

# **Microstructure and Rheology of Colloidal Natural Clay Mineral Dispersions**

Zur Erlangung des akademischen Grades einer  
DOKTORIN DER INGENIEURWISSENSCHAFTEN (Dr.-Ing.)

von der Fakultät für Chemieingenieurwesen und Verfahrenstechnik des  
Karlsruher Institut für Technologie (KIT)

genehmigte  
DISSERTATION

von  
M. Sc. Müge Pilavtepe  
aus Izmir, Türkei

Tag der mündlichen Prüfung: 05.02.2018

Erstgutachter: Prof. Dr. Norbert Willenbacher

Zweitgutachterin: PD Dr. Katja Emmerich



### Acknowledgements

First of all I would like to thank my supervisor Prof. Dr. Norbert Willenbacher for his encouraging support and advice throughout this work. I am grateful to PD. Dr. Katja Emmerich for being the second reviewer and for her help to understand the complex structure of natural clay minerals.

I gratefully acknowledge the German Academic Exchange Service for their financial support for the most part of my doctoral study. I really appreciate the graduate school for Climate and Environment (GRACE-KIT) for the financial support for my last and most difficult phase of my doctoral study and for the grant for international rheology conference in Japan, whereby I had an opportunity for precious networking. I would like to thank Karlsruhe House of Young Scientists (KHYS) for the grant for my research abroad at MIT in Cambridge, USA, where I gained excellent scientific and social experiences.

I want to thank Dr. Annett Steudel, Dr. Florian Schnetzer and especially Dr. Laure Delavernhe for the sample purification and physicochemical characterization as well as for their help and fruitful discussions. I thank Marita Heinle for performing the ICP-OES analysis. I would like to thank again Dr. Laure Delavernhe for calculation of data from ICP-OES and CEC analyses and her worthwhile graphical interpretations. I want to thank Dr.-Ing Rainer Schuhmann for his sustained support.

I also want to thank my students Dilek Dönmez, Barbara da Silva Lopez, Tabea Stadler, Sandra Saad, Sandra Haas, Rebekka Maria Cséki and especially Steffen Michael Recktenwald for doing excellent work in the lab conducting lots of experiments that are used in this thesis.

I am grateful to all my colleges for their collaboration, guidance and help in scientific and personal concerns. I would like to thank my parents and my friends Gülcin and Güney for their all support even from Turkey. Special thanks go to my boyfriend Michael for all his help and patience during the last year.

## Acknowledgements

---

## Abstract

Colloidal clay mineral dispersions consist of plate-like dispersed layers having negative charges at their faces based on isomorphic substitutions within the clay mineral structure and pH depending charges at their edges. The counter-ions of internal crystal structure of clay mineral particles diffuse out in water to form an electrical double layer on the clay mineral layer. The ionic strength of the dispersion determines the size of the electrical double layer, whereas the layer charge of dispersed layer determines the electrical potential of the clay mineral layer in diffusive double layer. Since the charge of the edge is pH dependent, the orientation of the clay mineral layers to each other is strongly influenced by the pH of dispersion. Their edges are positively charged at  $\text{pH} < \text{pH}_{\text{PZC,edge}}$  (point of zero charge at the edges) and negatively charged at  $\text{pH} > \text{pH}_{\text{PZC,edge}}$ . Competing attractive van der Waals interactions and repulsive or attractive electrostatic interactions between clay mineral layers in aqueous solution result in arrested states with different structural features. Depending on various physico-chemical parameters like ionic strength, solids content and pH, clay mineral dispersions form either fluid, gel-like or glass structure. At high ion concentration the compression of the electrical double layer allows for direct layer contacts and attractive gel states are formed. At  $\text{pH} > \text{pH}_{\text{PZC,edge}}$ , edge(-) to edge(-) (EE) and/or face(-) to face(-) (FF) contacts are formed resulting in so-called partially parallel overlapped (PPO) gel structure. At  $\text{pH} < \text{pH}_{\text{PZC,edge}}$ , edge(+) to face(-) (EF) contacts may occur resulting in arrested gel states with so-called house of cards (HOC) structure. In the absence of ions or at very low ionic strength, the sufficiently large electrical double layer around charged clay mineral layers leads to the repulsive glass state.

The rich variety of arrested states of clay mineral dispersions make them attractive for industrial applications and scientific studies. Most specific properties of clay mineral dispersions are viscoelasticity, time and shear rate dependent flow behavior, which are linked to the valence interlayer cations, chemical composition, structural charge localization as well as to the aspect ratio of clay mineral layers. The colloidal behavior of natural and synthetic clay minerals with different octahedral structure, e.g. di- and trioctahedral, layer charge (from 0.19 to

## Abstract

---

0.26 eq/FU) and average layer diameter (270, 100 and 30 nm) was investigated in this study. For this purpose synthetic hectorite (Laponite® with trioctahedral smectite), natural hectorite (natural clay mineral with trioctahedral Na-rich smectite, 0.2  $\mu\text{m}$  fraction of SHCa-1 Source Clay) and montmorillonite (natural bentonite with dioctahedral Na-rich smectite, 0.2  $\mu\text{m}$  fraction of Volclay) are used. The clay mineral specific  $\text{pH}_{\text{PZC,edge}}$  of dioctahedral smectites is lower than  $\text{pH}_{\text{PZC,edge}}$  of trioctahedral smectites.

Kinetics of structure formation, aging and broad bandwidth viscoelastic response ( $10^{-2}$  -  $10^6$  rad/s) of natural and synthetic clay mineral dispersion in different arrested states were characterized employing mechanical shear and squeeze flow rheometry combined with diffusing wave spectroscopy and multi particle tracking microrheology. Covering a wide range of solids (1-7 wt%) and salt (up to  $10^{-1}$  M NaCl) concentrations at different pH glasses, strong, and weak gels with prevailing EF or FF layer contacts were formed.

The differences between arrested states with different layer configurations were identified for the Laponite® dispersions using macro- and microrheological measurements, as a model system. Then the same measurements were applied to the more complicated system, i.e. natural hectorite and montmorillonite dispersions, and the data were compared with those obtained for the Laponite® system to see the effect of aspect ratio and layer charge of clay minerals on their rheological behavior.

The kinetics of structure formation of these three clay mineral dispersions was determined using small amplitude oscillatory shear measurement. They reach the arrested states following different routes but in their arrested states storage modulus  $G'$  is always higher than loss modulus  $G''$ . In all cases, gel formation takes place much faster than the transition from the sol to the glass state and gels at  $\text{pH} < \text{pH}_{\text{PZC,edge}}$  with preferred EF contacts form distinctly faster than at  $\text{pH} > \text{pH}_{\text{PZC,edge}}$  with prevailing FF contacts. A slower, more gradual structure formation of the natural clay mineral dispersions in glass state was observed than Laponite® dispersions in glass state which exhibited a fast increase in shear modulus after an extended induction time.

Aging has been studied at inherent  $\text{pH}=\text{pH}_{\text{inh}}$  of the respective clay mineral dispersions using shear modulus measurements for a period of 8-16 weeks. Strong gels of Laponite® dispersion with  $\text{pH}_{\text{inh}} < \text{pH}_{\text{PZC,edge}}$  show little aging and exhibit a weak increase of  $G' \sim t^\alpha$  with  $\alpha = 0.11 \pm 0.03$ , higher  $\alpha$  values are found for weak gels and strongest aging is observed in glasses. Aging turned out to be less pronounced for natural hectorite with  $\text{pH}_{\text{inh}} < \text{pH}_{\text{PZC,edge}}$  compared to arrested montmorillonite dispersions with  $\text{pH}_{\text{inh}} > \text{pH}_{\text{PZC,edge}}$ . For both natural clay mineral dispersions, aging is weaker in the glass state than for the investigated gels, in contrast to Laponite® glasses.

On the basis of the values derived from the rotational and oscillatory shear experiments during 8 weeks the rheological state diagrams for natural and synthetic clay mineral dispersions were created at their  $\text{pH}_{\text{inh}}$ . The main parameters for a state diagram, e.g. clay mineral and NaCl concentration as well as sample aging, were considered. The clay mineral content required to form arrested states increases with increasing clay mineral average layer diameter and higher salt concentrations are required to form attractive gel states of natural clay mineral dispersions due to their higher layer charge compared to Laponite®.

All three types of clay mineral dispersions in arrested state exhibit a frequency independent storage modulus  $G' \gg G''$  at low frequencies and the absolute value varies with clay mineral and salt concentration. The loss modulus  $G''$  is almost independent of the ionic strength of the dispersion, but changes significantly with pH in the frequency range between  $10^{-2}$  and  $10^3$  rad/s. High frequency relaxation is dominated by a characteristic power law scaling  $G'' \sim \omega^{3/4}$  and absolute values depend only weakly on sample composition. For natural clay mineral dispersions this characteristic crossover at which  $G' = G''$  occurs at lower frequencies than for Laponite® dispersions, i.e. the characteristic crossover frequency decreases with increasing layer size.

MPT microrheology data of Laponite® dispersions reveal structural refinement on the submicrometer length scale going on during aging for weak gels but not for glasses. Strong structural heterogeneity in Laponite® dispersion most pronounced at  $\text{pH} < \text{pH}_{\text{PZC,edge}}$  occurs during gel or glass formation, but at longer

## Abstract

---

times all arrested states appear homogenous on the 0.2 nm length scale. The characteristic time determining the transition to the arrested state obtained from bulk rheometry and MPT microrheology agree very well for the montmorillonite dispersions forming a glass or a strong gel. Similar behavior was observed for Laponite® dispersions in the glass state. However, for the natural hectorite dispersion forming a weak gel the sol/gel transition is delayed on the microscopic scale by about two orders of magnitude in time compared to bulk measurements, i.e. a structural refinement takes place long after the gel has formed on the macroscale, qualitatively in line with the Laponite® gels.

The variety of methods applied in this study and the broad range of physico-chemical parameters investigated here provide a comprehensive scientific and practical view on the rheological differences between natural and synthetic di- and trioctahedral smectite dispersions for industrial applications.

# Zusammenfassung

Tonmineraldispersionen bestehen aus plättchenförmigen kolloidalen Partikeln mit negativen Ladungen an ihren Oberflächen auf der Basis von isomorphen Substitutionen innerhalb der Tonmineralstruktur und mit pH-abhängigen Ladungen an ihren Kanten. Um eine elektrische Doppelschicht am Schichtpaket zu bilden, diffundieren die Zwischenschichtionen der Kristallstruktur von Tonmineralteilchen im Wasser. Die Ionenstärke der Dispersion bestimmt die Größe der elektrischen Doppelschicht, während die Schichtladungsdichte das elektrische Potential an der Schichtpaketen bestimmt. Da die Ladung der Kanten pH-abhängig ist, wird die Orientierung der Schichtpakete zueinander stark durch den pH-Wert der Dispersion beeinflusst. Ihre Kanten sind bei  $\text{pH} < \text{pH}_{\text{PZC,edge}}$  ( $\text{pH}_{\text{PZC,edge}}$ , an dem die Summe der Kantenladungen Null ist) positiv geladen und bei  $\text{pH} > \text{pH}_{\text{PZC,edge}}$  negativ geladen. Durch die Überlagerung von attraktiven van der Waals und abstoßenden oder anziehenden elektrostatischen Wechselwirkungen zwischen geladenen Tonmineralschichtpaketen in wässriger Lösung entstehen arretierte Zustände mit unterschiedlichen Strukturmerkmalen. In Abhängigkeit von verschiedenen physikalisch-chemischen Parametern, wie Ionenstärke, Feststoffgehalt und pH-Wert, bilden Tonmineraldispersionen entweder flüssige, gel- oder glasartige Strukturen. Bei hoher Ionenkonzentration ermöglicht die Kontraktion der elektrischen Doppelschicht direkte Kontakte der Schichtpakete und dadurch bilden sich attraktive Gelzustände. Bei  $\text{pH} > \text{pH}_{\text{PZC,edge}}$  werden Kanten(-) mit Kanten(-) (EE) und/oder die Plättchenoberflächen(-) mit Plättchenoberflächen(-) (FF) in Kontakt kommen, was zu einer sogenannten partiell parallelen überlappenden (PPO) Gelstruktur führt. Bei  $\text{pH} < \text{pH}_{\text{PZC,edge}}$  entstehen Kontakte zwischen positiv geladenen Kanten(+) und negativ geladenen Oberflächen(-) (EF), die zu arretierten Gelzuständen mit sogenannter House of Cards (HOC) - Struktur führen. Ohne Zugabe von Ionen oder bei sehr geringer Ionenstärke führt die ausreichend große elektrische Doppelschicht um die geladenen Schichtpakete zum abstoßenden Glaszustand.

Aufgrund der Vielfalt ihrer arretierten Zustände sind Tonmineraldispersionen für industrielle Anwendungen und wissenschaftliche Forschungen sehr attraktiv. Ihre spezifischen Eigenschaften sind die Viskoelastizität und das zeit- und

## Zusammenfassung

---

scherratenabhängige Fließverhalten, die von den Zwischenschichtkationen, der chemischen Zusammensetzung, der strukturellen Ladungslokalisierung sowie dem Aspektverhältnis von Tonmineralschichtpaketen beeinflusst werden. Das kolloidale Verhalten von natürlichen und synthetischen Tonmineralien mit unterschiedlicher oktaedrischer Struktur, z.B. di- und trioktaedrisch, Schichtladungsdichte (von 0,19 bis 0,26 eq/FU) und Teilchengröße (270, 100 und 30 nm) wurde in dieser Arbeit untersucht. Zu diesem Zweck wurden synthetischer Hectorit (Laponite®, trioktaedrischer Smectit), natürlicher Hectorit (trioktaedrischer Na-ausgetauschter Smectit, 0,2 µm Fraktion von SHCa-1 Source Clay) und Montmorillonit (dioktaedrischer Na-ausgetauschter Smectit, 0,2 µm Fraktion von Bentonit Volclay) verwendet. Der tonmineralspezifische  $\text{pH}_{\text{PZC,edge}}$  von dioktaedrischen Smectiten ist niedriger als der  $\text{pH}_{\text{PZC,edge}}$  von trioktaedrischen Smectiten.

Die Kinetik der Strukturbildung, die Alterung und die viskoelastische Reaktion in der umfassenden Bandbreite ( $10^{-2}$  -  $10^6$  rad/s) der natürlichen und synthetischen Tonmineraldispersionen in verschiedenen arretierten Zuständen wurden mit Hilfe einer mechanischen Scher- und Quetschströmungsrheometrie und optischer Mikrorheologiemethoden, wie dynamische Lichtsteuerung (Diffusing Wave Spectroscopy (DWS)) und die Multiple Particle Tracking (MPT), charakterisiert. Mit einem breiten Spektrum von Feststoffgehalt (1-7 Gew. %), Salzgehalt (bis zu  $10^{-1}$  M NaCl) und bei verschiedenen pH-Werten wurden Glaszustände sowie starke und schwache Gele mit vorherrschenden EF- oder FF-Schichtpaketenkontakten gebildet.

Die Unterschiede zwischen arretierten Zuständen mit unterschiedlichen Schichtpaketenkonfigurationen wurden für die Laponite®-Dispersionen mittels makro- und mikrorheologischer Messungen als Modellsystem festgestellt. Dann wurden die gleichen Methoden auf die komplizierteren natürlichen Systeme der Hectorit- und Montmorillonitdispersionen angewendet. Um den Effekt des Aspektverhältnisses und der Schichtladungsdichte von Tonmineralien auf ihr rheologisches Verhalten zu sehen, wurden die Daten mit dem Laponite®-System verglichen.

Die Kinetik der Strukturbildung dieser drei Tonmineraldispersionen wurde mittels oszillatorischen Schermessungen bei geringer Amplitude bestimmt. Sie erreichen die arretierten Zustände auf verschiedenen Wegen, aber in den arretierten Zuständen ist der Speichermodul  $G'$  immer höher als den Verlustmodul  $G''$ . In allen Fällen findet die Gelbildung viel schneller als den Übergang vom Sol zum Glaszustand statt und die Gele bei  $\text{pH} < \text{pH}_{\text{PZC,edge}}$  mit bevorzugten EF-Kontakten bildeten sich deutlich schneller als bei  $\text{pH} > \text{pH}_{\text{PZC,edge}}$  mit vorherrschenden FF-Kontakten. Es wurde eine langsamere, allmählichere Strukturbildung der natürlichen Tonmineraldispersionen beim Übergang in den Glaszustand als bei der Glasbildung der Laponite®-Dispersionen beobachtet, die nach einer verlängerten Induktionszeit einen schnellen Anstieg des Schermoduls zeigten.

In einem Zeitraum von 8-16 Wochen wurde die Alterung beim inhärenten pH-Wert der jeweiligen Tonmineraldispersionen mit Hilfe oszillatorischer Schermessungen untersucht. Die starken Gele der Laponite®-Dispersion bei  $\text{pH}_{\text{inh}} < \text{pH}_{\text{PZC,edge}}$  zeigen wenig Alterung und eine schwache Zunahme von  $G' \sim t^\alpha$  mit  $\alpha = 0,11 \pm 0,03$  wurde festgestellt. Höhere  $\alpha$ -Werte für schwache Gele und stärkste Alterung im Glaszustand wurden beobachtet. Die Alterung der natürlichen Hectoritdispersionen bei  $\text{pH}_{\text{inh}} < \text{pH}_{\text{PZC,edge}}$  war weniger ausgeprägt als bei Montmorillonitdispersionen mit  $\text{pH}_{\text{inh}} > \text{pH}_{\text{PZC,edge}}$ . Im Gegensatz zu Laponite® ist für beide natürlichen Tonmineraldispersionen die Alterung im Glaszustand schwächer als für die untersuchten Gelzustände.

Auf der Basis der in einem Zeitraum von 8 Wochen ermittelten rheologischen Daten wurden die Zustandsdiagramme für natürliche und synthetische Tonmineraldispersionen bei ihrem inhärenten pH erstellt. Die Hauptparameter für ein Zustandsdiagramm, z.B. Tonmineral- und NaCl-Konzentration sowie Probenalterung, wurden berücksichtigt. Der Tonmineralgehalt, der zur Bildung von arretierten Zuständen erforderlich ist, nimmt mit zunehmendem Tonmineralplättchendurchmesser zu. Um attraktive Gelzustände von natürlichen Tonmineraldispersionen zu bilden, sind aufgrund der höheren Ladungsdichte von natürlichen Tonmineralen im Vergleich zu Laponite® höhere Salzkonzentrationen erforderlich.

## Zusammenfassung

---

Alle drei Arten von Tonmineraldispersionen im arretierten Zustand weisen bei niedrigen Frequenzen einen frequenzunabhängigen Speichermodul  $G' \gg G''$  auf und der Absolutwert variiert mit Tonmineral- und Salzkonzentration. Der Verlustmodul  $G''$  ist nahezu unabhängig von der Ionenstärke der Dispersion, ändert sich aber signifikant mit dem pH-Wert im Frequenzbereich zwischen  $10^{-2}$  und  $10^3$  rad/s. Die Hochfrequenzrelaxation wird von einem charakteristischen Potenzgesetz  $G'' \sim \omega^{3/4}$  beherrscht und der absolute Wert hängt nur geringfügig von der Probenzusammensetzung ab. Für natürliche Tonmineraldispersionen tritt dieses charakteristische Crossover ( $G' = G''$ ) bei niedrigeren Frequenzen als für Laponite®-Dispersionen auf, d.h. die charakteristische Frequenz bei der sich Module schneiden nimmt mit zunehmender Plättchengröße ab.

Aus den Untersuchungen mit Hilfe der optischen Mikrorheologie ergibt sich für die Laponite®-Dispersionen eine strukturelle Verfeinerung im Submikrometerbereich, die während des Alterns für schwache Gele aber nicht für den Glaszustand auftritt. Die strukturelle Heterogenität in der Laponite®-Dispersion tritt am stärksten bei  $\text{pH} < \text{pH}_{\text{PZC,edge}}$  und beim Übergang vom Sol zum Glas- und Gelzustand auf, aber bei längeren Zeiten erscheinen alle arretierten Zustände auf der 0,2 nm Längenskala homogen. Die den Übergang zum arretierten Zustand bestimmende charakteristische Zeit wurde mit Hilfe der Rotationsrheometrie und der MPT-Mikrorheologie ermittelt. Die auf Makro- und Mikrolängenskala ermittelten Zeiten stimmen für die Montmorillonitdispersionen in den Glas- oder starken Gelzuständen sehr gut miteinander überein. Ähnliches Verhalten wurde für Laponite®-Dispersionen im Glaszustand beobachtet. Für die natürliche Hectoritdispersion, die ein schwaches Gel bildet, wurde der Sol/Gel-Übergang auf der mikroskopischen Skala um etwa zwei Größenordnungen im Vergleich zu Rotationsrheometriemessung verzögert. Das heißt, eine lange strukturelle Verfeinerung erfolgt, nachdem sich das Gel auf der Makroskala gebildet hat. Diese strukturelle Verfeinerung im schwachen Gelzustand von Hectoritdispersion ist qualitativ in Übereinstimmung mit den Ergebnissen die für Laponite®-Gele ermittelt werden.

Die vielfältigen in dieser Arbeit angewendeten Methoden und das breite Spektrum der hier untersuchten physikalisch-chemischen Parameter bieten eine

umfassende wissenschaftliche und praktische Analyse der rheologischen Unterschiede zwischen natürlichen und synthetischen di- und trioktaedrischen Smectitdispersionen im Hinblick auf industrielle Anwendungen.

# Content

<b>Acknowledgements</b> .....	<b>I</b>
<b>Abstract</b> .....	<b>III</b>
<b>Zusammenfassung</b> .....	<b>VII</b>
<b>Content</b> .....	<b>XII</b>
<b>List of Symbols</b> .....	<b>XIV</b>
<b>1 Introduction</b> .....	<b>1</b>
1.1 Clay mineral dispersions .....	1
1.2 Natural and synthetic smectites .....	2
1.3 Layer interaction in clay mineral dispersions.....	7
1.4 Effect of electrolytes and pH of the medium on layer interaction .....	13
1.5 State of the art .....	17
1.6 Scope of this study .....	24
<b>2 Materials</b> .....	<b>26</b>
2.1 Montmorillonite.....	26
2.2 Natural hectorite.....	26
2.3 Synthetic hectorite – Laponite® RD .....	27
2.4 Physicochemical properties of materials .....	27
2.5 Sample preparation.....	31
<b>3 Methods</b> .....	<b>33</b>
3.1 Overview .....	33
3.2 Transient oscillatory shear at fixed frequency and amplitude.....	38
3.3 Amplitude sweep experiments .....	38
3.4 Frequency sweep experiments .....	38
3.5 Oscillatory squeeze flow .....	39
3.6 Diffusing wave spectroscopy.....	40
3.7 Multiple particle tracking (MPT).....	41

<b>4 Results and Discussion .....</b>	<b>42</b>
4.1 Macro- and microscale structure formation and aging in different arrested states of Laponite® dispersions.....	42
4.1.1 Structure formation in glass and gel states of Laponite® dispersions.	43
4.1.2 Effect of pH on structure formation .....	44
4.1.3 Aging of Laponite® dispersions in different arrested states.....	46
4.1.4 Broad bandwidth linear viscoelastic relaxation of Laponite® dispersions in different arrested states .....	49
4.1.5 Microrheology and microstructural heterogeneity .....	51
4.2 Formation of arrested states in natural di- and trioctahedral smectite dispersions compared to synthetic hectorite - a macro and microrheological study .....	58
4.2.1 Comparison of structure formation of natural and synthetic clay mineral dispersions at their inherent pH .....	58
4.2.2 Effect of pH on structure formation of natural clay mineral dispersions .....	61
4.2.3 Aging of natural clay mineral dispersions in different arrested states .	62
4.2.4 State diagram of clay mineral dispersions at their inherent pH.....	64
4.2.5 Broad bandwidth linear viscoelastic response of natural clay mineral dispersions with different aspect ratio .....	66
4.2.6 Microstructures of natural clay mineral dispersions .....	68
<b>5 Conclusion .....</b>	<b>71</b>
5.1 Summary .....	71
5.2 Outlook .....	74
<b>6 List of Figures .....</b>	<b>76</b>
<b>7 List of Tables.....</b>	<b>79</b>
<b>8 References.....</b>	<b>80</b>

## List of Symbols

### Latin symbols

symbol	description	unit
$A$	effective Hamaker constant	J
$A_1$	Hamaker constant of liquid medium	J
$A_2$	Hamaker constant of dispersed particle	J
$a_s$	specific surface area	$\text{m}^2 \text{g}^{-1}$
$a_{s,edge}$	specific edge surface area	$\text{m}^2 \text{g}^{-1}$
BF	birefringence	
BV-M0.2Na	Na-exchanged montmorillonite	
$c_i$	ion concentration	M ( $\text{mol dm}^{-3}$ )
$c_{NaCl}$	NaCl concentration	M ( $\text{mol dm}^{-3}$ )
$c_s$	solids content	wt%
$c_{Laponite}$	Laponite concentration	wt%
$c_{SHCa-0.2Na}$	natural hectorite concentration	wt%
$c_{BV-M0.2Na}$	Na-exchanged montmorillonite concentration	wt%
CEC	cation exchange capacity	
$d$	diameter of tracer particle	$\mu\text{m}$
$D$	average layer diameter	nm
DLS	dynamic light scattering	
DWS	diffusing wave spectroscopy	
$e$	electron charge	$1.602 \times 10^{-19} \text{ C}$
$E_R$	repulsive energy or potential	$\text{J m}^{-2}$
$E_A$	van der Waals attractive energy	$\text{J m}^{-2}$
$E_T$	total interaction energy	$\text{J m}^{-2}$
$E_{max}$	maximum interaction energy	$\text{J m}^{-2}$
$E_{min}$	minimum interaction energy	$\text{J m}^{-2}$
$\Delta E_b$	barrier energy ( $V_{max} - V_{min}$ )	$\text{J m}^{-2}$
eq/FU	equivalent per formula unit	

## List of Symbols

EE	edge-to-edge layer contact	
EF	edge-to-face layer contact	
FF	face-to-face layer contact	
$f$	frequency	Hz
$F$	Faraday constant	96485.33 C mol <sup>-1</sup>
$G$	shear modulus	Pa
$G'$	storage modulus	Pa
$G'_{0,n}$	normalized plateau storage modulus	
$G''$	loss modulus	Pa
$G^*$	complex shear modulus	Pa
$H$	distance between two plate-like particles	nm
$\bar{H}_{exp}$	experimental average interparticle distance	nm
HOC	house of cards layer contact	
HR	heterogeneity ratio	
ICP-OES	inductively coupled plasma optical emission spectrometry	
$I$	ionic strength	M (mol dm <sup>-3</sup> )
$k_B$	Boltzmann constant	1.28x10 <sup>-23</sup> J K <sup>-1</sup>
LS	light scattering	
$M$	molecular weight	kg mol <sup>-1</sup>
$Me^{\nu+}$	interlayer cation with the charge $\nu$	
MPT	multiple particle tracking technique	
MSD	mean square displacement	
$M_1(\tau)$	estimator for the ensemble average of MSD	
$M_2(\tau)$	estimator for the ensemble variance of MSD	
$N_A$	Avogadro constant	6.022 x 10 <sup>23</sup> mol <sup>-1</sup>
PAV	piezoelectric axial vibrator	
pH <sub>inh</sub>	inherent pH of dispersion	
pH <sub>PZC,edge</sub>	pH of point of zero charge at the layer edge	
PPO	parallel partially overlapped layer contact	

## List of Symbols

---

PZC	point of zero charge	
PZNC	point of zero net charge	
PZNPC	point of zero net proton charge	
$R$	radius of cone-plate geometry	mm
$R_G$	gas constant	8.314 J K <sup>-1</sup> mol <sup>-1</sup>
$R_1$	inner cylinder radius of Searle system	mm
$R_2$	outer cylinder radius of Searle system	mm
$q_{max}$	the maximum in the oscillations of the scattering intensity in SAXS measurement	nm <sup>-1</sup>
SAXS	small-angle X-ray scattering	
SHCa-0.2Na	natural hectorite	
SIM	numerical simulation	
SLS	static light scattering	
$t$	time	s
$t_c$	crossover or gelation time	s
$t_p$	thickness of the clay mineral platelet	nm
$T$	absolute temperature	K
$x$	distance from the clay mineral basal surface	nm
$V_{uc}$	unit cell volume	m <sup>3</sup>
VI	visual inspection	

### Greek symbols

symbol	description	unit
$\alpha$	power law exponent describing the dependence of storage modulus on time	
$\beta$	power law exponent describing the dependence of loss modulus on frequency	
$\varepsilon$	permittivity of the medium	kg <sup>-1</sup> m <sup>-3</sup> s <sup>4</sup> A <sup>2</sup>
$\xi$	layer charge	eq/FU
$\delta$	phase angle	°
$\tan \delta$	loss factor (loss tangent)	
$\theta$	cone angle of cone-plate geometry	°

## List of Symbols

---

$\rho$	counter-ion density	
$\rho_s$	specific density	$\text{g cm}^{-3}$
$\kappa^{-1}$	thickness of double layer	nm
$\eta_p$	Bingham plastic viscosity	Pa s
$\gamma$	deformation (strain)	%
$\gamma_0$	strain amplitude	%
$\dot{\gamma}$	shear rate	$\text{s}^{-1}$
$\sigma$	shear stress	Pa
$\sigma_0$	stress amplitude	Pa
$\sigma_y$	yield stress	Pa
$\tau$	lag time	s
$\nu$	valence of the ion	
$\omega$	angular frequency	$\text{rad s}^{-1}$
$\psi$	electrical potential	mV
$\psi_0$	surface potential	mV
$\psi_s$	Stern-layer potential	mV



# 1 Introduction

## 1.1 Clay mineral dispersions

The synthetic clay mineral Laponite® is distinguished from natural clay minerals by the monodisperse layer size distribution, the uniform plate-like particle shape and the homogeneous layer charge distribution. Due to the relatively high monodispersity of Laponite® particles this synthetic clay mineral widely used as academic model system. On the other side, natural clay minerals are abundant in nature, and are low cost versatile materials with a large spectrum of properties that make them very attractive for the industrial and research viewpoints. Phase behavior, structure and dynamics of clay mineral colloidal dispersions are of high technical relevance and great scientific interest. The variety of different dynamically arrested states observed in such systems has stimulated the interest of soft matter scientists. Clay minerals are widely used as a rheology-modifier in many industrial products, such as electrically conductive, antistatic and barrier coatings, ceramic glazes, paint polymer, print paper, household cleaners and personal care products, as well as nanocomposites (Claire Greaves et al. 1995; Caruso et al. 2001; Loiseau & Tassin 2006; Pálková et al. 2010). The effect of natural clay mineral properties on rheological behavior of dispersion is very important in new geotechnical and industrial applications like geologic CO<sub>2</sub> injection (Loring et al. 2012), radioactive waste repository (Grangeon et al. 2015; Reiche et al. 2016), high-tech nanomaterials for drug delivery (Dawson & Oreffo 2013; Rives et al. 2014), soil and water purification (Lee & Tiwari 2012; De Oliveira & Guegan 2016). In the application of radioactive waste repository, the viscoelastic character of clay mineral dispersions should be considered because of the erosion of backfill material and sealing by injection techniques (Baik et al. 2007; Eriksson & Schatz 2015). Most specific properties of clay mineral dispersions (e.g. time and shear rate dependent flow behavior and viscoelasticity) are linked to the chemical composition, structural charge localization in the clay mineral layer (Paineau et al. 2011a), as well as to aspect ratio of clay mineral layers and particles (Michot et al. 2004; Paineau et al. 2011b). Their rheological behavior is complex but important for processing and applications.

### 1.2 Natural and synthetic smectites

The family of clay mineral materials encompasses many groups depending on their chemistry, structure and net charge (Jasmund & Lagaly 1993). Montmorillonite, natural and synthetic hectorites were used in this study, which are 2:1 layer silicates from smectite group. Clay mineral particles consist of stack of layers and are also called tactoid (see Figure 3). They are composed of two  $[\text{SiO}_4]$ -tetrahedral sheets encompassing an  $[\text{Me}(\text{O},\text{OH})_6]$ -octahedral sheet (Figure 1 and 2). The tetrahedrons are linked via oxygen ions to form a tetrahedral sheet by sharing corners, while an octahedral sheet is condensed to this tetrahedral sheet via oxygen ions (Figure 2). Octahedral sheet consists of octahedrons, which are connected by edge sharing (Figure 1).

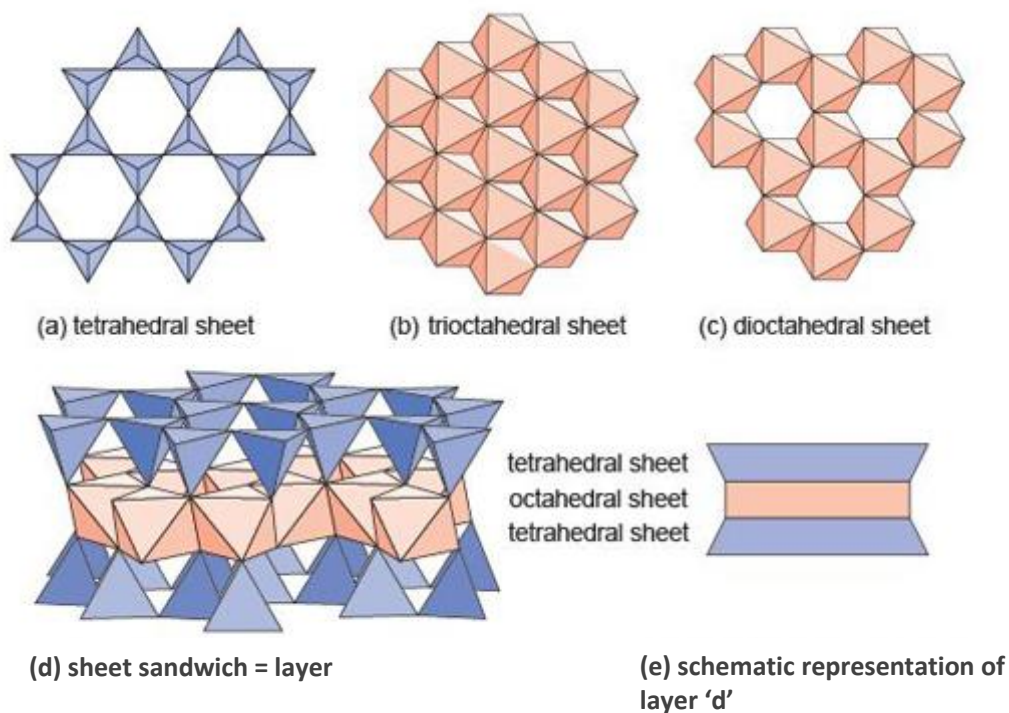


**Figure 1.** Building blocks of layer silicate minerals **a)** tetrahedral sheet **b)** trioctahedral sheet **c)** dioctahedral sheet **d)** an oblique view of a sheet sandwich (=layer), formed by two tetrahedral sheets bonded to an octahedral sheet **e)** a schematic representation of the layer in d) (web course materials [www.open.edu](http://www.open.edu), modified).

A distinction is made between trioctahedral and dioctahedral smectites depending on whether all sites or four of six octahedral sites are occupied by metal ions ( $Me^{v+}$ ) in a unit cell. In the 2:1 layer structure, the unit cell includes six octahedral and eight tetrahedral sites. If all six octahedral sites are occupied by divalent cations ( $Mg^{2+}$ ), the structure is called trioctahedral. If only four octahedral sites in a unit cell are occupied by trivalent cations ( $Al^{3+}$  or  $Fe^{3+}$ ), the structure is called dioctahedral.

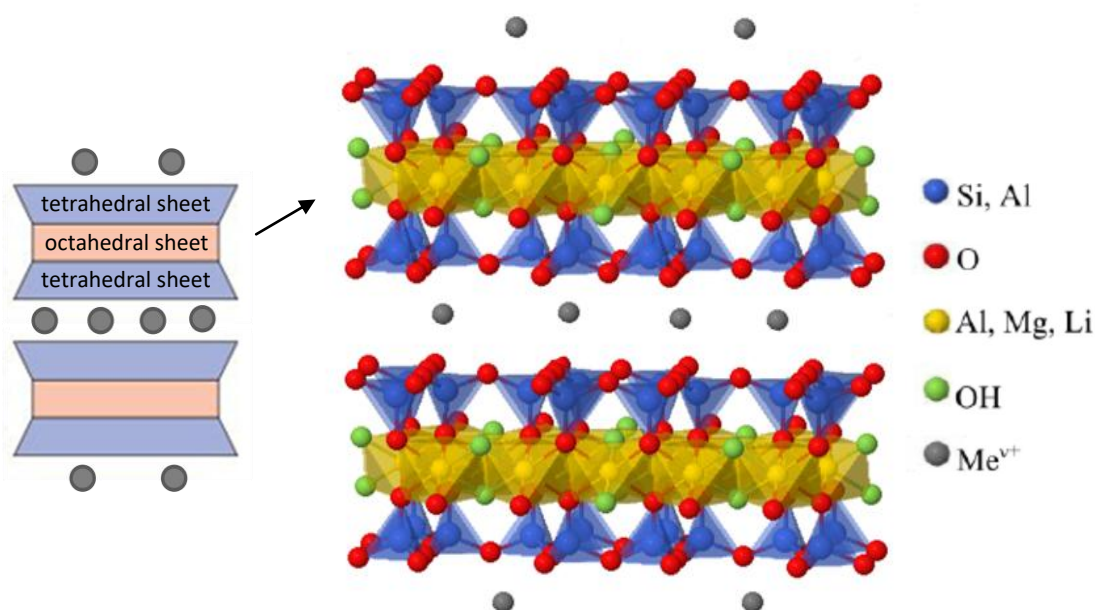


**Figure 2.** Representation of the layer structure of the three-layer clay minerals (2:1 layer silicates). The blue tetrahedrons represent the position of the  $[SiO_4]$ -tetrahedral sheet, the yellow octahedrons represent the  $[Me(O,OH)_6]$ -octahedral sheet. Depending on the clay mineral, the octahedral coordinated metal ions (yellow spheres) can be replaced by metal ions of different valence. Between the layers are counter-ions  $Me^{v+}$  (gray spheres) bound (ChemTube3D, University of Liverpool, [www.chemtube3d.com](http://www.chemtube3d.com), modified).

Montmorillonite is dioctahedral smectite, whereas natural and synthetic hectorites are trioctahedral smectites. For all of these three samples, isomorphous substitutions occur mainly in octahedral sheets. It causes negative charges on the layers. In trioctahedral clay minerals (hectorite), divalent metal ions ( $Mg^{2+}$ ) in the octahedral sheet can be substituted by monovalent metal ions ( $Li^+$ ), or in dioctahedral clay minerals (montmorillonite) trivalent metal ions ( $Al^{3+}$  or  $Fe^{3+}$ ) can be substituted by divalent metal ions ( $Mg^{2+}$ ). The negative charge of the layers is

## Introduction

balanced by hydrated exchangeable cations in the interlayers (mostly  $\text{Ca}^{2+}$ ,  $\text{Mg}^{2+}$ ,  $\text{Na}^+$ ) (Jasmund & Lagaly 1993) (see Figure 2). The degree of substitution changes from layer to layer within certain limits so that the cation density also varies from interlayer to interlayer, which causes heterogeneous charge distribution of natural clay minerals (Lagaly & Ziesmer 2003). The layer charge, the charge location and the kind of interlayer cations strongly influence the chemical and physical properties of the smectites (Emmerich et al. 2009).

The exchangeable cations (in this study  $\text{Na}^+$ ) can be hydrated, thus allowing the system to swell in water, as shown in Figure 3. The extent of hydration varies greatly and depends on many factors related to the composition of the layers and the nature of interlayers cations (Madejová et al. 1998; Abend & Lagaly 2000; Schnetzer et al. 2016).

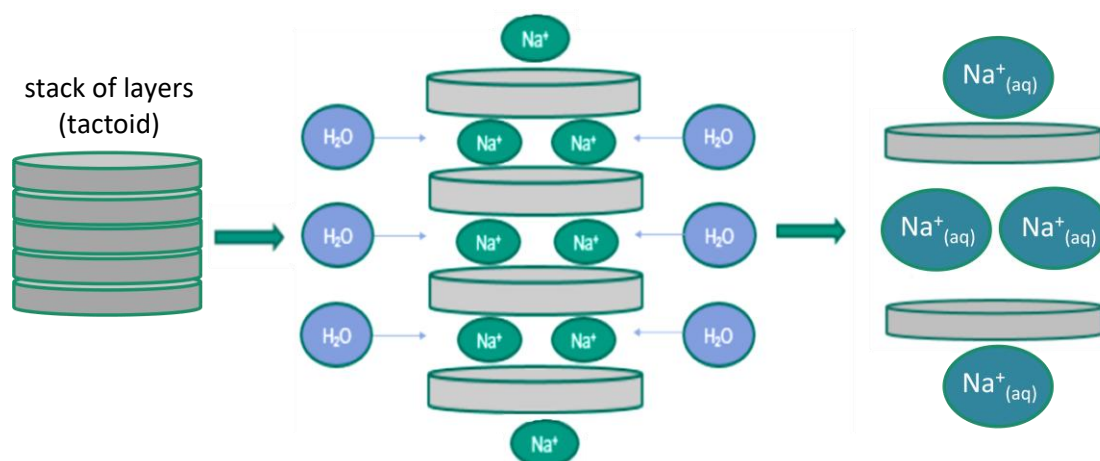


**Figure 3.** Swelling and complete delamination of clay mineral layers in aqueous dispersion. During dispersion, water or weak electrolyte solution is used to expand the distance between the individual plates. The  $\text{Na}^+$  ions are hydrated through water storage in the interlayers.

Paineau et al. (2011a) estimated the thickness of a single clay layer in such natural clay mineral dispersions from the slope of the swelling law derived from SAXS measurements. Swelling law is relating to the volume fraction  $\phi$  [%] and the experimental average interparticle distance  $\bar{H}_{exp}$  [nm], which can be deduced from the position of the maximum in the oscillations of the SAXS scattering

intensity,  $q_{max}$  [nm].

$$\bar{H}_{exp} \approx \frac{2\pi}{q_{max}} \quad (1.1)$$

Whatever the clay type, size fraction, or ionic strength, the swelling law exhibits two distinct domains. At low volume fractions, the  $\bar{H}_{exp}$  tends to scale as  $\phi^{-1/3}$ , which was assigned to the freely rotating objects. At higher volume fractions, a swelling regime with a power law  $\bar{H}_{exp} \sim \phi^{-1}$  was found with regard to the local lamellar order of the clay particles. In the  $\phi^{-1}$  regime, the average thickness of the individual platelets  $t_p$  [nm] can be derived from the slope of the swelling law by considering the Equation 1.2.

$$\bar{H}_{exp} = \frac{t_p}{\phi} \quad (1.2)$$

They reported the average thickness of a single clay layer in such natural clay mineral dispersions between 0.7 and 1 nm. According to this work we assumed perfect delamination of clay mineral layers in dispersion.

Whereas the negative charge of the clay mineral layers arises from isomorphological substitutions, the charge at the edges is pH dependent. Permanent charge induced by the layer charge and variable edge charges dependent of the pH induced by the amphoteric sites (silanols/aluminols/Mg-OH) at the edges of the clay mineral layer govern the charge heterogeneity of layers (Delavernhe et al. 2015). The variable edge charge of clay mineral layers becomes increasingly important for fine particles (Kaufhold & Dohrmann 2013).

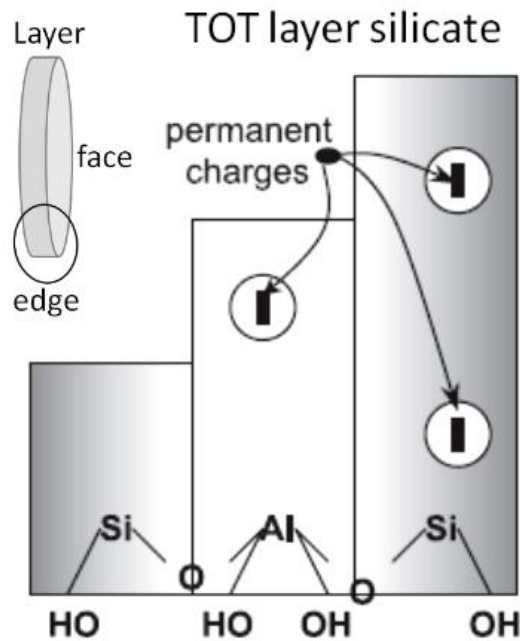
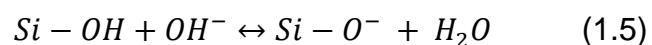
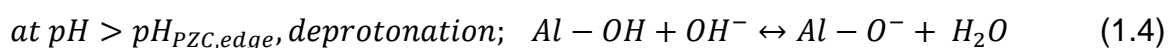
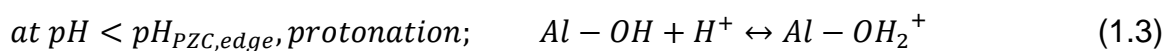


**Figure 4.** Development of surface charge heterogeneity on montmorillonite particles dispersed in aqueous solutions due to permanent negative charges on faces and surface pH-dependent charges on edges (Tombácz & Szekeres 2004, modified).

Polar sites, mainly octahedral Al–OH and tetrahedral Si–OH groups, are situated at the broken edges (Tombácz & Szekeres 2004), see Figure 4. These amphoteric sites are conditionally charged, and so variable (either positive or negative) charges can develop at the edges by direct H<sup>+</sup> or OH<sup>-</sup> transfer from aqueous phase depending on the pH. At lower pH a protonation process (Eq. 1.3) of the OH<sup>-</sup> groups, localized where the crystal structure terminates, forms a positive charge, which is slightly decreasing with increasing pH and neutralized at the pH of point of zero charge at edge pH<sub>PZC,edge</sub>. The deprotonation (Eq. 1.4-1.5) of Si–OH then that of the Al–OH sites takes place with increasing pH of solution resulting in negative charges at edges. The pH dependent edge sites play a significant role with respect to the stability and reactivity of the smectite (Delavernhe et al. 2015).



The term point of zero charge (PZC) defined as a unique pH, where the net surface charge is zero for amphoteric oxides bearing only pH-dependent charges, is not appropriate for clay minerals with both permanent and pH dependent charges. Additional point of zero charge definitions have to be introduced. The point of zero net proton charge (PZNPC) and the point of zero net charge (PZNC) have been introduced by Sposito (1981 and 1992). The PZNPC seems to be correct for the unique case of surface charge heterogeneity on clay mineral platelets, however, protons have specific affinity to the permanent charges (Tombacz et al. 1990; Janek & Lagaly 2001; Penner & Lagaly 2001) and so the use of  $\text{pH}_{\text{PZC,edge}}$ , i.e. the pH of the PZC belonging to the amphoteric edge sites, is unambiguous (Tombácz & Szekeres 2004).

The pH of point of zero charge at edge  $\text{pH}_{\text{PZC,edge}}$ , where positive and negative edge charges are in equilibrium, is a clay mineral specific value and sensitive to ionic strength of dispersions. Delhorme et al. (2010) defined the edge charge of 2:1 clays depending on pH and ion concentration using acid-base titration. The titration curve is shifted to acidic pH with increasing ion concentration. This shift is explained by the strong repulsive electrostatic interactions between edge sites (mainly aluminols) and negative layer charges sitting on the basal faces, as the change in the ionic strength modulates the screening of the repulsive electrostatic interactions. The rim charges of synthetic and natural hectorite layers are neutralized around  $\text{pH}=10-11$  (Tawari et al. 2001; Delavernhe et al. (accepted) 2017). The  $\text{pH}_{\text{PZC,edge}}$  of montmorillonite is much lower and lays between pH 5 and 7 (Tombácz & Szekeres 2004; Rozalén et al. 2009; Delhorme et al. 2010; Delavernhe et al. 2015).

### 1.3 Layer interaction in clay mineral dispersions

Fundamental investigations about clay mineral dispersions address phase behavior and in particular structure and dynamics of different arrested states (Mourchid et al. 1998; Levitz et al. 2000; Tanaka et al. 2004; Mongondry et al. 2005; Ruzicka et al. 2006; Jabbari-Farouji et al. 2008b; Ruzicka & Zaccarelli 2011). Depending on various physico-chemical parameters like ionic strength, layer size distribution, solids concentration and pH, clay mineral dispersions form

either fluid, gel-like or glass structure (Ruzicka et al. 2004; Tanaka et al. 2004; Ruzicka et al. 2008). Dispersions of clay minerals display a rich variety of arrested states differing in the complex arrangement of anisotropic disk-like clay mineral layers. The orientation of colloidal clay mineral layers is controlled by the balance between repulsive and attractive electrostatic forces and van der Waals forces between nano-sized plate-like particles.

When a clay mineral layers, having crystal structure that carries a negative charge due to isomorphic substitution, is placed in water, its counter-ions diffuse out to form an electrical double layer. Electrical double layer can be viewed as being composed of two layers (see Figure 5): an inner layer (Stern-layer) that may include adsorbed ions and a diffuse layer where ions are distributed according to the influence of electrical forces (Schramm 2006). There are two theories, e.g. the Stern theory and the Gouy-Chapman diffuse double layer theory (without Stern-layer), to determine electrokinetic and electro-chemical properties, potential energy and swelling pressure of clay-water electrolyte systems by considering either a constant charge or constant electrical potential at the surfaces of the clay mineral platelets (Tripathy et al. 2014). Sposito (2008) stated that the thickness of Stern-layer may vary between 0.5 and 0.6 nm. Sridharan and Satyamurty (1996) considered that the dimension of Stern-layer is equal to the hydrated ionic radii of exchangeable cations.

The Gouy-Chapman theory predicts an approximate exponential decay of the electrical potential  $\psi$  [mV] in the electrolyte solution at a distance  $x$  [nm] from the plane surface. This is represented by the following equation:

$$\psi = \psi_0 \exp(-\kappa x) \quad (1.6)$$

Where  $\psi_0$ [mV] is the surface potential and  $\kappa$  [nm<sup>-1</sup>] reciprocal of the extension or thickness of the double layer. The above expression is valid for a distance from the charged surface, where the potential is relatively low (Luckham & Rossi 1999).

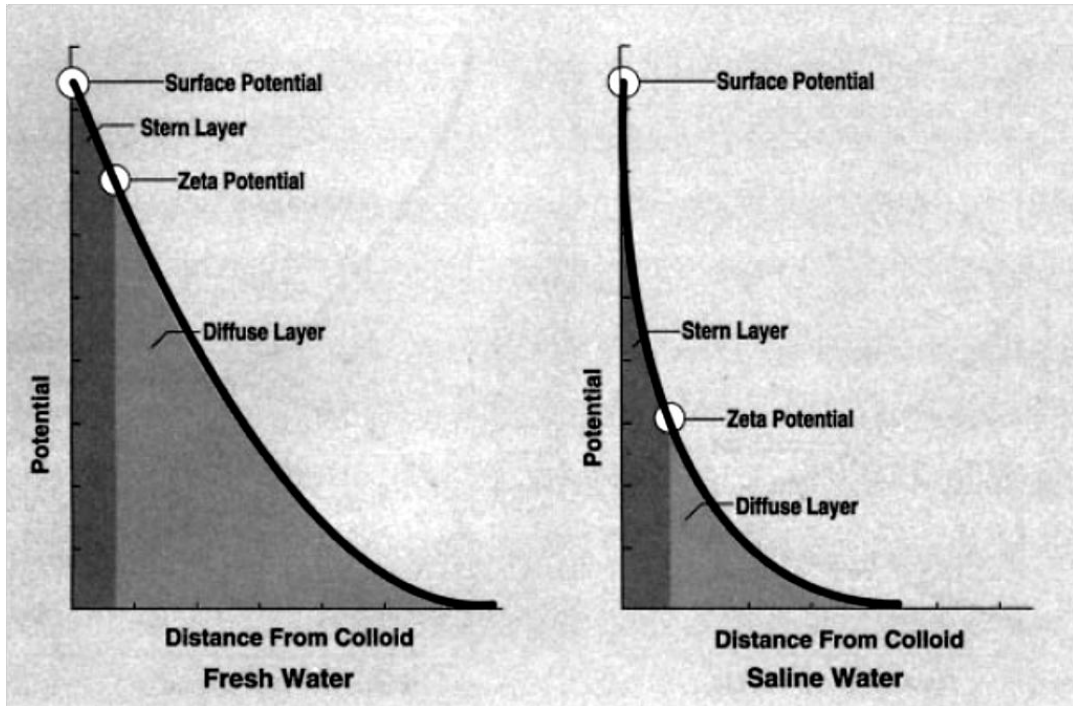


**Figure 5.** The diffuse electrical double layer showing the decay of potential away from the surface in fresh and saline water (Schramm 2006).

The surface potential  $\psi_0$  [mV] depends on both the layer charge  $\xi$  [eq/FU] at the surface and (through  $\kappa$ ) on the ionic composition of the medium as follows:

$$\xi = \epsilon \kappa \psi_0 \quad (1.7)$$

The thickness of the electrical double layer  $\kappa^{-1}$  [nm] can be calculated as:

$$\kappa^{-1} = \sqrt{\frac{\epsilon R_G T}{F^2 \sum_{i=n} c_i \nu_i^2}} \quad (1.8)$$

where  $F$  is the Faraday constant (96485.33 C mol<sup>-1</sup>),  $c_i$  [mol dm<sup>-3</sup>] the ion concentration,  $\nu_i$  the valence of the ion,  $\epsilon$  [kg<sup>-1</sup> m<sup>-3</sup> s<sup>4</sup> A<sup>2</sup>] the permittivity of the medium,  $R_G$  the gas constant (8.314 J K<sup>-1</sup> mol<sup>-1</sup>) and  $T$  [K] the absolute temperature,  $\kappa^{-1}$  is often also called Debye length (Shaw 1992).

## Introduction

It can be inferred from Eq. 1.8 that as the ion concentration increases the thickness of the double layer  $\kappa^{-1}$  decreases or is compressed, represented in Figure 5. The double layer thickness for an aqueous solution of a symmetrical electrolyte at 25 °C is given by:

$$\kappa^{-1} = 0.304 \sqrt{I} \quad (1.9)$$

$$I = (1/2) \sum_i c_i \nu_i^2 \quad (1.10)$$

where  $I$  [M] is ionic strength. For 1-1 electrolyte (NaCl aqueous solution in this study),  $\kappa^{-1}$  is 1 nm for  $I = 10^{-1}$  M, and 10 nm for  $I = 10^{-3}$  M (Schramm 2006).

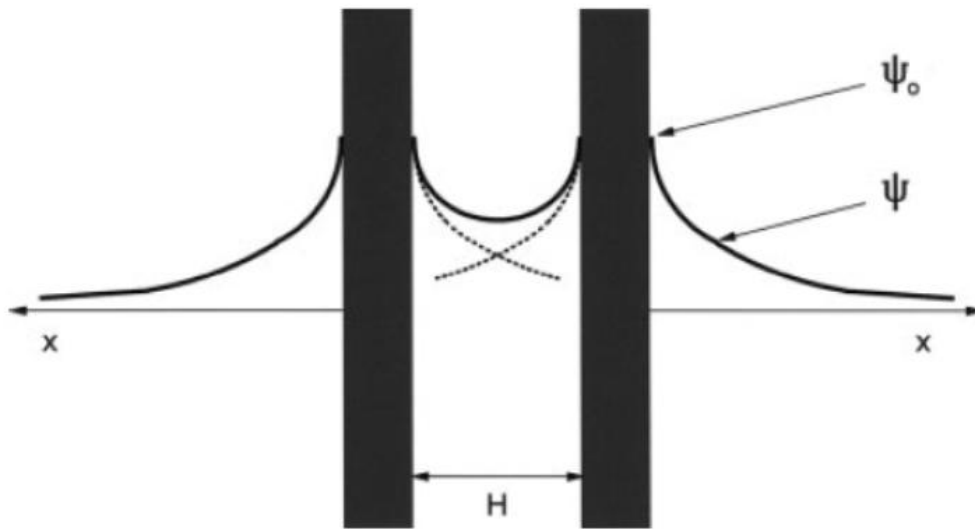


**Figure 6.** Two plate-like clay mineral layers approached to a separation distance,  $H$  with overlapping their diffuse double layers (Schramm 2006).

As two clay mineral layers approach each other in dispersion due to Brownian motion or convection, their diffuse double layers begin to interfere and stabilize by the repulsive forces. The repulsive energy or repulsive potential  $E_R$  [ $\text{J m}^{-2}$ ] between two clay mineral platelets oriented parallel to each other can be computed from the diffuse double layer theory as (Luckham & Rossi 1999):

$$E_R = \frac{64\rho k_B T}{\kappa} \left( \tanh \frac{ve\psi_s}{4k_B T} \right)^2 e^{-\kappa H} \quad (1.11)$$

where  $\rho$  is the counter-ion density,  $k_B$  the Boltzmann constant ( $1.28 \times 10^{-23} \text{ J K}^{-1}$ ),  $T$  [K] the absolute temperature,  $\psi_s$  [mV] the Stern-layer potential,  $H$  [nm] the distance between two clay mineral layers,  $\nu$  the valence of the ion,  $e$  the electron charge ( $1.602 \times 10^{-19} \text{ C}$ ) and  $\kappa$  [ $\text{nm}^{-1}$ ] the reciprocal Debye length. The repulsive potential decreases exponentially with increasing particle separation (Figure 6) and the range of repulsion is considerably reduced with electrolyte concentration (Figure 5).

In this study, the symbol  $E$  is used to represent the interaction energy between clay mineral layers and volume of particles is represented with the symbol  $V$ , which is usually used to symbolize the interaction energy between particles.

The van der Waals attractive energy  $E_A$  [ $\text{J m}^{-2}$ ] between parallel plate-like particles can be calculated as:

$$E_A = - \frac{A}{12\pi} \left( \frac{1}{H^2} + \frac{1}{(H+2t_p)^2} - \frac{1}{(H+t_p)^2} \right) \quad (1.12)$$

where  $A$  [J] is the Hamaker constant and  $H$  [nm] is the distance between the surfaces of the plates, and  $t_p$  [nm] is the thickness of the clay mineral layer (Ramos-Tejada et al. 2001b). The Hamaker constant depends on the nature of the material of the particles. In this case where liquid is the dispersion medium, rather than a vacuum, this constant must be replaced by an effective Hamaker constant, calculated from the expression:

$$A = (\sqrt{A_2} - \sqrt{A_1})^2 \quad (1.13)$$

where  $A_1$  is the Hamaker constant of the liquid medium and  $A_2$  is the Hamaker constant of the dispersed particle.

The fundamental feature of what is known as the DLVO theory is that this interaction is determined by a combination of the interparticle double layer repulsion energy ( $E_R$ ) and the Van der Waals attractive energy ( $E_A$ ). Colloidal stability can be explained by means of the sum of both energies (Luckham & Rossi 1999). The total interaction energy,  $E_T$  [ $\text{J m}^{-2}$ ] is represented as:

$$E_T = E_R + E_A \quad (1.14)$$

A representation of  $E_R$ ,  $E_A$  and  $E_T$  as a function of the interplate separation is shown in Figure 7. As seen in Figure 7,  $E_R$  decreases exponentially with increasing separation distance, while  $E_A$  decreases inversely to the separation distance squared.

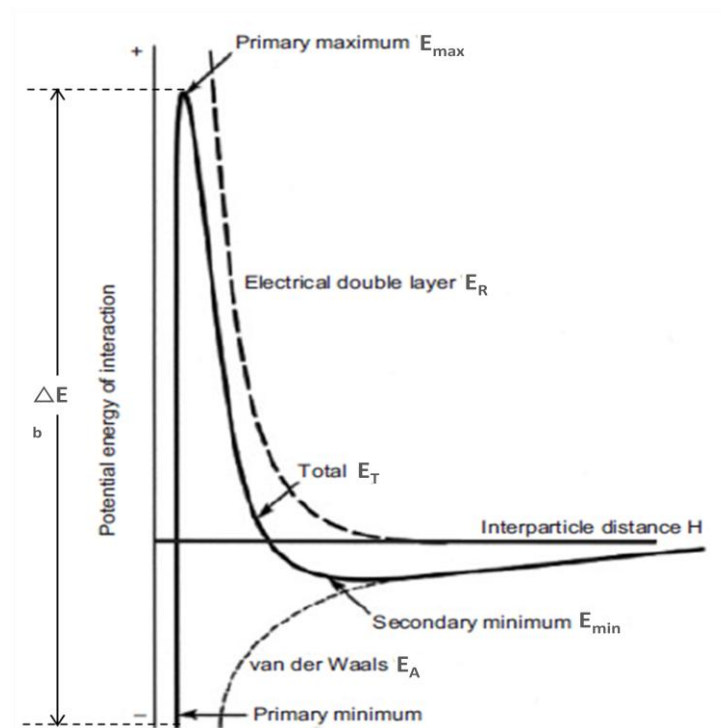


**Figure 7.** Potential energy of interaction between two parallel colloidal plate-shaped particles as a function of separation distance (Luckham & Rossi 1999; Schramm 2006, modified).

Of significant importance is the occurrence of a maximum energy ( $E_{max}$ ) at intermediate distances, which is considered as an energy barrier that the particles must overcome if they are to fall into the deep primary minimum at close distances and thus come together (Luckham & Rossi 1999). The height of  $E_{max}$  determines the relative stability of the system and the term  $\Delta E_b$  represents the barrier to redispersion (Figure 7). At large interparticle separations, a secondary minimum may occur since  $E_R$  falls off more rapidly with increasing distances than  $E_A$ .

The addition of electrolytes in the system will reduce  $E_{max}$ , and so the clay mineral layers will come into contact with each other and agglomerate. The aggregation of layers is known as coagulation or flocculation (Ramos-Tejada et al. 2001b; Lagaly & Ziesmer 2003). The dynamics of layer coagulation depends on the degree of compression of the double layer, which is influenced by the concentration and valence of the ions of opposite sign to the layer charge. Low electrolyte concentration produces slow coagulation, which is delayed by a long-range repulsion (Rand et al. 1980). At high electrolyte concentration, attraction dominates at any layer distance except at very close approach. In this case, layer agglomeration occurs at a maximum rate and the process is called rapid coagulation (Missana & Adell 2000). When a dispersion of plate-like clay mineral layers coagulates, three different modes of layer association may occur: face-to-face (FF), edge-to-face (EF) and edge-to-edge (EE) (Van Olphen 1977).

The EE and FF aggregations result from the overlapping of similar electrical double layers, while the EF aggregation results from the overlapping of dissimilar electrical double layers. EF association involves positive and negative surfaces, respectively, so there is no potential energy barrier to aggregation. This makes the EF coagulation rapid. The EE and FF kinds of aggregation, since they involve similar charges, are influenced by a potential energy barrier. Thus, EE and FF aggregation tend to be very slow unless there is sufficient electrolyte to reduce the energy barrier. For each type of association the van der Waals forces will vary, being highest for the FF type (Schramm 2006).

### **1.4 Effect of electrolytes and pH of the medium on layer interaction**

The ion concentration and pH of dispersion are decisive for electrostatic layer interaction and structure formation in clay mineral dispersions (Ramos-Tejada et al. 2001b; Mourad et al. 2008). The ionic strength of the dispersion determines the electrical double layer surrounding the layer, whereas the pH of surrounding medium determines the charge on the edges of clay mineral layers (Tombácz & Szekeres 2004). Since the charge of the edge is pH dependent, the orientation of

## Introduction

the layers to each other is strongly influenced by the pH of the dispersion. Edges are positively charged at  $\text{pH} < \text{pH}_{\text{PZC,edge}}$  slightly decreasing with increasing pH. The negative edge charges occur at  $\text{pH} > \text{pH}_{\text{PZC,edge}}$ . Even if the pH of clay mineral dispersions is lower than its  $\text{pH}_{\text{PZC,edge}}$ , in the absence of electrolyte or at very low ionic strength, the extended electrical double layer around the dispersed layers leads to the formation of an arrested glass structure (Bonn et al. 1998; Tanaka et al. 2004; Jabbari-Farouji et al. 2008b). Setting pH and adding an electrolyte leads to a contraction of the electrical double layer allowing for direct layer contacts and so-called attractive arrested states also termed gels are formed (Tanaka et al. 2004; Jabbari-Farouji et al. 2008b). These features are schematically sketched in Figure 8.

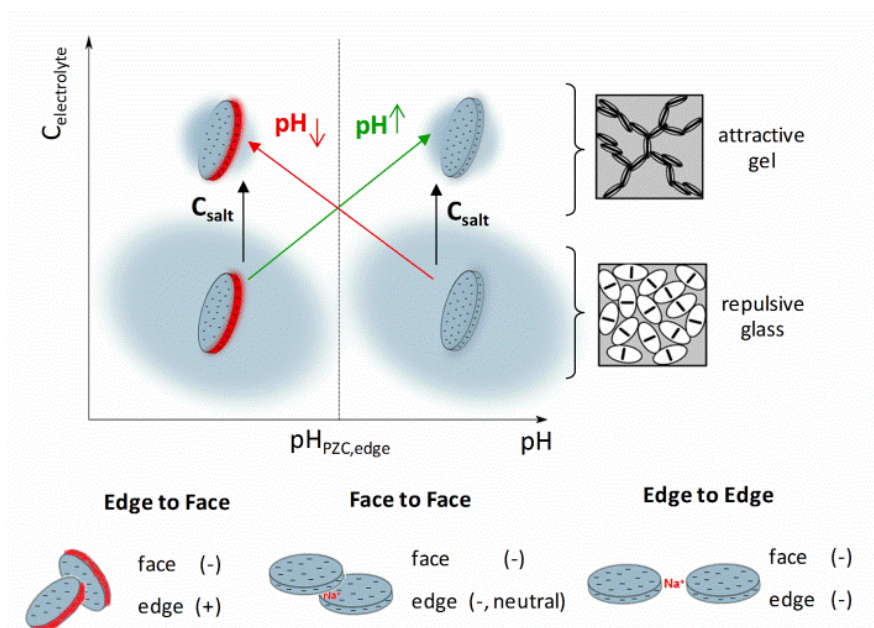


**Figure 8.** Effect of electrolyte concentration and pH on surface charge and range of electrical double layer in clay mineral dispersions. Negative charges are marked in blue, positive charges in red. The different path ways of changing surface charge and electrostatic interaction are marked by arrows. The illustrations for arrested states of clay mineral dispersion in square frames were taken from Tanaka et al. (2004).

At  $\text{pH} > \text{pH}_{\text{PZC,edge}}$ , FF (Tawari et al. 2001) and/or EE (Lagaly & Ziesmer 2003) layer contacts with  $\text{Na}^+$  in between are formed resulting in so-called partially

parallel overlapped (PPO) (Odriozola et al. 2004; Jönsson et al. 2008) gel structure. At high pH and high ion concentration, the possibility of FF layer orientation is higher than EE interaction (Lagaly & Ziesmer 2003). At  $\text{pH} < \text{pH}_{\text{PZC,edge}}$ , edges and faces are oppositely charged and EF layer contacts occur supposed to result in arrested gel states with so-called house of cards (HOC) structure (Van Olphen 1977; Dijkstra et al. 1995; Okamoto et al. 2001). Vali & Bachmann (1988) argued that an increase of solids content results in stacks of 2:1 layers with EF associations between FF stacks, also called honeycomb structure. Models for structure formation in clay mineral dispersions are often based on these assumptions about different types of layer contacts mentioned above. The existence of so-called PPO or HOC structures is widely accepted in the clay mineral science community (Van Olphen 1977; Durán et al. 2000; Abend & Lagaly 2000; Tawari et al. 2001; Ramos-Tejada et al. 2001b; Lagaly & Ziesmer 2003; Tombácz & Szekeres 2004). However, there is no direct experimental evidence for these layer contacts except for Monte Carlo simulations (Dijkstra et al. 1995) regarding gelation in clay mineral dispersions taking into account electrostatic interactions among the plate-like particles and from TEM images of clay/polymer nanocomposites (Okamoto et al. 2001). The physical motivation for these structural models is the experimental fact that the rim or edge charge changes from positive at  $\text{pH} < \text{pH}_{\text{PZC,edge}}$  to negative at higher pH. Quantitative determination of the edge charge for Laponite® layer (Giannakopoulos et al. 2006) as well as for Na-saturated montmorillonite layer (Tournassat et al. 2004a) and natural hectorite layer (Tournassat et al. 2004b) has been done using potentiometric and mass titration techniques. Tombacz and Szekeres (2004) implied that the formation of stacks of layers ordered in parallel to each other is hindered with decreasing pH, whereas EF heterocoagulated assembly of lamellae formed only at  $\text{pH} < \text{pH}_{\text{PZC,edge}}$ . They applied X-ray diffraction measurements on oriented montmorillonite clay films and showed that the intensity of basal plane reflection considerably decreases with decreasing pH. Similarly Lagaly (1989) claim that the card house structure (EF-structure) of kaolinite dispersion in acidic medium breaks down with increasing pH (see Figure 9).

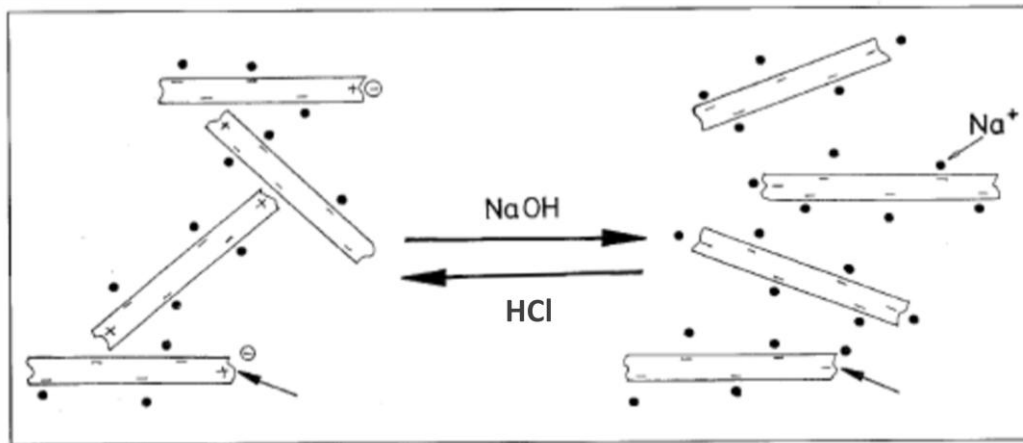


**Figure 9.** Illustration of change of kaolinite layer orientations subject to layer charges which are changing with adding NaOH or HCl into the medium (Lagaly 1989, modified).

The clay mineral layers in aqueous solution must overcome the barrier of particle interaction energy to come into contact with each other and agglomerate. The critical concentration of electrolyte at which agglomeration occurs is known as the critical flocculation/coagulation value (Luckham & Rossi 1999). Lagaly and Ziesmer (2003) reported that the critical coagulation concentration of NaCl in acidic medium at approximately pH 3.5 with E(+)/F(-) contacts is significantly lower than the critical NaCl concentration at pH > 6 with F(-)/F(-) coagulation for very dilute (0.025 wt%) montmorillonite dispersion. Tombacz and Szekeres (2004) revealed that at least 25 mM of NaCl concentration for 0.05 wt% Wyoming montmorillonite dispersion at pH 4 was needed to have EF coagulation, where the hidden electrical double layer of positively charged edge region has emerged. On the other side, the coagulation with FF aggregates requires higher salt concentration (around 90 mM) to compress the dominant electrical double layer on the highly negatively charged faces of layers at pH 8.5. They obtained the critical coagulation concentration of NaCl determining the size evolution of aggregates in dilute montmorillonite dispersion at constant pH and different NaCl concentrations using dynamic light scattering and the type of layer configuration was distinguished from X-ray diffraction measurements at different pH.

## 1.5 State of the art

Natural clay minerals are distinguished from synthetic clay mineral Laponite® by the highly anisometric and often irregular particle shape, the broad layer size distribution and the heterogeneity of layer charge. The majority of clay mineral studies have been done with Laponite® dispersions due to their relatively high monodispersity (Mourchid et al. 1998; Jabbari-Farouji et al. 2008b; Ruzicka & Zaccarelli 2011). Laponite® dispersions have been investigated as a model system for clay mineral dispersions (Fossum 1999) and disk like colloids (Dijkstra et al. 1995; Nicolai & Cocard 2001; Mori et al. 2001) in general.

Structure formation and aging in clay mineral dispersions strongly depend on solids and salt concentration as well as pH (Ruzicka et al. 2004; Ruzicka et al. 2006). The kinetics of the gel/glass formation in Laponite® dispersions at different solids content and electrolyte concentration has been studied by numerous authors covering time intervals from hours to years using light and X-ray scattering (Knaebel et al. 2000; Ruzicka et al. 2004; Mongondry et al. 2005; Jabbari-Farouji et al. 2007; Ruzicka et al. 2008; Jabbari-Farouji et al. 2012) as well as rheological methods (Willenbacher 1996; Bonn et al. 1998; Bonn et al. 2002; Labanda & Llorens 2008; Oppong et al. 2008; Jabbari-Farouji et al. 2008a; Shahin & Joshi 2010). Mourchid et al. (1998) discussed the isotropic to nematic phase transition of Laponite® dispersions. Only clay minerals subjected to the strongest electrostatic repulsions present a true isotropic to nematic phase transition in their phase diagrams. In contrast to the usual isotropic phase, the clay layers in the nematic phase tend to align parallel to each other. Since the isotropic/nematic transition is masked by gelation process for all octahedrally substituted clay mineral dispersions, only sol-gel phase transition is observed in most dispersions of octahedral smectites (Paineau et al. 2011a). In subsequent work of Ruzicka et al. (2010), they realized that restructuring at low Laponite® concentration still continues on the year timescales. But after three years they observed a separation process into clay-rich and clay-poor phases in very low clay mineral concentration ( $c_s < 1$  wt%). On the other side, even after 3 years, samples with solids concentration higher than 1 wt% exhibit a stable (transparent) arrested state (Figure 10).

$c_s = 0.1 \text{ wt\%}$  0.2 wt% 0.3 wt% 0.4 wt% 0.6 wt% 0.7 wt% 0.9 wt% 1.0 wt% 1.2 wt%

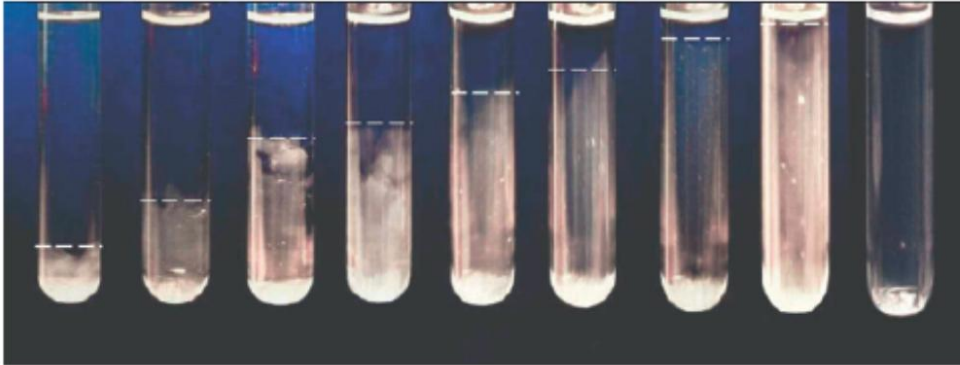


**Figure 10.** Photograph of samples in the concentration range  $0.1 \leq c_s \leq 1.2 \text{ wt\%}$  of Laponite® at very long waiting time (about 30000 h). The samples with  $< 1 \text{ wt\%}$  Laponite® aqueous dispersion show evidence of a phase separation, while the 1.2 wt% gel sample remains homogeneous at all times (Ruzicka et al. 2010, modified).

Willenbacher (1996) found a power law relationship between complex viscosity and time ( $|\eta^*| \sim t^{0.13 \pm 0.02}$ ) for gel like Laponite® dispersions (1 to 3 wt% Laponite® in 0.009 M NaCl dispersion) holding within the time regime up to  $10^6 \text{ s}$ . Due to the short-range attractive forces among Laponite® layers, gel structures form faster than glass structures built by long-range repulsive forces (Tanaka et al. 2004; Jabbari-Farouji et al. 2008a). The repulsive glass structure is also called Wigner glass (low-density glass) (Bonn et al. 1998). Tanaka et al. (2004) assumed that the glass structure of Laponite® dispersions has smaller characteristic length than gel structure and did not show any experimental evidence. Since elasticity inversely depends on the characteristic length cubic, they argued that glass structure of Laponite® dispersion is more rigid than gel structure. Their argument is not consistent with the results found in this study. Jabbari-Farouji et al. (2008a) expected that aged gel samples have a lower viscoelastic modulus than glass samples comparing the gel structure of 0.8 wt% Laponite® in 6 mM NaCl dispersion with the glass structure of 3.2 wt% Laponite® in pure water, without considering the effect of clay mineral concentration on the viscoelastic behavior. In this study, the gel and glass structures with same solids concentration are compared regarding their viscoelastic properties. Abend and Lagaly (2000) revealed that the mechanical strength of the attractive gel states is

higher than that of the repulsive glass states according to rheological measurements of montmorillonite dispersion. But it is clear that the strength of clay mineral dispersions increases with increasing solids content (Mourchid et al. 1995b; Paineau et al. 2011a) and ion concentration (Mourchid et al. 1995a; Nicolai & Cocard 2000). There is still no agreement about the origin of the resistance to mechanical load for arrested states with different layer orientation obtained at different pH and ionic strength for clay mineral dispersions.

As pointed out by Ruzicka and Zaccarelli (2011), a deficiency of some other early studies on Laponite® phase behavior is neglecting sample aging (Mourchid et al. 1995a; Mourchid et al. 1998) and may have led to inaccurate interpretation of arrested states of dispersions. Therefore, lots of different phase diagrams of Laponite® dispersions are available (Kroon et al. 1998; Mourchid et al. 1998; Tanaka et al. 2004; Ruzicka et al. 2006; Jabbari-Farouji et al. 2012). As seen in Figure 11, Ruzicka and Zaccarelli (2011) summarized the previous studies performed by different groups and provided a unifying phase diagram of Laponite® considering the main control parameters, e.g. clay mineral and salt concentration, and aging time. Because the clay mineral dispersions do not reach equilibrium state (Willenbacher 1996), we prefer the term state diagram instead of phase diagram in agreement with Ruzicka and Zaccarelli (2011).

Abend and Lagaly (2000), and Shalkevich et al. (2007) proposed a similar phase diagram with nose shape, like in Figure 11, for natural Na-saturated montmorillonite presenting a repulsive glass at low ionic strength ( $< 10^{-3}$  M) and high volume fraction, whereas at higher ionic strength only attractive interactions were involved whatever the clay mineral concentration. The similar nose shape in the phase diagram of clay minerals has recently been experimentally observed for Laponite® (Levitz et al. 2000) and theoretically predicted for charged colloidal disks (Trizac et al. 2002).

The state diagrams of natural clay minerals, like nontronite (Michot et al. 2006) and montmorillonite (Abend & Lagaly 2000; Michot et al. 2004; Shalkevich et al. 2007) have been investigated with considering solids and electrolyte concentration but not all of them considered the sample aging (Abend & Lagaly 2000; Michot et al. 2004) and pH of dispersion (Michot et al. 2004; Michot et al.

## Introduction

2006; Shalkevich et al. 2007). The positional and orientational orders of the natural clay mineral layers in aqueous solution at different pH and electrolyte concentration have been examined by using small-angle X-ray scattering (SAXS) measurements (Norrish 1954; Tombácz & Szekeres 2004; Michot et al. 2006; Shalkevich et al. 2007; Paineau et al. 2011a) and rheological measurements (Rand et al. 1980; Khandal & Tadros 1988; Sohm & Tadros 1989; Tombácz & Szekeres 2004; Shalkevich et al. 2007). By applying X-ray diffraction measurements on oriented montmorillonite clay films, Tombacz and Szekeres (2004) proved that the formation of stacks of layers ordered in parallel to each other and EF coagulated layers at high and low pH, respectively. Other former studies had supported the EF layer contacts in Na-saturated montmorillonite dispersions (Khandal & Tadros 1988; Brandenburg & Lagaly 1988; Lagaly 1989; Sohm & Tadros 1989; Lagaly & Ziesmer 2003). Hence, a clear picture about layer interaction at different pH and electrolyte concentration, and its influence on the kinetics of phase transition of clay mineral dispersion is still lacking.

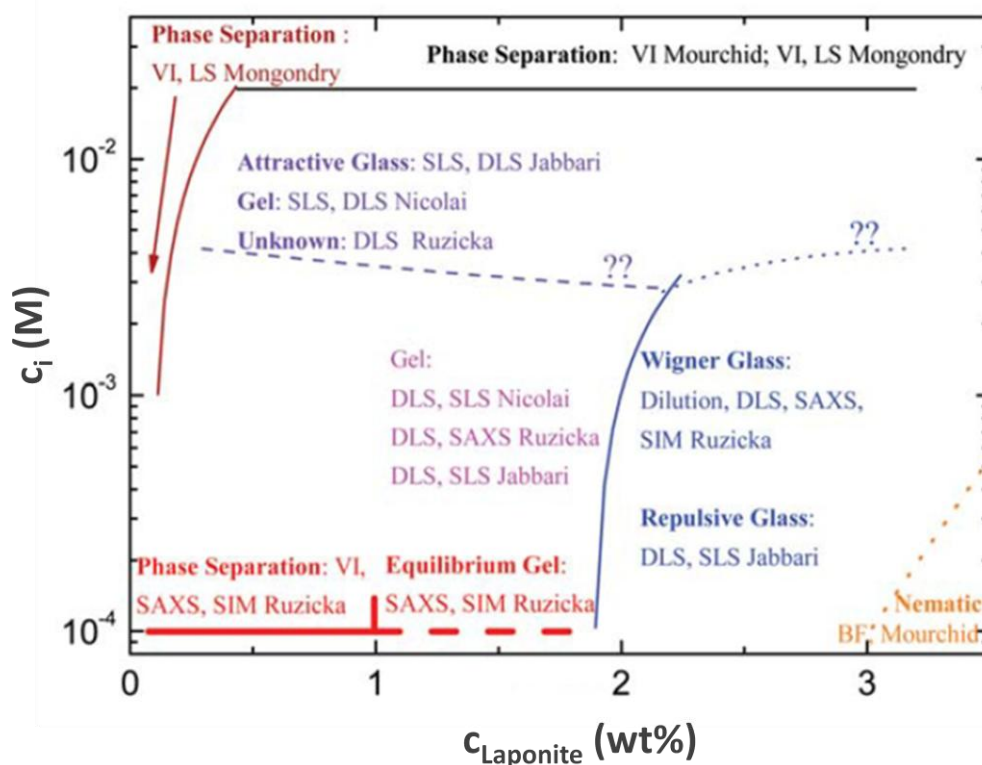


**Figure 11.** Proposed non-equilibrium phase/state diagram for aqueous Laponite® dispersions. Various nonergodic states are possible at long aging time, depending on the ion concentration and the Laponite® concentration here given in weight % (Ruzicka & Zaccarelli 2011, modified).

Michot et al. (2004) showed that the average layer size of Na-saturated montmorillonite ( $410 \pm 130$  nm,  $295 \pm 100$  nm and  $75 \pm 50$  nm) has the main effect and polydispersity of layer size distribution has almost no effect on the osmotic pressure and linear viscoelastic behavior of dispersions. However, the investigated size and polydispersity range ( $295 \pm 100$  nm and  $250 \pm 180$  nm) was fairly small. Furthermore, they did not find a significant dependency of storage modulus ( $G'$ ) on electrolyte concentration, which might be related to neglecting of sample aging. However, they observed the solids content corresponding to the sol/gel or sol/glass transition of Na-saturated montmorillonite dispersions increases linearly with increasing average layer size and Paineau et al. (2011b) explained this feature based on the statistical hydrodynamic layer trapping. When the interaction energy between hydrodynamic volume of dispersed clay mineral layers in aqueous dispersion is stronger than Brownian energy of dispersed layer, layers might hydrodynamically trap each other. The interplay between layer charge, anisotropy of layers and ionic strength and their effects on rheological behavior of clay mineral dispersion are still far from being understood.

Not too much work has been published on the theoretical prediction (using DLVO theory (Secor & Radke 1985; Missana & Adell 2000; Arroyo et al. 2000)) of the pH-dependent stability of natural clay mineral dispersions. At low pH, clay minerals may react with hydrogen ions which dissolves the mineral structure and releases  $Mg^{2+}$  ions. The rate of this reaction decreases with increasing pH and is negligible for montmorillonite dispersion at  $pH \geq 4$  (Delavernhe et al. 2015) for Laponite® dispersions at  $pH \geq 8$  (Mongondry et al. 2005), and as well as for natural hectorite at  $pH \geq 8$  (Delavernhe et al. (accepted) 2017). Benna et al. (1999) analyzed pH influence on rheological properties of three different natural montmorillonite dispersions without considering the electrolyte effect on  $pH_{PZC,edge}$ . The required concentration of NaCl for layer coagulations of natural clay minerals at  $pH < pH_{PZC,edge}$  is lower than the critical NaCl concentration at  $pH > pH_{PZC,edge}$  (Lagaly & Ziesmer 2003; Tombácz & Szekeres 2004). On the other hand, Au et al. (2015) reported pH effect on the rheological properties of Laponite® dispersions in gel state without considering the time influence on the strength of clay mineral dispersion. Since at lower ion concentration the

sufficiently large electrical double layer slips over the pH dependent edge charges and hinders the layer interaction, the effect of pH and electrolytes on colloidal behavior of clay mineral dispersions should be considered together (Tombácz & Szekeres 2004; Delhorme et al. 2010; Pilavtepe et al. (submitted) 2017).

The rheology of natural clay mineral dispersions has been investigated for several decades by varying dispersion concentration, the quality and quantity of added salts (Abend & Lagaly 2000; Lagaly & Ziesmer 2003), polymers and thinning agents (Ramos-Tejada et al. 2001a; Alemdar et al. 2005; Laribi et al. 2005; Kleshchanok et al. 2012), as well as pH of dispersion (Brandenburg & Lagaly 1988; Lagaly 1989; Yildiz et al. 1999; Benna et al. 1999; Arroyo et al. 2000; Ramos-Tejada et al. 2001b; Janek & Lagaly 2001; Tombácz & Szekeres 2004). Laribi et al. (2005) compared the rheological behavior of pure and interstratified smectite for the purpose of preventing the sedimentation in drilling fluids with enhancing its yield stress and they found qualitatively similar flow behavior. Paineau et al. (2011b) found that tetrahedrally substituted clay minerals are more repulsive than octahedrally substituted ones, using dynamic and steady-state rheological measurements. Galambos et al. (2012) compared the adsorption properties of radionuclides on di- and trioctahedral smectites based on different mineralogical structures. But there is no significant study about rheological differences between natural and synthetic di- and trioctahedral smectites.

So far, the linear viscoelastic properties of natural clay mineral dispersions were analyzed only in the frequency range up to 100 rad/s with bulk rheological measurements (Mourad et al. 2008; Paineau et al. 2011b; Ali & Bandyopadhyay 2016). Jabbari-Farouji et al. (2008a) used optical tweezer microrheology to determine the linear viscoelastic response of Laponite® dispersions at their inherent pH at high frequencies up to  $6 \times 10^5$  rad/s. They found strongly frequency-dependent viscoelastic shear modulus at high frequencies  $G \sim \omega^{0.7}$ . Similar exponents of  $\frac{3}{4}$  have been reported for solutions of semi-flexible polymers, protein filaments or worm-like surfactant micelles in the high frequency regime

where internal relaxation modes of the individual stiff building blocks are prevailing (Willenbacher et al. 2007).

Since Laponite® dispersions with low concentration and without added salt need more time to reach an arrested state and cluster size changes during this time (Ruzicka et al. 2004), such dispersions are called inhomogeneous gels on a macroscopic length scale. At higher clay mineral concentration the arrested state forms faster and there is no evidence for structural heterogeneity from DLS or SAXS measurements and accordingly such states are called homogeneous gel or attractive glass (Jabbari-Farouji et al. 2007; Ruzicka et al. 2008). On the other side, microrheological studies using particle tracking methods revealed that heterogeneous gel like structures occur in Laponite® dispersions at low concentration and high ionic strength (Oppong et al. 2008; Rich et al. 2011b) and homogeneous repulsive glass structures were observed in the absence of electrolyte (Jabbari-Farouji et al. 2008a). Oppong et al. (2008) observed an increase of heterogeneity during structure formation until the characteristic crossover time at which  $G' = G''$  was reached and no further change beyond that time. But their results may be obscured by aging effects as they added the tracer particles (1  $\mu\text{m}$  diameter) one month after sample preparation assuming that complete rejuvenation is possible by vigorous sonication. Rich et al. (2011b) observed a gradual shift of sol-gel transition in their particle tracking experiments depending on the size of the used tracer particles (from 0.9 to 0.2  $\mu\text{m}$  diameters) and also found an increase in heterogeneity up to the crossover time but did not continue to monitor this at longer times. Jabbari-Farouji et al. (2008a) claim that Laponite® dispersions in glass state are homogeneous based on microrheological experiments using probe particles with 1.16  $\mu\text{m}$  diameter, but observed heterogeneity in the weak gel they investigated using 0.5  $\mu\text{m}$  probe particles. However, this optical tweezer based study suffers from poor statistical significance, since the viscoelastic response of the gel sample was only probed at 5-8 different positions. The structural heterogeneity of natural hectorite dispersion was investigated using the optical MPT technique with tracer particles in 1.16  $\mu\text{m}$  diameter (Houghton et al. 2008). This provides local information of the viscoelastic properties of the surrounding medium on a micrometer length scale

of 1  $\mu\text{m}$ . There is no other microrheological study of natural clay minerals to reveal their structural refinement depending on length scale.

### 1.6 Scope of this study

A wide-ranging rheological comparison of natural tri- and dioctahedral smectites, hectorite and montmorillonite, respectively, with synthetic trioctahedral smectite Laponite® will be presented in this study. For an accurate characterization, we used purified natural smectites to avoid the effect of soluble impurities (carbonate, iron (hydr)oxides and organic matter) in the samples on rheological behavior. The solids content was varied between 1 and 7 wt% depending on clay mineral, while NaCl content was increased up to  $10^{-1}$  M.

The kinetics of structure formation and aging for different types of repulsive or attractive arrested states subject to clay mineral type, aspect ratio and pH depending layer orientation was characterized using the classical oscillatory shear rheometry and MPT optical microrheology. A distinction between repulsive glasses and attractive gels from bulk rheological measurements alone is not trivial and sometimes maybe not possible (Bonn et al. 1999). Therefore, the bulk rheology has been combined with microrheology to shed new light on the long-standing controversy about rheological behavior of arrested states of clay mineral dispersion on the macro- and micro-length scales.

Their state diagrams were determined at their inherent pH considering clay mineral and NaCl concentration as well as sample aging. The chemical stability of synthetic and natural clay mineral dispersions was analyzed in a wide range of pH 4 to 12 with the help of CEC method.

The effect of the main control parameters, i.e. clay mineral content and salt concentration, as well as pH and aspect ratio on microscopic heterogeneity and structural refinement on submicrometer length scale for different attractive and repulsive arrested states of synthetic and natural clay mineral dispersions will be discussed based on MPT experiments.

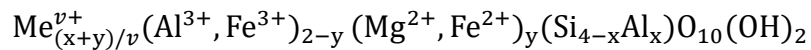
Complementary to the classical oscillatory shear rheometry and MPT microrheology covering the frequency range  $\omega < 100$  rad/s, the high frequency squeeze flow mechanical rheometry as well as DWS optical microrheology have been performed to determine linear viscoelastic properties of clay mineral dispersions in the frequency range up to  $10^6$  rad/s. Clay mineral dispersions with a broad range of clay mineral and electrolyte content at lower and higher pH than corresponding  $\text{pH}_{\text{PZC,edge}}$  have been investigated to figure out the effect of layer interactions and layer dimension on linear viscoelastic response of clay mineral dispersions.

The variety of methods applied in this study and the broad range of physico-chemical parameters investigated provide a comprehensive scientific view on differences between arrested states with different layer orientations and rheological differences between synthetic and natural clay mineral dispersions with different layer size and layer charge.

## 2 Materials

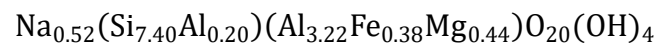
### 2.1 Montmorillonite

The most common dioctahedral smectites belong to the montmorillonite–beidellite series with a general formula;



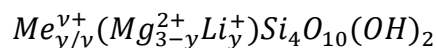
Here,  $\xi = (x + y)$  is the layer charge resulting from the substitutions within the tetrahedral and octahedral sheets ranging from 0.2 to 0.6 eq/FU and  $Me^{v+}$  denotes the interlayer monovalent or divalent cations. Montmorillonites and beidellites are defined by a main layer charge located in the octahedral sheets ( $x \ll y$ ) and in the tetrahedral sheets ( $x \gg y$ ), respectively (Emmerich et al. 2009; Wolters et al. 2009).

The montmorillonite used in this study was separated from the bentonite Volclay (supplied by Süd-Chemie AG, Germany). Chemical composition of Na-exchanged montmorillonite (BV-M0.2Na) was determined from X-ray fluorescence analysis (XRF) (Schnetzler et al. 2016);



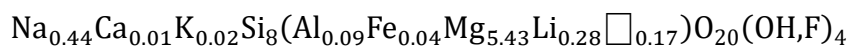
### 2.2 Natural hectorite

The hectorite is a swellable trioctahedral 2:1 layer silicate of the smectite group with the general formula;



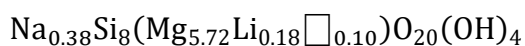
where  $Me^{v+}$  is a mono- or divalent cation in the interlayer and  $\xi = y$  is the layer charge created by substitution in the octahedral sheet ( $Li^+$  for  $Mg^{2+}$ ) (Brigatti et al. 2006).

The natural hectorite, which is one of the main components of SHCa-1, was supplied by the Clay Mineral Society for this study. The chemical formula for natural hectorite (SHCa-0.2Na) is deduced from chemical analyses;



### 2.3 Synthetic hectorite – Laponite® RD

The synthetic hectorite, Laponite® RD (registered trademark of BYK Additives) was donated by BYK Additives & Instruments, Germany. Its general formula is;



The quadrat symbol  $\square$  in the structural formula of natural and synthetic hectorites indicates the vacancies in clay mineral structure.

### 2.4 Physicochemical properties of materials

Chemical pre-treatments were applied only on natural clay minerals to reduce the cementing interactions of carbonates, iron (hydr)oxides and organic materials in natural clay minerals according to the procedure detailed in Wolters et al. (2009) and Delavernhe et al. (2015). The < 0.2  $\mu\text{m}$  fraction of the natural clay minerals was separated by centrifugal sedimentation (Delavernhe et al., 2015). The major elements in natural clay minerals were quantified chemically by XRF (Philips MagiX PRO spectrometer).

Laponite® layers are nearly monodisperse with a diameter of 30 nm (Avery & Ramsay, 1986). The disk geometry and size of Laponite® layers were verified by SAXS measurements (Mourchid et al. 1995a; Kroon et al. 1998). SHCa-0.2Na and BV-M0.2Na have broader layer size distribution with a mean weighted equivalent diameter of 100 nm (Bosbach et al., 2000) and 270 nm (Delavernhe et al., 2015), respectively. Specific surface area  $a_s$  [ $\text{m}^2 \text{g}^{-1}$ ] was measured by argon gas adsorption (Autosorb-1-MP, Quantachrome Instrument) (Table 1).

## Materials

The layer charge  $\xi$  was determined with the alkylammonium method and varied between  $0.19 \pm 0.01$ ,  $0.24 \pm 0.01$  and  $0.26 \pm 0.01$  eq/FU for Laponite®, SHCa-0.2Na and BV-M0.2Na, respectively (Table 1). Cation exchange capacity (CEC) of clay minerals was measured using the Cu-trien method according to Meier & Kahr (1999) over a pH range of 4-10 for BV-M0.2Na (Delavernhe et al. 2015) and 6-13 for SHCa-0.2Na and Laponite® (Delavernhe et al. (accepted) 2017). The pH dependency of the CEC is shown in Figure 12.

The CEC were measured  $78 \pm 1$  cmol(+) kg<sup>-1</sup> at pH = 8.9 for Laponite® RD,  $81 \pm 1$  cmol(+) kg<sup>-1</sup> at pH = 7.9 for SHCa-0.2Na and  $92 \pm 2$  at pH = 7.1 for BV-M0.2Na without any addition of acid or base. It should be noticed that the addition of the Cu-trien solution to the dispersions induced a decrease of pH compared to the natural pH of the materials, which were  $10 \pm 0.2$ ,  $8.8 \pm 0.4$  and  $9.7 \pm 0.3$  for Laponite®, SHCa-0.2Na and BV-M0.2Na, respectively.

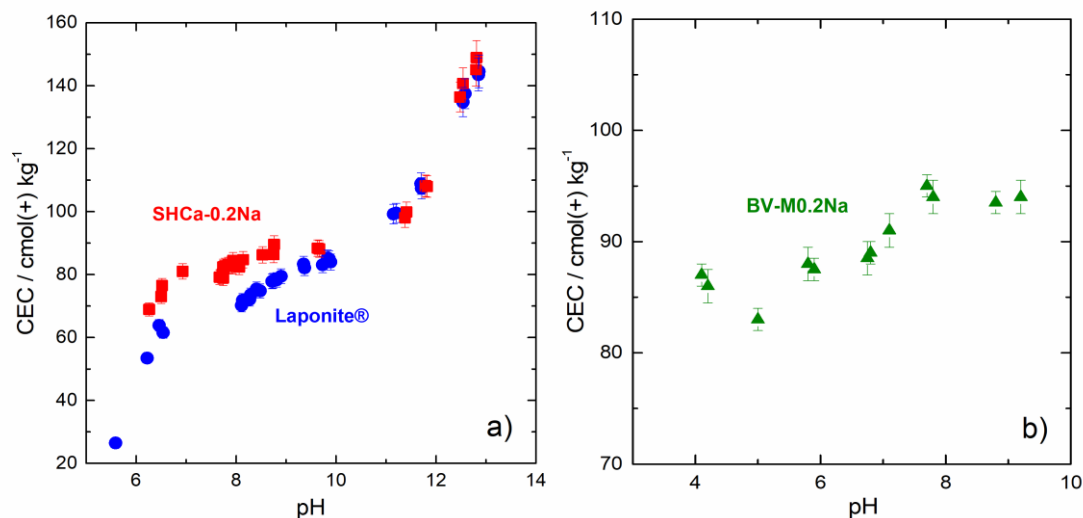


**Figure 12.** CEC values as a function of pH **a)** for natural and synthetic hectorite, SHCa-0.2Na and Laponite®, respectively. Data are submitted in Delavernhe et al. (2017, accepted) **b)** for Na-saturated montmorillonite BV-M0.2Na. Data are taken from Delavernhe et al. (2015).

The CEC originates from the layer charge. However, about 10-20% of CEC are due to variable charges depending on the pH and ionic strength of dispersion. The CEC trend can be divided in two parts for hectorites: the first one at pH < 10

with a slower CEC increase for SHCa-0.2Na than for Laponite® and the second part at pH >10 with a strong CEC increase similar for SHCa-0.2Na and Laponite® RD (see Figure 12a). The larger CEC increase observed for Laponite® RD at pH <10 could be related to the higher edge surface area than SHCa-0.2Na. The specific edge surface area  $a_{s,edge}$  [ $m^2 g^{-1}$ ] was calculated to be  $75.5 m^2 g^{-1}$  resulting in a mean  $a_{s,edge}$  of 9.8% of the total  $a_s$  for Laponite® layers and to be  $15.7 m^2 g^{-1}$  equivalent to about 2% of the total  $a_s$  for SHCa-0.2Na layers.

A strong increase in CEC was observed at pH > 10 for Laponite® and SHCa-0.2Na dispersions, and a less pronounced increase in CEC was observed at around pH 6.5 for BV-M0.2Na (see Figure 12) that indicated deprotonation of (Mg-OH-Mg) edge surface sites (Tournassat et al. 2004b) and a strong increase of negative charges at the edges. The clay mineral specific  $pH_{PZC,edge}$  could be suggested from this significant change in the slope of pH dependent CEC relating to increase of pH dependent edge charges. The  $pH_{PZC,edge}$  was suggested around 11 for Laponite® and SHCa-0.2Na, and around 6.5 for BV-M0.2Na in good agreement with early findings (Tawari et al. 2001; Tombácz & Szekeres 2004; Rozalén et al. 2009; Delhorme et al. 2010; Delavernhe et al. 2015).

CEC strongly decreases at pH < 8 for Laponite® and at pH < 7.5 for SHCa-0.2Na. BV-M0.2Na sample does not show any dramatic change in CEC over pH range 4-10. It means the BV-M0.2Na samples remain stable in this pH range. At lower pH, clay minerals may react with hydrogen ions and autotransformation dissolves the mineral structure and releases  $Mg^{2+}$  and  $Al^{3+}$  from octahedral sheets (Janek & Lagaly, 2001). The rate of this reaction decreases with increasing pH. The strong decrease in CEC at low pH should be regarded with caution due to side reactions resulting from dissolution of mineral structure.

The chemical stability was predicted from soluble cation analysis in solution during pH dependent CEC measurement and analyzed by inductively coupled plasma optical emission spectrometry (ICP-OES) (Optima 8300 DV, Perkin Elmer). The evolution of the structural cations,  $Mg^{2+}$  and  $Li^+$  for the octahedral

## Materials

sheet and  $\text{Si}^{4+}$  for the tetrahedral sheets, in the supernatants over the pH revealed the dissolution behavior of the trioctahedral smectites. The soluble structural cations of Laponite® and SHCa-0.2Na after 72 h equilibrium in dispersion (24 h without Cu-trien solution + 48 h after addition of Cu-trien solution) were presented in Figure 13a and 13b, respectively, and compared with their total amount in structure (dashed lines in Figure 13). A minimum of dissolution based on the  $\text{Si}^{4+}$  release was observed at pH around 10 for both hectorites. The soluble  $\text{Mg}^{2+}$  at pH 10 for Laponite® is around  $3 \times 10^{-5}$  M (Figure 13a) and close to the concentration measured by Mohanty and Joshi (2016) for Laponite® dispersion at pH 10 after 5 days less than  $3 \times 10^{-3}$  M of background electrolyte. At pH > 10 dissolution of mineral structure results in the release of  $\text{Si}^{4+}$  for both hectorites, whereas the  $\text{Mg}^{2+}$  and  $\text{Li}^+$  concentrations were almost constant.

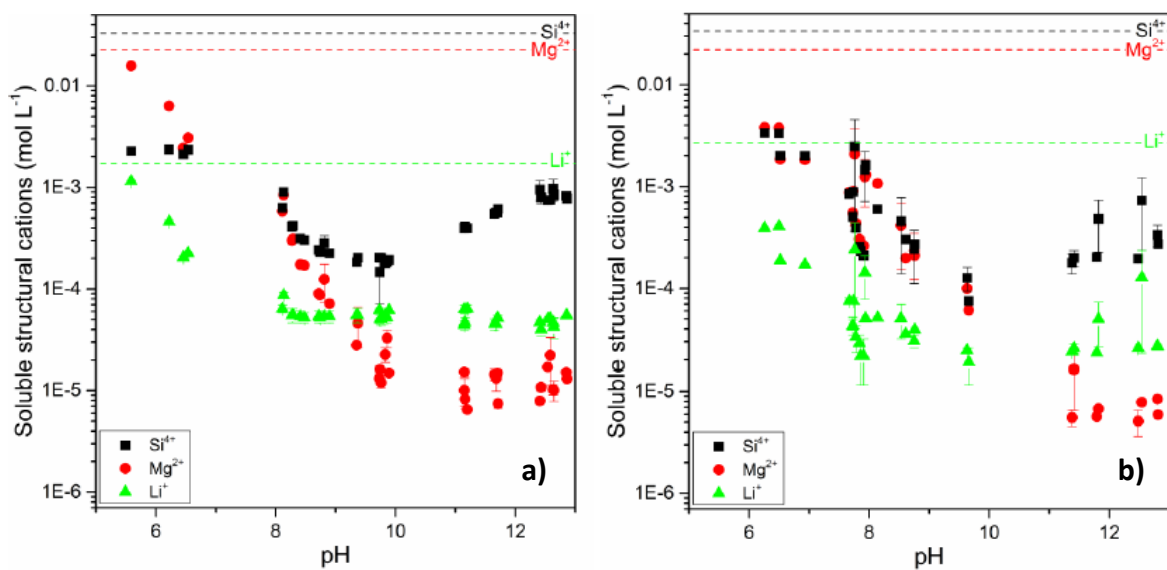


**Figure 13.** Soluble structural cations of **a)** Laponite® and **b)** SHCa-0.2Na after 72 h equilibrium in dispersion (24 h without Cu-trien + 48 h after addition of Cu-trien solution). Dashed lines determined from the XRF analysis. Data are submitted in Delavernhe et al. (2017, accepted).

The soluble structural cations for both hectorites shown in Figure 13 increase with decreasing pH. For BV-M0.2Na samples, they remain constant in the pH range of 4 to 10 (Tournassat et al. 2004a; Delavernhe et al. 2015). At pH < 8 for

Laponite® and at pH < 7.5 for SHCa-0.2Na samples the structure dissolution exceeded 5% of released structural cations. This results in a sharp increase in the amount of soluble cations and in a strong decrease in CEC at low pH, see Figure 12.

The exchangeable cations in clay mineral structure were subsequently analyzed by ICP-OES and 84 to 92 % of homoionic saturation by Na<sup>+</sup> was obtained (see Table 1).

The specific density ( $\rho_s = M/V_{uc}/N_A$  with  $N_A$  Avogadro constant) of montmorillonite and hectorite is quite similar at about 2.7 to 2.75 g/cm<sup>3</sup> because of the lower molecular weight  $M$  [kg/mol] of montmorillonite and larger unit cell volume  $V_{uc}$  [cm<sup>3</sup>] of trioctahedral smectites (Meunier, 2005).

**Table 1.** Physicochemical properties of synthetic and natural smectites.

			D	$a_s$	$\xi$	CEC	Na	pH <sub>inh</sub>	pH <sub>pzc,edge</sub>
			nm	m <sup>2</sup> /g	eq/FU	cmol(+)/kg	%	-	-
Laponite® RD synthetic hectorite	trioct.	synt.	30	320	0.19 (±0.01)	78 (±1)	90 (±3)	10 (±0.2)	≈ 11
SHCa-0.2Na natural hectorite		natural	100	129	0.24 (±0.01)	81 (±1)	84 (±3)	8.8 (±0.4)	≈ 10
BV-M0.2Na montmorillonite	dioct.	natural	270	60	0.26 (±0.01)	92 (±2)	98 (±1)	9.7 (±0.3)	≈ 6.5

## 2.5 Sample preparation

The effect of solids and ion concentration on the rheological behavior of clay mineral dispersions was studied in the range of 1 wt% to 7 wt% and 0 to 10<sup>-1</sup> M NaCl. The clay mineral powder was dispersed in NaCl aqueous solution under agitation for 30 min at room temperature. The solids and NaCl concentrations for corresponding clay mineral samples are listed in Table 2. The samples were homogenized by means of an ultrasonic bath for 20 min. Subsequently, a further

## Materials

treatment of the samples was carried out by means of an ultrasonic homogenizer (Digital Sonifier, Branson, USA) for 20 s at amplitude of 10% to ensure a homogeneous distribution of the clay mineral platelets and a complete delamination. After this homogenization process the time was noticed as initial point in time for sample aging, while samples are in the liquid or so-called sol state. The temperature of dispersion was checked at 5 min intervals during sample preparation to avoid any high increase in sample temperature, as this can influence the aging behavior of the clay mineral dispersions (Awasthi & Joshi 2009).

**Table 2.** Clay mineral and NaCl concentrations in samples used for this study.

$c_{NaCl} \backslash c_s$	1 wt%	2 wt%	3 wt%	4 wt%	5 wt%	6 wt%	7 wt%
$10^{-1}$ M			BV-M0.2Na		SHCa-0.2Na BV-M0.2Na		BV-M0.2Na
$10^{-2}$ M	Laponite®	Laponite®	Laponite® SHCa-0.2Na	SHCa-0.2Na	SHCa-0.2Na BV-M0.2Na	BV-M0.2Na	BV-M0.2Na
$10^{-3}$ M		Laponite®	Laponite®		SHCa-0.2Na BV-M0.2Na		SHCa-0.2Na
$10^{-4}$ M		Laponite®	Laponite®	SHCa-0.2Na	SHCa-0.2Na BV-M0.2Na	BV-M0.2Na	SHCa-0.2Na
0 M		Laponite®	Laponite®				

We measured the inherent  $pH=pH_{inh}$  of Laponite®, SHCa-0.2Na and BV-M0.2Na dispersions to be  $10 \pm 0.2$ ,  $8.8 \pm 0.4$  and  $9.7 \pm 0.3$ , respectively, similar to Delavernhe et al. (2017, accepted). The pH was set to higher and lower pH than corresponding  $pH_{PZC,edge}$  by adding 1 M NaOH or HCl to the dispersions at their  $pH_{inh}$ . In order to guarantee chemical stability of dispersions the minimum pH was set to  $pH=8.5$  for hectorite dispersions according to Figure 12 and 13 and to  $pH=4.5$  for montmorillonite dispersions according to Figure 12 and Delavernhe et al. (2015 and 2017, accepted). We checked pH of all samples for a period of three months and obtained no significant change in pH. Supportively, Mongondry et al. (2005) found that for Laponite® samples the pH remained above 8.5 for a period of at least two months, but it descended for some samples to pH 8 after a year.

## 3 Methods

### 3.1 Overview

The classic definition of rheology is the study of the deformation and flow of matter. Typically, rheology is distinguished from the broader fields of fluid mechanics and solid mechanics by its focus on ‘complex fluids’ and ‘soft solids’ (Morrison 2001). Rheological properties are closely connected with everyday experiences, e.g. spreading mayonnaise on a piece of bread; squeezing toothpaste onto a toothbrush; brushing, rolling, or spraying paint on a wall; applying cosmetic products; or stepping around muddy soil (Larson 1999).

In some colloidal dispersion, e.g. clay mineral dispersions, toothpaste, greases, lipstick and natural rubber polymers, the shear rate (flow) remains at zero until a threshold shear stress is reached, termed the yield stress ( $\sigma_y$ ), and then Newtonian or pseudoplastic flow begins. A common cause of such behavior is the existence of an interparticle or intermolecular network which initially acts like a solid and offers resistance to any positional changes of the volume elements. In this case flow only occurs when the applied stress exceeds the strength of the network.

Two of the most common empirical models used to describe the behavior of pseudoplastic fluids with yield stresses are the Bingham plastic and Herschel-Bulkley model (Schramm 2006). Clay mineral dispersions typically behave as Bingham plastic fluid (Ghezzehei & Or 2001):

$$\sigma = \sigma_y + \eta_p \dot{\gamma} \quad (3.1)$$

where  $\sigma$  [Pa] is the shear stress,  $\sigma_y$  [Pa] is the yield stress,  $\eta_p$  [Pas] is the Bingham plastic viscosity and  $\dot{\gamma}$  [s<sup>-1</sup>] is shear rate. Other types of time-independent flow behavior are shown in Figure 14a.

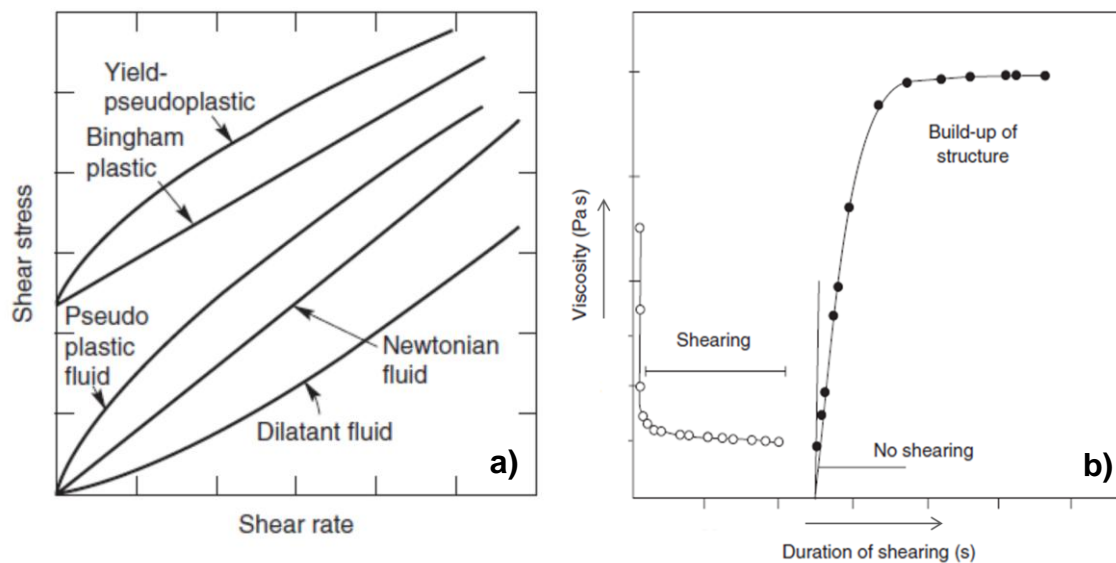


**Figure 14. a)** Types of time-independent flow behavior (Chhabra & Richardson 2008) **b)** Breakdown and re-formation of structure in a thixotropic dispersion (Chhabra & Richardson 2008).

Another important flow behavior of clay mineral dispersions is thixotropy (Willenbacher 1996; Barnes 1997). Thixotropy refers to time dependent flow. Thixotropic structures progressively break down on shearing and slowly rebuild at rest, see Figure 14b. The time-scales involved can range from many minutes in the case of breakdown to many hours in rebuilding (Barnes 1997). Other examples of materials exhibiting thixotropic behaviour include concentrated dispersions, emulsions, drilling fluids, waxy crude oils and protein solutions (Chhabra & Richardson 2008).

Additionally, viscoelastic properties of clay mineral dispersions make them attractive for industrial application. The rheological behavior of materials can be regarded as being between two extremes: Newtonian viscous fluids, typically low-molecular liquids, and Hookean elastic solids, like for example rubber. However, many real materials exhibit mechanical behavior with both viscous and elastic characteristics. Such materials are termed viscoelastic. Before considering the more complex viscoelastic behavior, here first the flow properties of ideally viscous and ideally elastic materials are elucidated.

The ideal elastic behavior of solids can be described by Hooke's law of elasticity:

$$\sigma = G\gamma \quad (3.2)$$

where  $\gamma$  [%] is deformation (also termed strain) and  $G$  [Pa] is the shear modulus which reveals information about the rigidity of a material. The shear modulus of an ideal elastic solid is independent of the shear stress and duration of the shear load. As soon as the deformation is reached, no further motion occurs. In contrast, viscoelastic materials deform at constant stress partially instantaneously, partially continuously over time. Thus, the time dependent stress relaxation is used to characterize the viscoelasticity of materials. When the stress relaxation is proportional to the strain we are talking about the so called linear viscoelastic regime. Above a critical strain the interparticle network of the sample breakup and the shear modulus becomes strain dependent. This is the so called nonlinear viscoelastic regime.

The most common way to quantify the viscoelastic character of a fluid is by measuring the response of a fluid sample to oscillatory shear at very small strain amplitudes.

When oscillatory shear strain is applied to a viscoelastic material it will be deformed sinusoidally by a deformation  $\gamma(t)$  with amplitude  $\gamma_0$  [%] and angular frequency  $\omega$  [rad s<sup>-1</sup>]:

$$\gamma(t) = \gamma_0 \sin \omega t \quad (3.3)$$

where  $t$  [s] is the time. Hence the shear rate can be expressed as the time derivative of the shear strain as follows:

$$\dot{\gamma}(t) = \frac{d\gamma(t)}{dt} = \gamma_0 \omega \cos(\omega t) \quad (3.4)$$

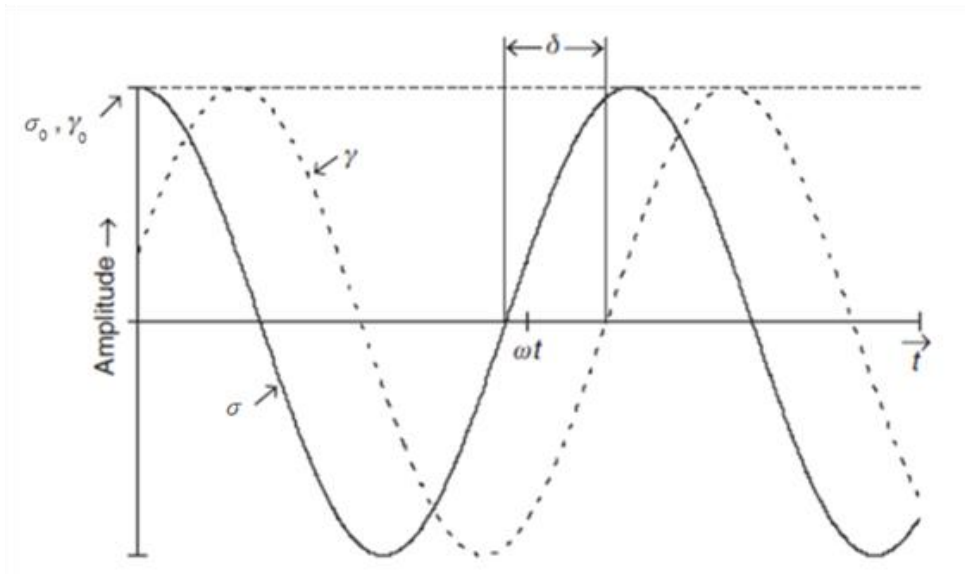


**Figure 15.** Oscillatory shear strain ( - - - ) out of phase with stress ( - ) by a phase angle  $\delta$ .

The oscillating system responds with sinusoidal course of shear stress  $\sigma(t)$  with amplitude  $\sigma_0$  [Pa] and angular frequency  $\omega$  [rad s<sup>-1</sup>], but phase shifted by an angle  $\delta$  [°] compared to the presented sine curve (Figure 15):

$$\sigma(t) = \sigma_0 \sin(\omega t + \delta) \quad (3.5)$$

Depending on material behavior, the phase shift angle  $\delta$  occurs between 0° and 90°. For ideal elastic materials the phase shift disappears, i.e.  $\delta = 0^\circ$  while for ideal viscous liquids  $\delta = 90^\circ$ . With respect to the analysis of oscillatory shear experiments the shear modulus is written in complex form:

$$G^*(\omega) = \frac{\sigma(t)}{\gamma(t)} \quad (3.6)$$

The complex shear modulus  $G^*$  [Pa] consists of two components: the storage modulus  $G'$  [Pa] and loss modulus  $G''$  [Pa]:

$$G^*(\omega) = G'(\omega) + iG''(\omega) \quad (3.7)$$

The  $G'$  value is a measure of the energy stored by the material during the cycle of deformation and represents the elastic behavior of the material, while  $G''$  is

measure of the energy dissipated or lost as heat during the shear process and represents the viscous behavior of a test material (Willenbacher & Georgieva 2013). The shear moduli  $G'$  and  $G''$  can be expressed as sine and cosine function of the phase shift angle  $\delta$  as follows:

$$G'(\omega) = \frac{\sigma_0}{\gamma_0} \cos \delta \quad (3.8)$$

$$G''(\omega) = \frac{\sigma_0}{\gamma_0} \sin \delta \quad (3.9)$$

Hence the tangent of the phase shift  $\delta$  can be defined as the ratio of loss and storage modulus:

$$\tan \delta = \frac{G''(\omega)}{G'(\omega)} \quad (3.10)$$

$\tan \delta$  is called the loss tangent or the loss factor, which is high for materials that are liquid-like, but approaches zero for materials that are solid-like (Larson 1999).

In order to characterize the rheological properties of clay mineral dispersions expressed above the cone-plate geometry and Searle system (in Figure 16) were used in this study.

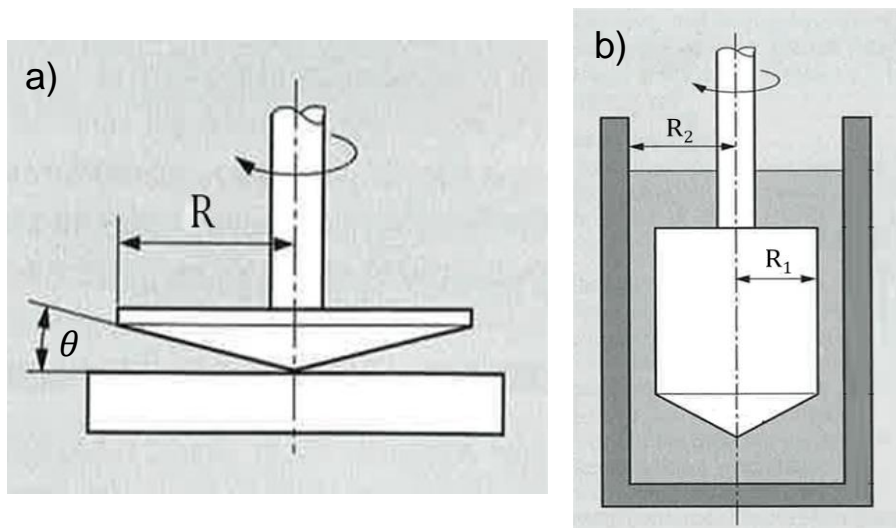


**Figure 16.** a) Schematic diagram of a cone-plate geometry of a rotational rheometer with a diameter  $R$  and a cone angle  $\theta$ , b) Searle system of a rotational rheometer with rotating inner cylinder radius  $R_1$  and outer cylinder radius  $R_2$ .

### 3.2 Transient oscillatory shear at fixed frequency and amplitude

A controlled stress rheometer (HAAKE Rheostress RS 150, Thermo HAAKE, Germany) equipped with a Searle system (Figure 16b), i.e. a concentric cylinder system with rotating inner cylinder (radius  $R_1 = 19.36$  mm) and fixed outer cylinder (radius  $R_2 = 20$  mm), was used to measure structure formation and aging dynamics of clay mineral dispersions. Directly after sample preparation in sol state, 10 ml dispersions were filled into the Searle system and sheared at sufficiently high shear stress ( $\sigma > \sigma_y$ ) for a given time interval  $\Delta t = 300$  s that guarantees complete destruction of possible sample structure. Subsequent recovery of the rest structure was monitored using small amplitude oscillatory shear measurements at a stress amplitude of  $\sigma_0 = 0.2$  Pa and a frequency of  $\omega = 0.6$  rad/s. The top of the sample chamber was covered with a plate in order to suppress evaporation of water.

### 3.3 Amplitude sweep experiments

We applied amplitude sweep experiments at time intervals of one week for a total lag time of up to 16 weeks in order to characterize the long term aging and change of mechanical strength of clay mineral dispersions. These experiments were carried out using a Physica Anton Paar MCR501 controlled stress rheometer with cone-plate geometry (Figure 16a) (diameter 25 mm, cone angle  $2^\circ$ , gap height at the tip of cone plate geometry  $47 \mu\text{m}$ ). The storage ( $G'$ ) and loss ( $G''$ ) moduli were determined by varying the shear stress amplitude from 1 to 500 Pa at constant frequency of 6 rad/s.

### 3.4 Frequency sweep experiments

Oscillatory shear flow experiments at varying frequencies were performed in the linear viscoelastic regime, where  $G'$  and  $G''$  are independent of the applied stress amplitude. The experiments were carried out using a Physica Anton Paar (MCR501) controlled stress rheometer, with cone-plate geometry (Figure 16a) (diameter 25 mm, cone angle  $2^\circ$ , gap height at the tip of cone plate geometry  $47 \mu\text{m}$ ). The experiments were executed at constant deformation amplitude

$\gamma_0 = 1\%$  from high to low frequency (60-0.006 rad/s). Preliminary amplitude sweep experiments confirmed that this deformation is within the linear viscoelastic response regime for the dispersions investigated here.

### 3.5 Oscillatory squeeze flow

The dependence of  $G'$  and  $G''$  on angular frequency  $\omega = 2\pi f$  between  $10^1$  and  $3 \times 10^4$  rad/s was measured by squeezing samples at very low deformation ( $< 0.1\%$ , depending on gap height) using a customized piezo-driven axial vibrator (PAV). The device illustrated in Figure 17 consists of four piezo actuators and four piezo detectors, which were connected to a quadratic copper tube carrying the lower plate of the sample fixture. The cover lid defines the upper wall of the cylindrical sample fixture. Piezo actuators are driven and detectors are read out using a lock-in amplifier (SR850, Stanford Research Systems, Inc., Sunnyvale, California, USA). The PAV was built at the Institute for Dynamic Materials Testing (IdM) at the University of Ulm.

$G'$  and  $G''$  were calculated from the detected phase shift and voltage amplitude determined in experiments with and without sample in the measuring cell as described in Crassous et al. (2005). Sample deformation in these experiments is so small that the resulting data are always in the linear viscoelastic regime (Crassous et al. 2005). Gap height was adjusted to 10-100  $\mu\text{m}$  depending on sample composition using appropriate distance rings. The exact gap width was determined from preliminary calibration with a Newtonian fluid of known viscosity. The required sample volume is about 100  $\mu\text{L}$ . In order to make an accurate comparison 8 weeks aged samples were used for these experiments as well as for frequency sweep and DWS experiments.

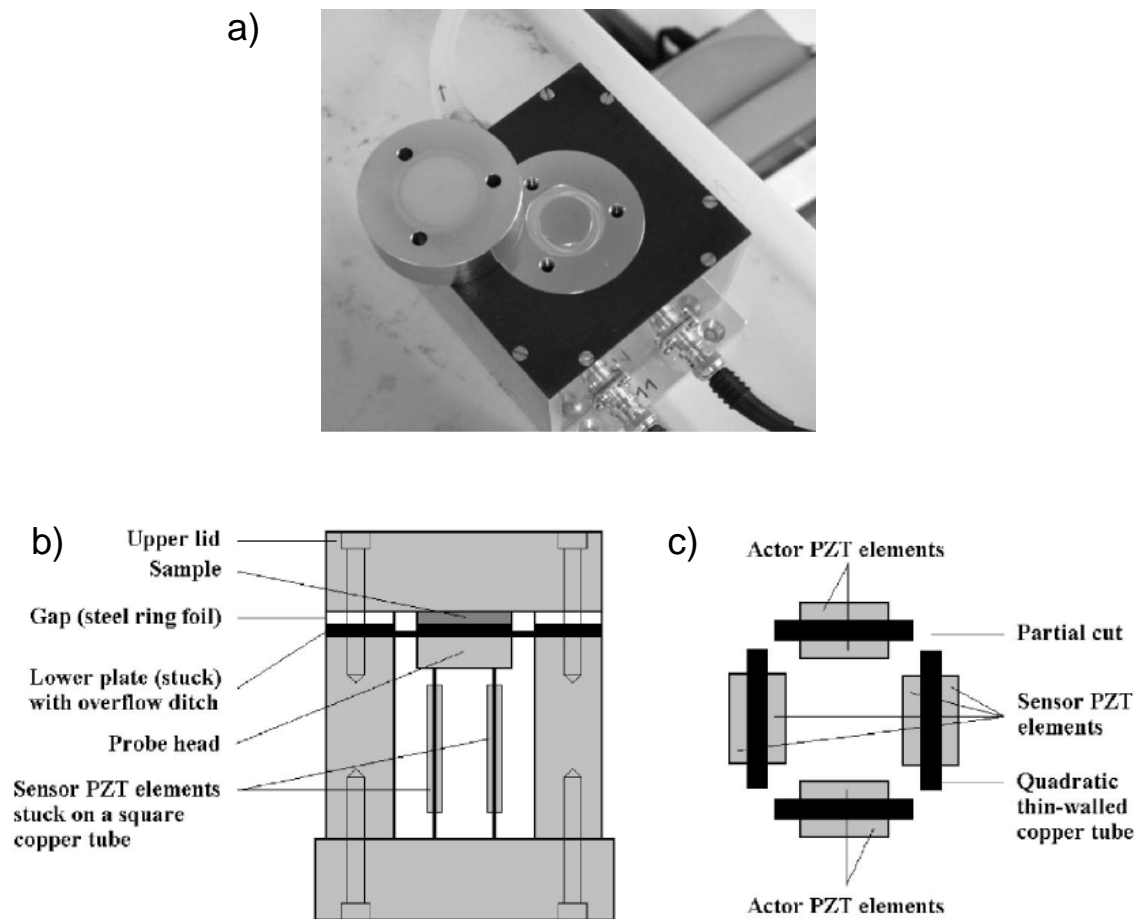


**Figure 17.** a) Piezoelectric axial vibrator (PAV) used in this study b) longitudinal cut of the PAV c) transversal cut of PAV (Crassous et al. 2005)

### 3.6 Diffusing wave spectroscopy

Diffusing wave spectroscopy (DWS) is an optical microrheological technique based on the thermal motion of embedded tracer particles and covers the angular frequency range from 1 to  $10^6$  rad/s. We used  $\text{TiO}_2$  nanoparticles (LS Instruments AG, Fribourg, Switzerland)  $0.36 \mu\text{m}$  in diameter as tracers, 0.5 wt% of  $\text{TiO}_2$  particles were added during preparation of clay mineral dispersions and  $800 \mu\text{l}$  samples were filled into cuvettes (Hellma, Müllheim, Germany) with 2 mm thickness. In accordance with Bonn et al. (2002), we observed that the addition of  $\text{TiO}_2$  particles does not affect the linear viscoelastic response of dispersions. Measurements were conducted and analyzed using the DWS ResearchLab (LS Instruments, Fribourg, Switzerland) with multi-tau correlator at an acquisition time of 270 s and echo duration of 5 s. The mean square displacement (MSD) of

tracer particles was calculated from the autocorrelation of the scattered light intensity and a generalized Stokes-Einstein equation was used to determine the complex shear modulus  $G^* = G' + iG''$  (Mason & Weitz 1995). The MSD was calculated for lag times between  $10^1$  and  $10^{-6}$  s and data analysis was done as described by Oelschlaeger et al. (2009).

### 3.7 Multiple particle tracking (MPT)

In order to do MPT video microscopy, 0.01 vol% of dragon green fluorescent polystyrene spheres with either 1.01, 0.52, 0.21 or 0.19  $\mu\text{m}$  in diameter (Bang Laboratories, USA) were added to the clay mineral dispersions. The samples including tracer particles were vortexed and homogenized for 5 min in an ultrasonic bath. Then they were directly injected into a commercial rectangular capillary of 0.1 mm thickness and 2 mm width (CM Scientific, UK) sealed with UV-curing glue. The microscope (Axio Observer D1, Carl Zeiss) equipped with a Fluar 100x, N.A. 1.3, oil-immersion lens, was focused roughly halfway into the sample and the Brownian motion of tracer particles was monitored in an  $127 \times 127 \mu\text{m}$  field of view, at a rate of 30 frames per second (sCMOS camera Zyla X) for 1 min. The experimental setup was described in detail by Kowalczyk et al. (2015). For each experiment about 150 particles were tracked simultaneously. After image processing (IPS Visiometrics), displacement of particle centers was monitored using a self-written MATLAB code (Kowalczyk et al. 2015) based on the widely used Crocker and Grier tracking algorithm (Crocker & Grier 1996). A highly elastic tri-block-copolymer gel Pluronic® F127 (BASF SE, Ludwigshafen, Germany) has been employed to determine the static error which sets the upper limit for the storage modulus accessible with a given setup (Kowalczyk et al. 2015) and the lower limit for heterogeneity ratio to be obtained with corresponding tracer particles (Savin & Doyle 2005).

# 4 Results and Discussion

Results and discussion will be presented in two parts. As model system the rheological characterization of Laponite® dispersions on the macro- and micro-length scale will be shown in the first part. After understanding the structure formation and aging in different arrested states of Laponite® dispersion as well as their viscoelastic behavior in a broad frequency range and the heterogeneous microstructure of their arrested states, we will compare the characteristic behavior of this model system with natural clay mineral systems, i.e. Na-saturated montmorillonite and natural hectorite. The wide-ranging rheological comparison of synthetic and natural clay mineral dispersions will be presented in second part of results and discussion. The results in these two parts were submitted for publication to two peer-reviewed scientific journals.

## 4.1 Macro- and microscale structure formation and aging in different arrested states of Laponite® dispersions

Covering a wide range of solids content and salt concentrations at different pH repulsive glasses, attractive strong and weak gels with prevailing EF or FF layer contacts were formed. The classical oscillatory shear rheometry and MPT optical microrheology have been used to characterize kinetics of structure formation and aging for different types of repulsive or attractive arrested states. Laponite® dispersions have been investigated with a broad range of clay mineral content (1-3 wt%), electrolyte concentration (up to  $10^{-2}$  M NaCl) and different pH (8.5, 10 and 12). The variety of methods applied in this study and the broad range of physico-chemical parameters investigated provide a comprehensive scientific view on differences between arrested states with different Laponite® layer orientations. A distinction between repulsive glasses and attractive gels from bulk rheological measurements alone is not trivial and sometimes maybe not be possible (Bonn et al. 1999). Therefore, bulk rheometry has been combined with microrheology to shed new light on the long-standing controversy about rheological behavior of Laponite® dispersions on the macro- and micro-length scales. The effect of the main control parameters, i.e. clay mineral content and

salt concentration, as well as pH on kinetics of structure formation, aging, mechanical strength, microscopic heterogeneity and structural refinement for different attractive and repulsive arrested states are discussed. Beyond that, the squeeze flow mechanical rheometry as well as diffusing wave spectroscopy (DWS) optical microrheology have been applied to determine linear viscoelastic properties in the frequency range up to  $10^6$  rad/s.

### 4.1.1 Structure formation in glass and gel states of Laponite® dispersions

In order to determine kinetics of structure formation and initial aging of different arrested states of Laponite® dispersions, the change of  $G'$  and  $G''$  was measured as a function of time using small amplitude oscillatory shear measurement (stress amplitude  $\sigma_0 = 0.2$  Pa, frequency  $\omega = 0.6$  rad/s). Glass and gel structures were obtained dissolving 2 wt% Laponite® in deionized water and  $10^{-2}$  M NaCl aqueous solution, respectively. Due to the high energy input during transfer of the sample into the rheometer fixture and during the initial steady shear period both samples are in sol state when oscillatory shear experiments start as confirmed by visual inspection. The sample without added electrolyte remains in this sol state characterized by a constant low  $G''$  value and an unmeasurably small  $G'$  for about  $10^3$  min until both moduli rapidly increase and finally  $G'$  is larger than  $G''$ . The characteristic point where  $G' = G''$  is generally assumed to mark the formation of a percolating network (Winter & Chambon 1986) and the corresponding time  $t_c$  is called cross-over or gelation time. Here it is attributed to the formation of a sample spanning arrested state, i.e. the repulsive glass (Figure 18a). The situation is different for the sample including  $10^{-2}$  M NaCl. In this case even the first modulus values accessible after about 50 s (corresponding to 5 oscillations) are orders of magnitude higher than in the sol state with  $G' > G''$  and in the subsequent time interval of about  $10^3$  min  $G''$  remains essentially constant whereas  $G'$  further increases without reaching a steady state (Figure 18a), as expected (Willenbacher 1996). This demonstrates that again a sample spanning arrested state is formed and this attractive gel-state forms orders of magnitude faster than the glass state. The characteristic crossover time or gelation time  $t_c$  is clearly below 1 min and from the shape of the  $G'$  and  $G''$  curves we estimate

## Results and Discussion

$t_c = 0.4$  min compared to  $t_c = 1258$  min for the glass formation. Similar experiments have been performed for other clay mineral contents and electrolyte concentrations and the corresponding  $t_c$  values are shown in Figure 18b. As expected arrested states generally form much faster at higher clay mineral content and for both clay mineral contents the strong gel forms much faster than the glass state (Figure 18b). The formation of so-called weak gels (Mongondry et al. 2005) at intermediate electrolyte concentration, however, takes about as much time as glass formation. This is attributed to the still strong electrostatic repulsion among layers delaying aggregation.

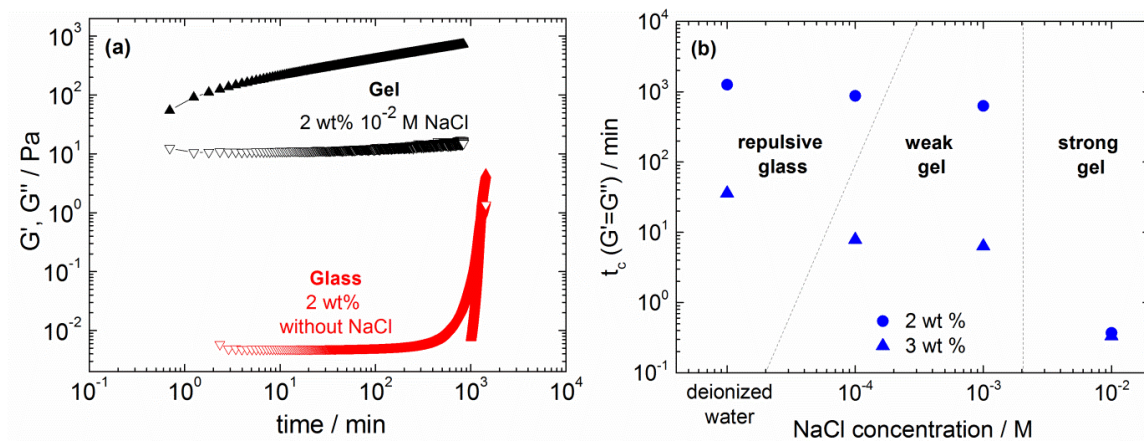


**Figure 18.** **a)** Structure formation for two arrested states of Laponite® dispersions at  $\text{pH}_{\text{inh}}=10$ . Filled up-triangle =  $G'$ , empty down-triangle =  $G''$ . **b)** Solids content and NaCl concentration effect on the crossover time  $t_c$  (where  $G' = G''$ ) of Laponite® dispersions.

### 4.1.2 Effect of pH on structure formation

The time dependent oscillatory shear measurements were applied to Laponite® dispersions at  $\text{pH}=8.5$ , 10 and 12 to see the pH effect on structure formation and aging. Two different Laponite® dispersions have been investigated, 2 wt% solids content without added electrolyte and 1 wt% solids content with  $10^{-2}$  M NaCl, respectively. Samples with high salt concentration, around  $10^{-2}$  M, became turbid after setting pH to 8.5. Such unstable samples were excluded in this study. In order to guarantee chemical stability of Laponite® dispersions, the minimum pH was set to 8.5, as discussed in the section 2.2. No turbidity was observed for samples with high electrolyte concentration at  $\text{pH}=12$ .

For all investigated samples a transition to an arrested state with  $G' \gg G''$  is observed. The sample with 2 wt% Laponite® without added electrolyte at its inherent pH forms a glass and this takes a long time ( $t_c = 1258$  min) as discussed above. The arrested states at pH=12 ( $t_c = 30$  min) and pH=8.5 ( $t_c = 0.3$  min) form much faster (Figure 19).

Changing pH from its inherent value of pH 10 to pH 8.5 or pH 12 results in a strong increase in electrolyte concentration in the aqueous phase and according electrical conductivity increases from 505  $\mu\text{S}/\text{cm}$  to 892  $\mu\text{S}/\text{cm}$  and 1869  $\mu\text{S}/\text{cm}$  at pH=8.5 and pH=12, respectively. This leads to a substantial compression of the electrical double layer resulting in the formation of attractive gel states. Moreover, we have to keep in mind, that  $\text{pH}_{\text{PZC,edge}}$  of Laponite® is around 10 to 11 as deduced from stability ratio measurements (Tawari et al. 2001) and confirmed by the cation exchange capacity (CEC) measurements from pH 8 to 12 according to Meier and Kahr (1999). The CEC results are shown in Figure 12.

At pH=8.5 the edges are positively charged and at pH=12 they are negatively charged. Accordingly, it is assumed that EF contacts are likely to form at pH=8.5 and FF contacts with  $\text{Na}^+$  in between prevail at pH=12. As seen in Figure 19a structure formation is much faster at pH 8.5 than at pH 12. Therefore, it is proposed that structures predominantly based on EF contacts form much faster than FF dominated structures. This conclusion is further corroborated by the results obtained for the 1 wt% clay mineral dispersions with  $10^{-2}$  M NaCl. Due to the high ionic strength, attractive interactions dominate in both cases at pH=10 and pH=12 and structure formation takes place rapidly (Figure 19b). At pH=10 edges are still slightly positively charged and the arrested state is assumed to have an EF structure, whereas FF contacts prevail at pH=12. Again, the structure supposed to be dominated by EF contacts forms faster than the gel including FF type layer contacts.

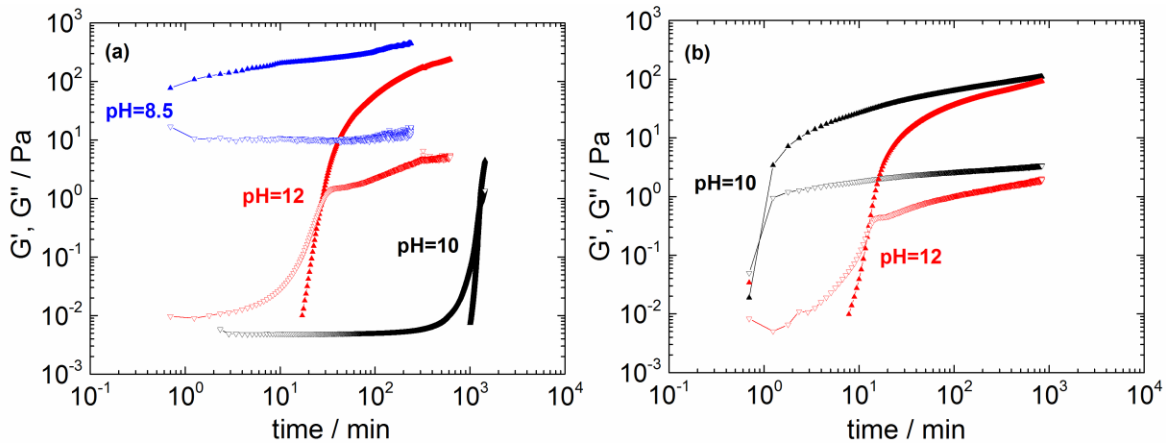


**Figure 19.** Effect of pH on kinetics of structure formation for **a)** 2 wt% Laponite® dispersion without NaCl and **b)** 1 wt% Laponite® dispersion at  $10^{-2}$  M NaCl concentration. Filled up-triangle =  $G'$ , empty down-triangle =  $G''$ . Blue, black and red symbols represent pH=8.5, 10 and 12, respectively.

### 4.1.3 Aging of Laponite® dispersions in different arrested states

Aging, i.e. the change of structure or dynamics over long periods of time is a common phenomenon in out-of-equilibrium systems such as amorphous polymers (Struik 1978), supersaturated solid solutions (Lifshitz & Slyozov 1961) or clay mineral dispersions (Willenbacher 1996; Knaebel et al. 2000; Ianni et al. 2007; Ruzicka & Zaccarelli 2011; Au et al. 2015). In the latter case aging corresponds to a perpetual re-arrangement of clay mineral layers and re-organization of the overall gel or glass structure and shows up, e.g. in a monotonic increase of the storage modulus over time. This phenomenon can already be seen from the transient  $G'$  data shown in Figures 17 and 18 covering a time interval of about one day. Willenbacher (1996) was the first to discuss aging in attractive gel Laponite® dispersions as a self-delaying process and reported an increase of  $G'$  over several weeks following a power law  $G' \sim t^\alpha$  with  $\alpha = 0.13 \pm 0.02$  independent of clay mineral content and mechanical pre-treatment of samples. Structural re-arrangement and aging have been shown to endure for more than one year in dilute Laponite® dispersions as revealed by light and X-ray scattering experiments (Ruzicka et al. 2010). Here the aging phenomenon in different arrested states of Laponite® dispersions has been studied using shear modulus measurements. The fixed frequency amplitude

sweep oscillatory shear experiments were performed at time intervals of one week covering a total time period of up to 16 weeks. In between measurements, samples were stored in tightly sealed vials to avoid any loss of solvent. Corresponding results for dispersions including 2 wt% Laponite® and  $10^{-4}$  M NaCl at pH=8.5, 10 and 12, are shown in Figure 20. The pH was periodically tested and confirmed to remain at its initial value during the extended storage time.

The attractive gel formed at pH=8.5 and assumed to have EF layer contacts exhibits the highest strength with a shear modulus  $G' \approx 10^3$  Pa. This structure also requires the largest critical stress  $\sigma_y = 70$  Pa to enable flow, here defined as the stress amplitude at which  $G' = G''$  often also termed apparent yield stress. When this stress is exceeded catastrophic failure destroys the structure and  $G'$  rapidly becomes immeasurably small. This structure shows very little aging and the modulus increases by only 10 % within 5 weeks of storage.

The attractive arrested state formed at pH=12 and supposed to have a prevailing FF structure exhibits a much weaker shear strength than the EF structure with an initial modulus  $G' = 10^2$  Pa and  $\sigma_y = 15$  Pa. This type of gel experiences a gradual structural breakdown when  $\sigma_y$  is exceeded and aging is clearly visible, the modulus increases by a factor of two within 5 weeks. The repulsive glass formed at pH=10 exhibits lower initial shear strength and yield stress than the attractive gel formed at pH=12. However, it exhibits a uniquely strong aging and  $G'$  increases by a factor of 4 within 16 weeks of storage. Moreover, the mode of failure changes from gradual break down for shortly stored samples to catastrophic failure at extended aging times.

## Results and Discussion

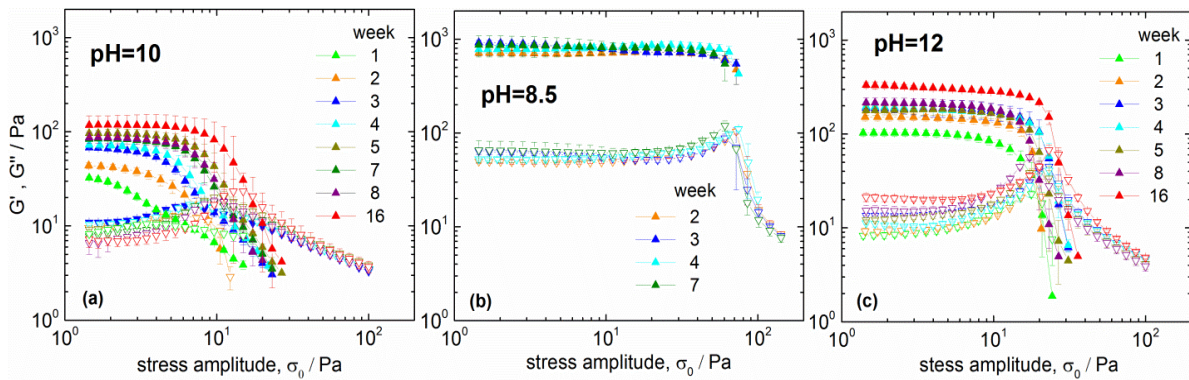


**Figure 20.** Amplitude sweep experiments at different aging times for 2 wt% Laponite® dispersions with  $10^{-4}$  M added NaCl **a)** at pH=10, **b)** at pH=8.5 and **c)** at pH=12. Filled up-triangle =  $G'$ , open down-triangle =  $G''$ .

Figure 21 compares the time evolution of the normalized storage modulus  $G'_{norm} = G'(t_{storage}) / G'(t_{storage} = 0)$  for different repulsive and attractive arrested states. In all cases the time dependence of  $G'$  may be approximated by a power law  $G' \sim t^\alpha$  with  $\alpha = 0.11 \pm 0.03$  for the attractive strong gel states (black lines) in excellent agreement with the early findings of Willenbacher (1996). In contrast, the weak gels (blue lines) and repulsive glass (red line) exhibit much stronger aging than strong gels. Here  $\alpha = 0.74 \pm 0.01$  was found for the glass with 2 wt% Laponite® and  $10^{-4}$  M NaCl at pH = 10 as well as  $\alpha = 0.36 \pm 0.01$  for the weak gels. Obviously, layer mobility is much higher for the layers arrested due to electrostatic repulsion of neighboring layers than for those trapped in contact with attractive neighbors in gel structures.

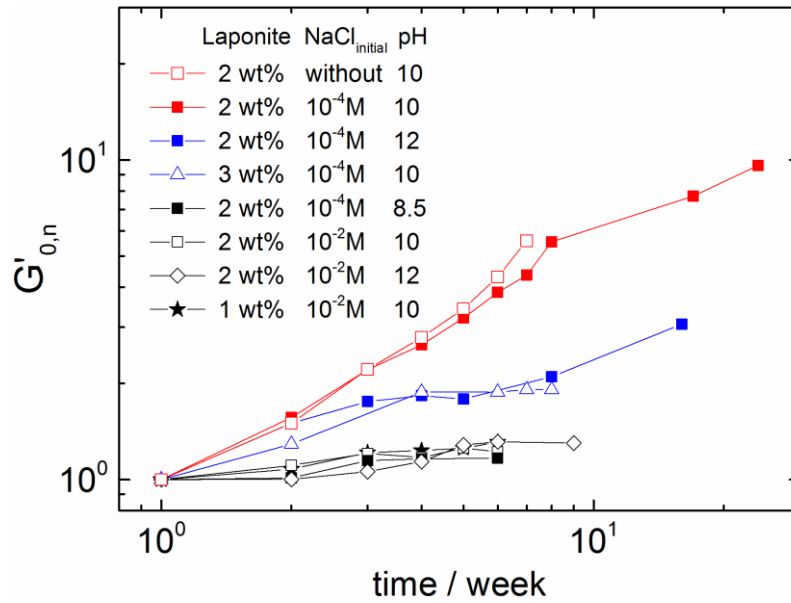


**Figure 21.** Normalized plateau moduli as a function of aging time for Laponite® dispersions at various solids content and NaCl concentrations at inherent pH of 10, at set pH 12 and 8.5. Black, blue and red lines represent strong gel, weak gel and repulsive glass samples.

#### 4.1.4 Broad bandwidth linear viscoelastic relaxation of Laponite® dispersions in different arrested states

Jabbari-Farouji et al. (2008a) described the frequency dependence of the shear modulus as a superposition of two power law contributions and found an exponent  $\beta \approx 0.7$  characterizing the high frequency relaxation of investigated samples. Here the bulk oscillatory shear and squeeze flow were combined with DWS microrheology to cover the frequency range from  $5 \times 10^{-3}$  to  $3 \times 10^6$  rad/s. Storage and loss modulus data for 2 wt% Laponite® dispersions with different pH and salt concentration are shown in Figure 22. Data obtained with different techniques agree very well and as expected  $G'$  is essentially constant over more than five decades in frequency but starts to increase around  $\omega \approx 10^3 - 10^4$  rad/s (Figure 22a). The absolute values of the frequency independent  $G'$  data in the low frequency range demonstrate that at a given Laponite® content the EF-type attractive gel assumed to be formed at pH = 8.5 is stronger than the FF-type arrested state supposed to exist at pH = 12 which in turn has a higher shear

## Results and Discussion

strength than the repulsive glass (pH = 10). At pH 10 and 12, adding NaCl results in an increase of  $G'$ , whereas added electrolyte has no effect at pH = 8.5.

At frequencies around  $10^3 - 10^4$  rad/s  $G''$  also starts to increase strongly according to a power law  $G'' \sim \omega^\beta$  with  $\beta = 0.75 \pm 0.03$  (Figure 22b). This exponent as well as the absolute values of  $G''$  are independent of pH or salt concentration within experimental uncertainty. Such a scaling law has been predicted for solutions of semi-flexible objects such as polymers, wormlike micelles or protein filaments (Lifshitz & Slyozov 1961; Ianni et al. 2007). It is attributed to intrinsic relaxation modes of the building blocks of the semi-flexible objects and directly related to the bending stiffness or persistence length of these chains. Here, this characteristic power law may be related to the bending modulus of the single clay mineral layers and thus should be independent of the mode of arrest in which the layers are trapped.

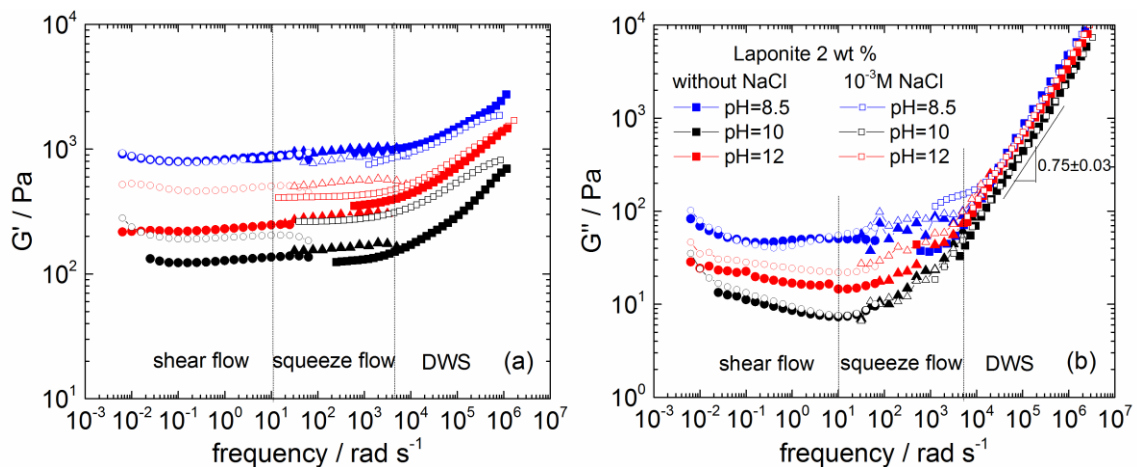


**Figure 22.** Linear viscoelastic **a)** storage modulus and **b)** loss modulus for 2 wt% Laponite® dispersions with and without NaCl at three pH. The broad frequency range was covered with the help of small amplitude oscillatory shear flow (square), squeeze flow (triangle) and DWS experiments (square). All experiments were performed on 8 weeks old samples.

#### 4.1.5 Microrheology and microstructural heterogeneity

Brownian motion of spherically shaped fluorescent tracer particles embedded in the clay mineral dispersions has been monitored to characterize the change in viscoelasticity and local particle dynamics during formation of different arrested states. At least 150 tracer particles were tracked simultaneously in a single experiment. From the particle positions in subsequent video images the mean square displacement  $\text{MSD}(\tau)$  of each particle is obtained as a function of lag time  $\tau$  and finally the average  $\text{MSD}(\tau)$  obtained in a single experiment is calculated.

In Figure 23a such average MSD data obtained at different time intervals after sample preparation are shown for a 3 wt% Laponite® dispersion with  $10^{-4}$  M NaCl. Immediately after sample preparation the MSD of the tracer particles depends linearly on  $\tau$ , i.e. the tracers diffuse in a viscous environment, the sol state. Then the slope of the  $\text{MSD}(\tau)$  curves gradually decreases with increasing waiting time until finally MSD data turn time-independent when the arrested gel state is reached.

The Laplace transform of the average MSD  $\langle \Delta \tilde{r}^2(i\omega) \rangle$  is related to the complex shear modulus  $G^*$  of the surrounding medium via the generalized Stokes-Einstein equation:

$$G^*(\omega) = G'(\omega) + iG''(\omega) = \frac{2k_bT}{\pi d i \omega \langle \tilde{r}^2(i\omega) \rangle} \quad (4.1)$$

where  $T$  is the temperature,  $k_b$  the Boltzmann constant and  $d$  the diameter of the tracer particles. This relationship has been used to calculate  $G'$  and  $G''$  data from the MSD (Kowalczyk et al. 2015). The transition from the liquid to the arrested state is clearly visible also from the representation of experimental data, see Figure 23b. Similar results have been reported earlier (Oppong et al. 2008; Rich et al. 2011b) demonstrating that MPT is a versatile, non-destructive way to characterize long-term changes in viscoelastic sample properties even if volatile components are included, since the specimen are kept in tightly sealed cuvettes.

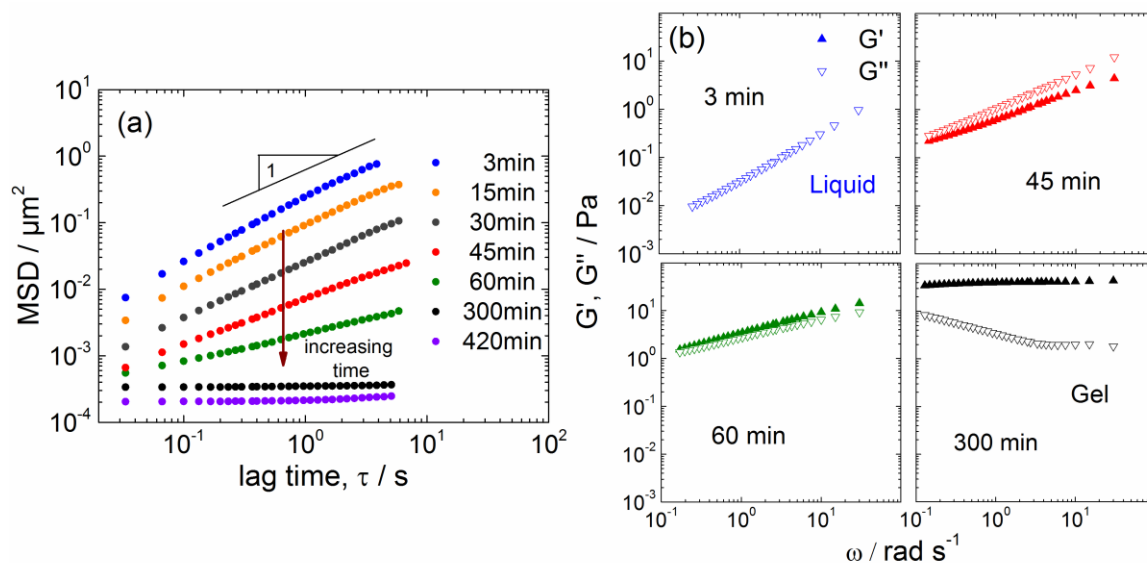


**Figure 23.** **a)** Mean value of MSD of  $0.21 \mu\text{m}$  tracer particles embedded in a 3 wt% Laponite® dispersion with  $10^{-4}$  M NaCl at  $\text{pH}_{\text{inh}}=10$  at different waiting times. **b)** Frequency dependence of the storage and loss moduli of 3 wt% Laponite® dispersion with  $10^{-4}$  M NaCl on corresponding length scale ( $0.21 \mu\text{m}$ ) at different waiting times.

Similar experiments have been performed for Laponite® dispersions in different arrested states and structure formation kinetics has been characterized using tracer particles of different size between  $0.19 \mu\text{m}$  and  $1.01 \mu\text{m}$ . Formation of the repulsive glass and the attractive gel structure for 3 wt% Laponite® dispersed in de-ionized water and a  $10^{-4}$  M NaCl solution, respectively, is shown in Figure 24a and 23b. Structure build-up is characterized via the corresponding change in  $G'$  and  $G''$  taken at fixed frequency  $\omega = 0.6 \text{ rad/s}$  over waiting time. For comparison, results from mechanical rheometry are also included.

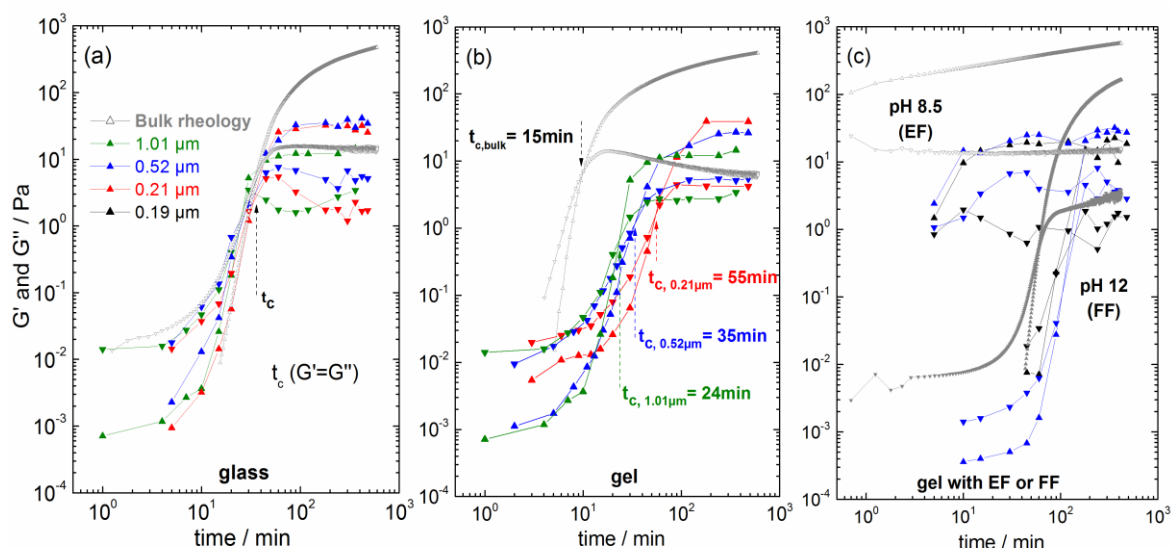


**Figure 24.** **a)** Glass structure; viscoelastic moduli as a function of time for 3 wt% Laponite® in deionized water at  $\text{pH}_{\text{inh}}=10$ . **b)** Gel structure; viscoelastic moduli as a function of time for 3 wt% Laponite® in  $10^{-4}$  M NaCl at  $\text{pH}=10$ . **c)** Gel structure with prevailing EF or FF; viscoelastic moduli as a function of time for 2 wt% Laponite® in  $10^{-4}$  M NaCl aqueous solution at  $\text{pH}=8.5$  (EF) and 12 (FF).  $G'$  (up-triangle) and  $G''$  (down-triangle).

For the glass sample, the characteristic structure formation time  $t_c$  at which  $G' = G''$  is independent of the size of the tracer particles and MPT data are in excellent agreement with bulk rheometry data. This is different from earlier observations (Strachan et al. 2006; Petit et al. 2009) showing a probe size dependence of tracer diffusivity but we have to keep in mind that the particle size in these dynamic light scattering and fluorescence recovery after photo bleaching studies is well below the size range investigated here. It should be noted, that the aging of the glasses as well as gel systems, i.e. the increase in  $G'$  for times  $t > t_c$  cannot be monitored using MPT. Due to the constraints defined by the noise-to-signal ratio of the setup the upper limit for the accessible modulus is  $G'_{\text{max}} \approx 30$  Pa, essentially independent of particle size (Kowalczyk et al. 2015).

A completely different scenario is observed for the sample with 3 wt% Laponite® and  $10^{-4}$  M NaCl considered as a weak gel. In this case the crossover times  $t_c$  from MPT are significantly longer than  $t_{c,\text{bulk}} = 15$  min obtained from bulk rheometry and increases systematically with decreasing tracer particle size. For

## Results and Discussion

---

$d = 0.21 \mu\text{m}$   $t_c = 55 \text{ min}$  is found. Similar results were obtained for the sample with 2 wt% Laponite® and  $10^{-4} \text{ M NaCl}$ , in this case  $t_{c,bulk} = 120 \text{ min}$  and  $t_c = 1224 \text{ min}$  was determined using tracer particles with  $d = 0.19 \mu\text{m}$ . Furthermore, Rich et al. (2011b) found a shift of  $t_c$  from  $t_{c,bulk} = 6 \text{ min}$  to  $t_c = 180 \text{ min}$  at a Laponite® concentration of 1 wt% using  $0.11 \mu\text{m}$  particles, i.e. the delay of the sol-gel transition increases with decreasing clay mineral concentration.

Similar results have been reported previously for Laponite® dispersions with solids content between 0.75 and 1.25 wt% at NaCl concentrations of  $1.8 \times 10^{-3} \text{ M}$  and  $1 \times 10^{-3} \text{ M}$ , respectively (Oppong et al. 2008; Rich et al. 2011b), which may also be considered as weak gels. This increase in gelation time with decreasing length scale seems to be consistent with the fractal network model proposed by Pignon et al. (1997), if layer re-arrangements and re-organization of micron-sized clusters assumed to build-up the fractal network are considered to take place at long times. On the macroscopic scale it shows up as slow aging, i.e. weak increase in  $G'$  over time as discussed above.

Finally, macro- and microstructure formation for Laponite® gels have been compared at pH=8.5 where EF layer contacts prevail and at pH=12 where FF is the preferred layer contact mode. As can be seen from Figure 24c in both cases gelation is significantly delayed on the microscale compared to the macroscale and structural refinement even takes place in the strong gel obtained at pH=8.5.

The delayed gelation time observed on the microscale and the corresponding structural refinement seems to indicate a heterogeneity of the attractive, gel-like arrested states, which is not observed in glass systems. MPT is a valuable tool to characterize sample heterogeneities on a sub-micrometer length scale offering good statistical significance. Oppong et al. (2008) quantified sample heterogeneity using the non-Gaussian parameter characterizing the deviation of the MSD distribution at fixed lag time for the ensemble of tracked particles from the Gaussian distribution function to be found in a homogeneous, ergodic system. For the weak gel they investigated this parameter increased sharply until the (microscopic) gelation time was reached and seemed to remain high even at somewhat longer aging times. Similar results were reported by Rich et al. (2011b)

using the so-called heterogeneity ratio  $HR$  as a quantitative measure of spatial heterogeneity obtained by MPT experiments.  $HR$  is calculated as (Savin & Doyle 2007):

$$HR = \frac{M_2(\tau)}{M_1(\tau)^2} \quad (4.2)$$

where  $M_1(\tau)$  is the estimator for the ensemble average of MSD and  $M_2(\tau)$  is the estimator for the ensemble variance of MSD, both quantities are calculated at a given lag time  $\tau$  from individual particle trajectories weighted by a factor proportional to their length. For the weak gel a monotonic increase of  $HR$  with waiting time was observed even somewhat beyond the gelation point obtained at the length scale of the respective tracer particles (Rich et al. 2011b).

Here the heterogeneity of Laponite® dispersions has been investigated varying clay mineral content and electrolyte concentrations as well as different pH (8.5, 10, 12), thus including glass as well as different arrested gel states. The parameter  $HR$  (Eq. 4.2) was used to quantify sample heterogeneity based on MPT experiments with different particle size ( $d=0.19, 0.21$  and  $0.52 \mu\text{m}$ ). Figure 25 displays these  $HR$  data as a function of waiting time  $t$  and the latter is normalized to the microscopic gelation time  $t_c$  determined for each sample using the respective tracer particles.

## Results and Discussion

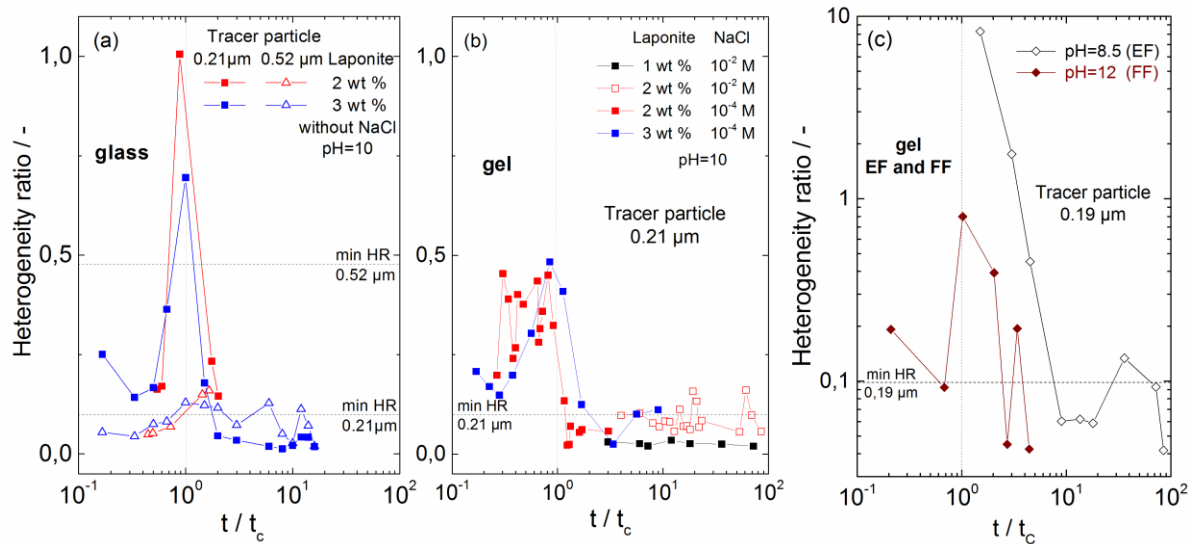


**Figure 25.** **a)** Heterogeneity ratio (HR) during sol-glass phase transition of Laponite® dispersions at pH=10 measured by MPT method and using 0.21 and 0.52 μm tracer particles **b)** HR during sol-gel phase transition of Laponite® dispersions at pH=10 measured by MPT method and using 0.21 μm tracer particle **c)** HR during phase transition of 2 wt% Laponite® in 10<sup>-4</sup> M NaCl aqueous solution at pH=8.5 and 12 measured by MPT method and using 0.19 μm tracer particle. The minimum HR for each tracer particle type was determined in homogeneous polymer hydrogel (Pluronic® F127) and plotted as horizontal dashed line. The phase transition point  $t_c$ , where  $G'$  and  $G''$  are equal, was marked at  $t/t_c = 1$  as vertical dotted line.

Note, non-zero  $HR$  values are found even for ideal homogeneous fluids due to limitations of experimental setup and data acquisition (Savin & Doyle 2007). This  $HR$  threshold has been determined experimentally using a homogenous, highly elastic polymer gel (Puronic F127,  $G'=10^4$  Pa at  $T=20^\circ\text{C}$ ), corresponding horizontal lines for the different particle sizes (Figure 25).

In these MPT experiments all investigated samples exhibit a pronounced heterogeneity at the sol-gel/glass transition, i.e. around  $t/t_c \approx 1$ . Consistent with earlier results (Jabbari-Farouji et al. 2008a) the glass samples exhibit this heterogeneity only at the length scale of tracer particle size of 0.21 μm but not a larger scales. The degree of heterogeneity seems to be most pronounced for the gel with the EF structure generated at pH 8.5 and weakest for the gels formed at pH 10.

All arrested states exhibit a uniform structure at a length scale of about 5-7 times the clay mineral layer diameter. Undoubtedly, there is no indication of sample heterogeneity for any of the investigated glasses, weak or strong gels at times  $t/t_c \gg 1$ . This surprising result is directly visible from the MSD ensembles exemplary shown in Figure 26.

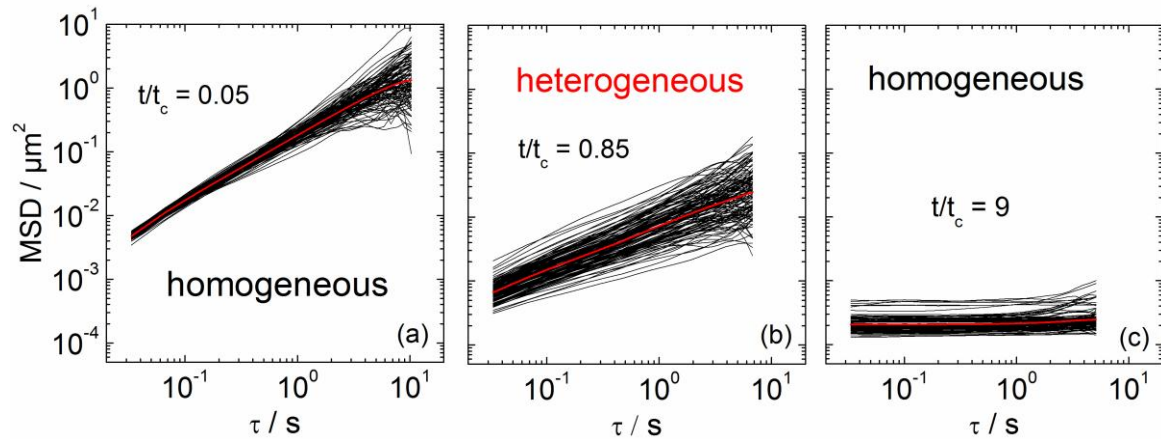


**Figure 26.** Ensemble of individual MSD for simultaneously tracked tracer particles ( $d = 0.21 \mu\text{m}$ ) in a 3 wt% Laponite® dispersion with  $10^{-4}$  M NaCl at different times normalized by crossover time; a broad distributions of MSDs for the heterogeneous structure **b)** at  $t/t_c \approx 1$  and narrow distributions of MSDs for homogeneous structures **a)** at  $t/t_c \ll 1$  and **c)** at  $t/t_c \gg 1$  are clearly visible.

### 4.2 Formation of arrested states in natural di- and trioctahedral smectite dispersions compared to synthetic hectorite - a macro and microrheological study

Colloidal behavior of natural clay minerals with different octahedral structure, e.g. di- and trioctahedral, was investigated using macro- and microrheological measurements and compared with the data of the synthetic hectorite system reported in the previous section. The Na-saturated montmorillonite (BV-M0.2Na), natural hectorite (SHCa-0.2Na) and Laponite® with different lateral layer dimension of 270, 100 and 30 nm, respectively, were used. The solids content was varied between 1 and 7 wt%, depending on clay mineral, and NaCl content was increased up to  $10^{-1}$  M at their corresponding inherent pH. The pH of dispersions was also set to higher and lower values than  $\text{pH}_{\text{PZC,edge}}$ , which is a clay mineral specific parameter. The differences in their structure formation subject to clay mineral type and pH depending layer orientation will be presented. Their linear viscoelastic behavior depending on particle size in a wide range of solids and ion concentrations, as well as their structural refinement on submicrometer length scale using MPT will be discussed in this chapter. Their state diagrams were determined at their inherent pH considering clay mineral and NaCl concentration as well as sample aging. Beyond that we have employed squeeze flow mechanical rheometry as well as diffusing wave spectroscopy (DWS) optical microrheology on natural clay mineral system to determine linear viscoelastic properties in the frequency range up to  $10^6$  rad/s.

#### 4.2.1 Comparison of structure formation of natural and synthetic clay mineral dispersions at their inherent pH

In order to determine kinetics of structure formation and initial aging of different arrested states of natural clay mineral dispersions, the change of  $G'$  and  $G''$  was measured as a function of time using small amplitude oscillatory shear measurement (stress amplitude  $\sigma_0 = 0.2$  Pa, frequency  $\omega = 0.6$  rad/s) and corresponding results are shown in Figure 27. Due to the high energy input during transfer of the sample into the rheometer fixture and during the initial

steady shear period, all samples are in sol state when oscillatory shear experiments start. The samples without or with a trace amount of added electrolyte remain for a while in this sol state characterized by  $G' < G''$ . The characteristic point where  $G' = G''$  is generally assumed to mark the formation of a percolating network (Winter & Chambon 1986) and the corresponding time  $t_c$  is called cross-over or gelation time. Here it is attributed to the formation of a sample spanning arrested state, i.e. the repulsive glass or attractive gel. For natural clay mineral dispersions gelation occurs faster than glass formation and in both arrested states the elastic modulus is always higher than the viscous modulus similar as for Laponite® dispersions in the frequency range  $< 10^2$  rad/s.

For Laponite® dispersions  $G'$  remains unmeasurably small for about  $10^3$  min until both moduli rapidly increase and finally  $G'$  is larger than  $G''$  in the glass state (see Figure 27a). SHCa-0.2Na and BV-M0.2Na dispersions with low electrolyte content gradually form the glass state with slow increases in  $G'$  and  $G''$ . It should be noted that the electrostatic repulsion is stronger for the Laponite® than for the natural clay minerals, since the ionic strength is clearly lower and presumably this is the reason for the delayed glass formation in the synthetic hectorite system.

The situation is different for the Laponite® and SHCa-0.2Na samples including high concentration of electrolyte ( $\geq 10^{-2}$  M NaCl). In this case the first modulus values accessible after about 50 s (corresponding to 5 oscillations) are orders of magnitude higher than in the sol state with  $G' > G''$  and in the subsequent time interval of about  $10^3$  min  $G''$  remains essentially constant whereas  $G'$  further increases without reaching a steady state (Figure 27a-b), as expected (Willenbacher 1996). Figure 18a is presented here again as Figure 27a for a better comparison of the dynamics of structure formation of SHCa-0.2Na and BV-M0.2Na systems with Laponite® system.

For BV-M0.2Na dispersion (Figure 27c) even with high amount of added electrolyte ( $10^{-1}$  M NaCl),  $G'$  and  $G''$  gradually increase. Here it should be considered that the inherent pH of BV-M0.2Na dispersion is higher than its  $\text{pH}_{\text{PZC,edge}}$ , whereas the situation is reverse for Laponite® and SHCa-0.2Na dispersions. As pointed out in the previous section 4.1, at  $\text{pH} > \text{pH}_{\text{PZC,edge}}$  and

## Results and Discussion

high ion concentration clay mineral layers are supposed to connect preferentially in FF configuration to form gel states and FF contacts form slower than EF contacts in accordance with Yariv and Cross (1979). Therefore, it is assumed at high electrolyte concentration the gel-state of the BV-M0.2Na dispersion is based on a gradual formation of FF contacts, whereas Laponite® and SHCa-0.2Na dispersions have rapid gel structure formation due to EF layer coagulation.

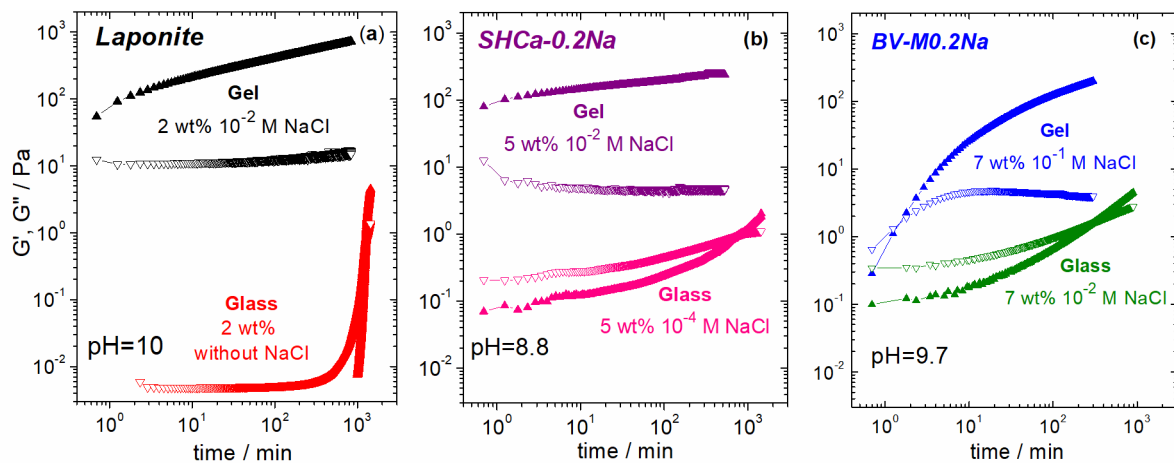


**Figure 27.** Structure formation for two arrested states of **a)** Laponite® (the same of Figure 18a) **b)** SHCa-0.2Na and **c)** BV-M0.2Na dispersions at  $\text{pH}_{\text{inh}}=10$ , 8.8 and 9.7, respectively. Filled up-triangle =  $G'$ , empty down-triangle =  $G''$ .

These three clay mineral dispersions reach the arrested states following different routes and similar results were found for other clay mineral and electrolyte concentrations. Most remarkably for natural clay mineral dispersions BV-M0.2Na and SHCa-0.2Na more solids content was needed to get arrested states and this is attributed to their larger layer diameter. Moreover, higher salt concentration was needed for BV-M0.2Na samples with higher layer charge ( $0.26 \pm 0.01$  eq/FU) than that of Laponite® and SHCa-0.2Na samples ( $0.19 \pm 0.01$  and  $0.24 \pm 0.01$  eq/FU, respectively) to obtain gel states tentatively dominated by FF contacts. The electrical potential of clay mineral layers is proportional to layer charge in electrical double layer, which is the charge per unit area needed to counterbalance the layer charge. As a result, high electrolyte concentration was needed to compress the electrical double layer of clay minerals with high layer charge and to form gel states.

### 4.2.2 Effect of pH on structure formation of natural clay mineral dispersions

The time dependent oscillatory shear measurements were applied on both natural clay mineral dispersions introduced here at  $\text{pH} < \text{pH}_{\text{PZC,edge}}$  and  $\text{pH} > \text{pH}_{\text{PZC,edge}}$  to see the pH effect on structure formation. Below  $\text{pH}_{\text{PZC,edge}}$  the positively charged edges of clay mineral layers can interact with the negative basal surface of layers, however, EF coagulation does not take place in the absence of electrolytes or at lower ionic strength due to the long range electrostatic repulsion emerging from negatively charged faces of the clay mineral layers (Secor & Radke 1985; Tombácz & Szekeres 2004). As discussed above, both natural clay mineral dispersions show slower glass formation than gel formation, similar as Laponite® samples (Figure 27). Moreover, the previous chapter 4.1.2 indicated that the EF structure forms faster than FF structure in dilute colloidal Laponite® dispersions.

Increasing pH of the weak gel sample with 5 wt% SHCa-0.2Na and  $10^{-3}$  M NaCl from its inherent  $\text{pH}=8.8$ , which is lower than the  $\text{pH}_{\text{PZC,edge}}$  of hectorite clay minerals, to  $\text{pH}=12$  results in an increase in electrolyte concentration in the aqueous phase and negative charges occur at the layer edges. Accordingly, FF coagulation is assumed to occur at  $\text{pH}=12$  whereas EF contacts should prevail at  $\text{pH}=8.8$  for SHCa-0.2Na dispersion. The time evolution of  $G'$  and  $G''$  at both pH values is shown in Figure 28a. Obviously, the gel at  $\text{pH}=8.8$  forms much faster than the gel at  $\text{pH}=12$ , indicating that the EF based structure forms much faster than the FF structure, similar as previously observed for Laponite® dispersions.

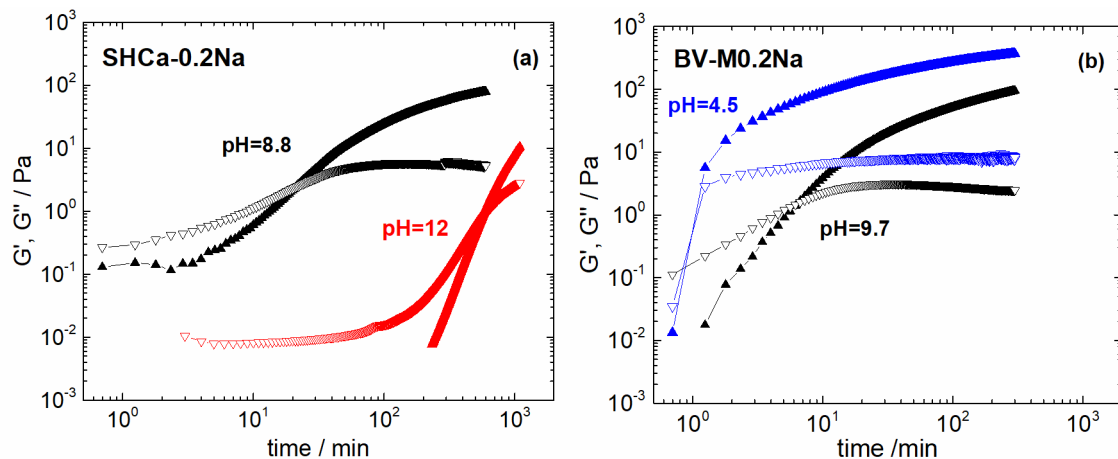


**Figure 28.** Effect of pH on kinetics of structure formation for **a)** 5 wt% SHCa-0.2Na dispersion with  $10^{-3}$  M added NaCl and **b)** 5 wt% BV-M0.2Na dispersion with  $10^{-1}$  M NaCl concentration. Filled up-triangle =  $G'$ , empty down-triangle =  $G''$ . Black color represents samples at their inherent pH, red and blue colors represent higher and lower set pH than corresponding  $\text{pH}_{\text{PZC,edge}}$ , respectively.

Because of the higher inherent  $\text{pH}=9.7$  of BV-M0.2Na dispersions than its  $\text{pH}_{\text{PZC,edge}}=6.5$ , attractive gel structure occurred at high ion concentration ( $10^{-1}$  M) predominantly based on FF contacts. As can be seen from Figure 28b,  $\text{pH}=4.5$  ( $< \text{pH}_{\text{PZC,edge}}$ ) the 5 wt% BV-M0.2Na dispersion with  $10^{-1}$  M NaCl built an arrested gel state presumably based on EF contacts distinctly and faster than the same sample at  $\text{pH}=9.7$  in gel state with prevailing FF structure again in line with the previous results for Laponite® reported in the first part of discussion and in accordance with Yariv and Cross (1979).

### 4.2.3 Aging of natural clay mineral dispersions in different arrested states

The aging of clay mineral dispersions corresponds to a perpetual re-arrangement of clay mineral layers and re-organization of the overall gel or glass structure. This shows up, e.g. in a monotonic increase of the storage modulus over time, which was monitored over a long time period for two natural clay mineral systems introduced here at their inherent pH. This aging phenomenon for natural clay mineral dispersions can already be seen from the transient  $G'$  data shown in Figure 27 covering a time interval of about one day. Previously the aging of

Laponite® dispersions as a self-delaying process was discussed in chapter 4.1.3. There an increase of  $G'$  over several weeks following a power law  $G' \sim t^\alpha$  with  $\alpha = 0.11 \pm 0.03$  for attractive strong gel state,  $\alpha = 0.74 \pm 0.01$  for glass state as well as  $\alpha = 0.36 \pm 0.01$  for weak gels was reported. Here the aging phenomenon in natural clay mineral dispersions has been studied using shear modulus measurements. The fixed frequency amplitude sweep oscillatory shear experiments were performed at time intervals of one week covering a total time period of up to 8 weeks. In between measurements, samples were stored in tightly sealed vials to avoid any loss of solvent. Figure 29 compares the time evolution of the normalized storage modulus  $G'_{norm} = G'(t_{storage})/G'(t_{storage} = 0)$  for natural clay mineral dispersions at their inherent pH.

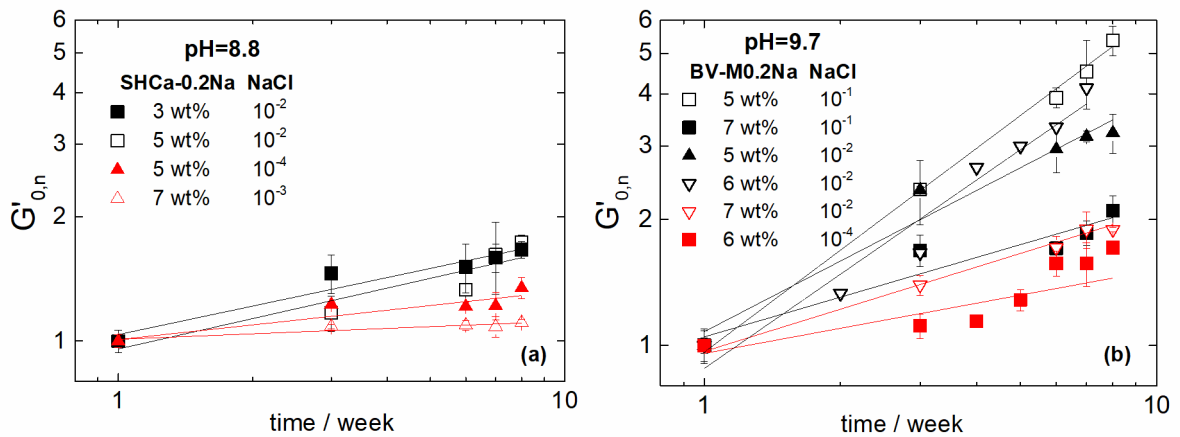


**Figure 29.** Normalized plateau moduli as a function of aging time for **a)** SHCa-0.2Na and **b)** BV-M0.2Na dispersions at various solids content and NaCl concentrations at their inherent pH of 8.8 and 9.7, respectively. Black and red colors represent the gel and glass arrested states of corresponding clay mineral dispersion, respectively.

Since the inherent pH of natural hectorite (SHCa-0.2Na) dispersions is lower than  $pH_{PZC,edge}$ , these samples with high ion concentration immediately form gel structure (see Figure 27b) with EF contacts and show a weak increase of  $G' \sim t^\alpha$  with  $\alpha = 0.24 \pm 0.01$  over 8 weeks aging time (Figure 29a). The SHCa-0.2Na dispersions with low ion concentration slowly building glass

structures do not show substantial aging over a time period of 8 weeks with  $\alpha$  values of  $0.11 \pm 0.01$  and  $0.06 \pm 0.03$ , respectively. Arrested BV-M0.2Na samples generally show stronger aging than the SHCa-0.2Na dispersions but again aging is less pronounced in the glass state compared to the gel state. These results are obviously in clear contrast to the previous findings for Laponite® (see Figure 21). This might be related to a slower more gradual structure formation of the natural clay mineral dispersions in the glass state whereas Laponite® dispersions exhibit a fast increase in shear modulus after an extended induction time (see Figure 27a).

#### 4.2.4 State diagram of clay mineral dispersions at their inherent pH

The rheological state diagrams for Laponite®, SHCa-0.2Na and BV-M0.2Na dispersions at their inherent pH were created on the basis of the values derived from the rotational and oscillatory shear experiments during 8 weeks. The main criterion for designating the approximate limit of arrested states in state diagram of clay mineral dispersions is the kinetics of structure formation in Figure 27. Because the clay mineral dispersions with low solids and electrolyte concentration need long time to form an arrested state, the sample aging was analyzed over a long period of time, i.e. 8 weeks, using shear modulus measurements (Figures 10, 20 and 28). The electrolyte concentration of the dispersion is decisive for the formation of attractive or repulsive forces dominated gel or glass states, whereas the pH of dispersions has an influence on the type of prevailing layer contacts in attractive gel state. We have to bear in mind that inherent pH of Laponite® and SHCa-0.2Na dispersions are lower and pH of BV-M0.2Na dispersion is higher than their  $\text{pH}_{\text{PZC,edge}}$ . But, at very low electrolyte concentration or in the absence of salt, long range electrostatic repulsion originating from negative face charges dominate irrespective of pH and hence so-called repulsive glass states form. The estimated state diagrams of synthetic and natural clay minerals dispersions used in this study are shown in Figure 30.

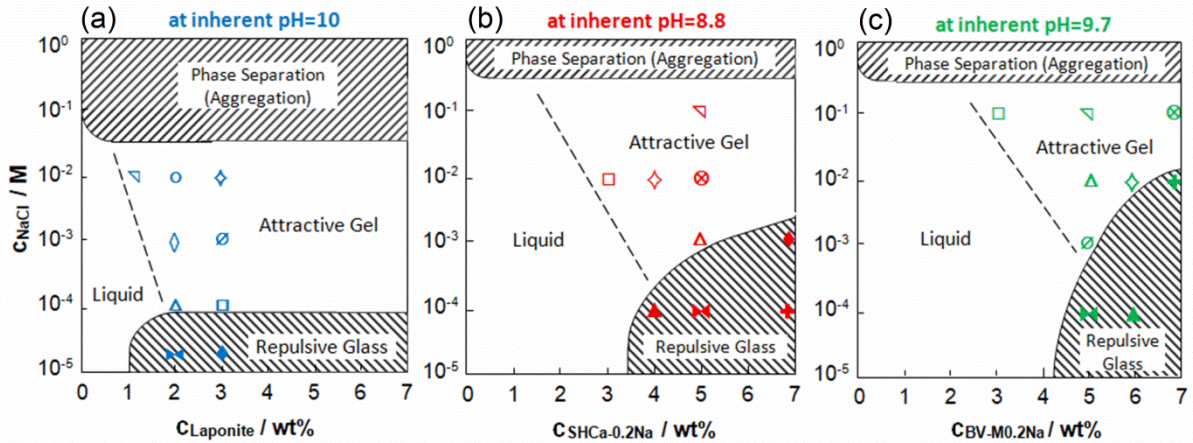


**Figure 30.** Estimated state diagrams **a)** for Laponite® dispersion from Tanaka et al. (2004) with blue symbols correspond the measured samples **b)** for SHCa-0.2Na dispersion with red symbols correspond the measured samples and **c)** for BV-M0.2Na dispersion with green symbols correspond the measured samples. All samples were analyzed using rotational and oscillatory shear rheometry during 8 weeks aging time.

The estimated areas of arrested states in state diagram for Laponite® dispersion are in excellent agreement with the early findings of Tanaka et al. (2004) and Ruzicka and Zaccarelli (2011). The lower limit of solids needed to get arrested states of natural clay mineral dispersions is shifted to higher values compared to Laponite® and the transition from the repulsive glass to the attractive gel state occurs at higher NaCl concentration due to their larger layer size and layer charge. The estimated line between liquid and gel state for Laponite® dispersions at  $10^{-2}$  M NaCl concentration is near to 1 wt% solids content (Figure 30a), while for the natural smectite samples this transition shifted to higher solids concentrations, between 2 and 3 wt% for SHCa-0.2Na (Figure 30b) and between 3 and 4 wt% for BV-M0.2Na (Figure 30c). The maximum amount of NaCl for a stable dispersion is around  $5 \times 10^{-2}$  M NaCl for Laponite® and for natural smectites this value increase by one order of magnitude to about  $5 \times 10^{-1}$  M NaCl.

### 4.2.5 Broad bandwidth linear viscoelastic response of natural clay mineral dispersions with different aspect ratio

The bulk oscillatory shear and squeeze flow rheometry were combined with DWS microrheology to capture relaxation behavior in arrested natural clay mineral dispersions covering the frequency range from  $6 \times 10^{-3}$  to  $3 \times 10^6$  rad/s. Data obtained with these different techniques are shown for SHCa-0.2Na and for BV-M0.2Na dispersions with various solids and NaCl concentration in Figure 31a-b and obviously agree very well. A frequency independent  $G' \gg G''$  at low frequencies is a typical feature for all kinds of gels and here is found in the frequency range up to  $\omega \approx 100$  rad/s typically covered by oscillatory shear rheometry. However, the absolute value of  $G'$  increases with increasing clay mineral and ion concentration (Figure 31a-b).  $G'$  is essentially constant over large frequency range for viscoelastic samples, e.g. for natural clay mineral dispersions as shown in Figure 31 and for Laponite® dispersions as obtained in previous section 4.1.4 in this study. The same behavior has been observed for other natural clay mineral dispersions (Paineau et al. 2011b) and gibbsite colloidal dispersion (Mourad et al. 2009).

The frequency dependence of the loss modulus of Laponite® dispersions in the high frequency range  $\omega > 10^4$  rad/s is well described by a power law  $G'' \sim \omega^\beta$ ,  $\beta = 0.75 \pm 0.03$ . This exponent as well as the absolute values of  $G''$  for Laponite® dispersions are independent of pH and initial salt concentration within experimental uncertainty, see Figure 22. For SHCa-0.2Na and BV-M0.2Na dispersions similar power law dependence of  $G''$  with  $\beta = 0.72 \pm 0.03$  and  $\beta = 0.74 \pm 0.01$  at high frequencies, respectively, and a slight variation in absolute values with clay mineral and salt concentration were found, see Figure 31a-b.

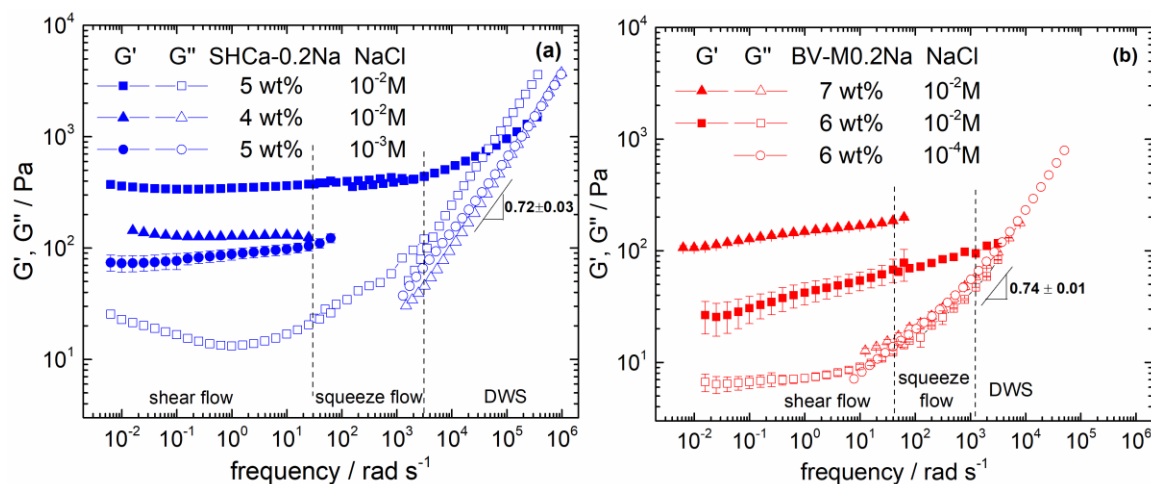


**Figure 31.** Linear viscoelastic storage modulus and loss modulus **a)** for SHCa-0.2Na and **b)** for BV-M0.2Na dispersions at their  $pH_{inh}$ . The broad frequency range was covered with the help of small amplitude oscillatory shear flow, squeeze flow and DWS experiments. All experiments were performed on 8 weeks old samples.

The linear viscoelastic response of these synthetic and natural clay mineral dispersions was compared plotting the mechanical loss factor  $\tan \delta = G''/G'$  over frequency. Accordingly, a high loss factor indicates predominantly viscous stress relaxation. For the comparison we used the 8 weeks old attractive gel samples of 2 wt% Laponite®, 5 wt% SHCa-0.2Na and 6 wt% BV-M0.2Na dispersions with  $10^{-2}$  M NaCl at their inherent pH, results are shown in Figure 32.

Natural hectorite differs only slightly from Laponite® showing similar trend of  $\tan \delta$  over a large frequency range. In both cases  $\tan \delta$  starts around 0.1 at low frequencies and strongly increases for  $\omega > 10^2$  rad/s. For BV-M0.2Na dispersion, the shape of the  $\tan \delta$  vs.  $\omega$  curve is similar but the absolute values of  $\tan \delta$  are about a factor of 3-4 higher than for the other two samples. This means that the BV-M0.2Na dispersion in its gel state has a less perfect network structure allowing for more viscous stress relaxation than natural and synthetic gel like hectorite dispersions (Figure 32). We should also keep in mind that at high ion concentration the BV-M0.2Na dispersion at its  $pH_{inh}$  is supposed to have FF layer contacts, whereas the two hectorites samples presumably have EF layer contacts at their  $pH_{inh}$ .

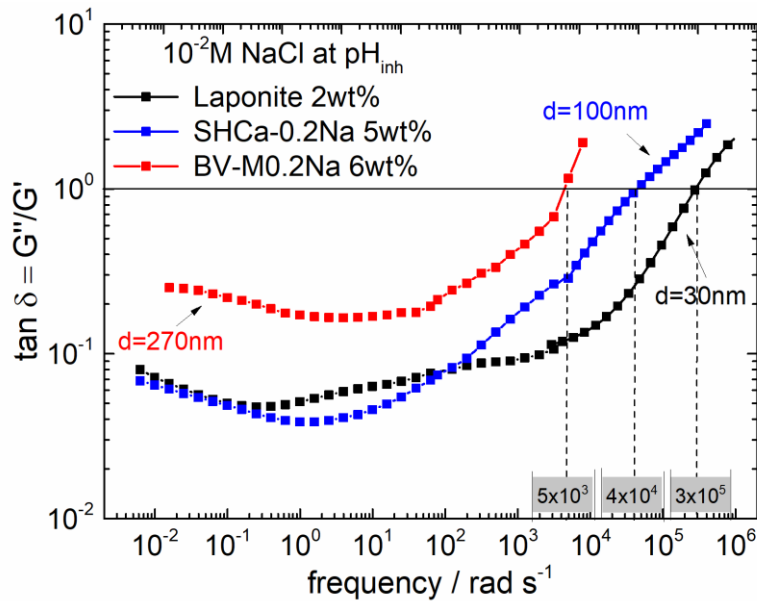


**Figure 32.** The ratio of linear viscoelastic storage modulus ( $G'$ ) and loss modulus ( $G''$ ) of 2 wt% Laponite® (black line), 5 wt% SHCa-0.2Na (blue line) and 6 wt% BV-M0.2Na (red line) dispersions with  $10^{-2}$  added NaCl at their corresponding inherent pH over broad frequency range. All experiments were performed on 8 weeks old samples.

At low frequencies  $G'$  dominates and is essentially frequency independent. At high frequencies  $G''$  strongly increases with frequency according to a universal power law  $\beta = 3/4$  and its absolute value is almost independent of electrolyte and solids concentration. Consequently, there is a crossover of  $G'$  and  $G''$ , i.e.  $\tan \delta = 1$  at a characteristic frequency  $\omega_c$ , and this  $\omega_c$  varies with sample composition. For Laponite®, this characteristic frequency was found  $6 \times 10^4 < \omega_c < 3 \times 10^5$  rad/s, for SHCa-0.2Na  $1 \times 10^4 < \omega_c < 5 \times 10^4$  rad/s and for BV-M0.2Na  $1 \times 10^3 < \omega_c < 5 \times 10^3$  rad/s. Apparently, this crossover frequency range is a clay mineral specific feature and decreases with increasing layer size, i.e. aspect ratio of clay mineral layer.

### 4.2.6 Microstructures of natural clay mineral dispersions

Optical MPT was applied using spherical fluorescent tracer particles of different size between 1 and 0.2  $\mu\text{m}$  to see microstructural differences in arrested states of natural clay mineral dispersions with different layer size. For this purpose, we analyzed 5 wt% SHCa-0.2Na (layer size=100nm) dispersion with  $10^{-3}$  M added

NaCl as a weak gel, 5 wt% BV-M0.2Na (layer size=270 nm) dispersion with  $10^{-1}$  M NaCl as a strong gel and 7 wt% BV-M0.2Na in  $10^{-2}$  M NaCl aqueous solution as glass sample (Figure 33). Brownian motion of at least 150 tracer particles embedded in clay mineral dispersions was monitored simultaneously to characterize the change in viscoelasticity and local particle dynamics during formation of arrested states. From the particle positions in subsequent video images the mean square displacement  $MSD(\tau)$  of each particle is obtained as a function of lag time  $\tau$  and finally the average  $MSD(\tau)$  obtained in a single experiment is calculated. The generalized Stokes-Einstein equation (Eq. 4.1) has been used to calculate  $G'$  and  $G''$  data from the MSD as a function of frequency. Here, structure build-up is characterized via the change in  $G'$  and  $G''$  taken at fixed frequency  $\omega = 0.6$  rad/s over waiting time. Corresponding data are shown in Figure 33 and for comparison results from mechanical rheometry are also included.

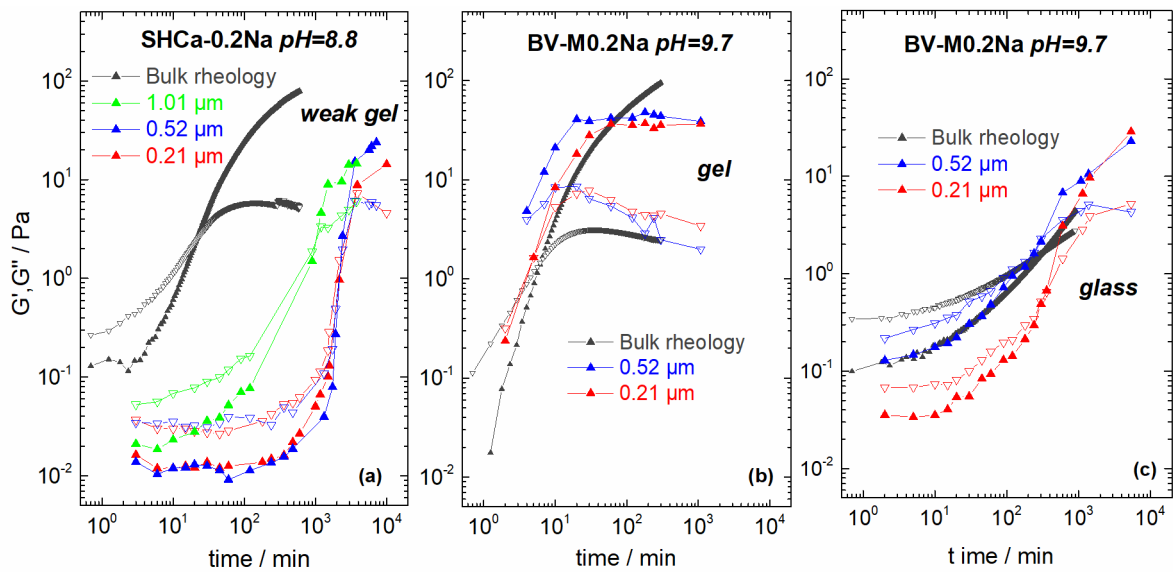


**Figure 33.** **a)** Weak gel structure with prevailing EF; viscoelastic moduli as a function of time for 5 wt% SHCa-0.2Na in  $10^{-3}$  M NaCl at pH=8.8. **b)** Gel structure with prevailing FF; viscoelastic moduli as a function of time for 5 wt% BV-M0.2Na in  $10^{-1}$  M NaCl at pH=9.7. **c)** Glass structure; viscoelastic moduli as a function of time for 7 wt% BV-M0.2Na in  $10^{-2}$  M NaCl aqueous solution at pH=9.7.  $G'$  (up-triangle) and  $G''$  (down-triangle).

## Results and Discussion

---

Despite some deviations in absolute modulus values the characteristic crossover times  $t_c$  obtained from MPT using 0.21  $\mu\text{m}$  and 0.52  $\mu\text{m}$  tracer particles as well as bulk rheometry agree very well for BV-M0.2Na dispersion at pH=9.7 in the strong gel state ( $10^{-1}$  M NaCl) with its prevailing FF contacts in contrast to Laponite® dispersion in the gel state. No such refinement is found for BV-M0.2Na dispersion in the glass state similar to what has been observed in the previous section for Laponite® dispersions in the glass state (see Figure 24).

A completely different scenario is observed for the 5 wt% SHCa-0.2Na dispersion with  $10^{-3}$  M NaCl which is considered to be a weak gel predominantly built up from EF contacts. In this case the network formation is substantially delayed on the microscale compared to the bulk and the corresponding  $t_c$  values from MPT data are about two orders of magnitude larger than the one obtained from bulk rheometry. For the small 0.21  $\mu\text{m}$  and 0.52  $\mu\text{m}$  tracer particles gelation occurs even later than probed by the 1.01  $\mu\text{m}$  particles. So even long after a macroscopic gel state is formed the sample is still in a sol state on the microscale, i.e. a structural refinement takes place qualitatively consistent with the fractal network model proposed by Pignon et al. (1997). Similar results were previously found for Laponite® dispersion in a weak gel state but with FF contacts prevailing, see Figure 24c. In that case, however, the shift in gelation or crossover-time was only one order of magnitude.

## 5 Conclusion

### 5.1 Summary

Firstly, we have investigated structure formation and aging of Laponite® dispersions in different arrested states. By varying clay mineral content (1-3 wt%), electrolyte concentration (up to  $10^{-2}$  M NaCl) and pH (8.5, 10, 12) glasses, strong gels and weak gels with different layer contacts were formed for Laponite® dispersions. Additional insight into structural refinement and sample heterogeneities on a length scale  $0.2 \mu\text{m} - 1 \mu\text{m}$  was obtained from MPT experiments. High frequency linear viscoelastic response of arrested dispersions was determined using oscillatory squeeze flow mechanical rheometry and DWS optical microrheology.

After that, based on same macro- und microrheological measurements we have studied formation and aging of arrested states of natural di- and tri-octahedral smectite dispersions in comparison to the synthetic hectorite Laponite® (trioctahedral smectites). The natural clay minerals used in this study are natural hectorites (SHCa-0.2Na, trioctahedral smectites), and montmorillonite (BV-M0.2Na, dioctahedral smectite) with different aspect ratio and octahedral structure.

This study covered a broad range of natural clay mineral content (up to 7 wt%) and NaCl concentration (up to  $10^{-1}$  M) as well as pH above and below the respective  $\text{pH}_{\text{PZC,edge}}$ . Below this critical pH EF contacts among clay mineral layers are assumed to prevail whereas FF contacts should be preferred above  $\text{pH}_{\text{PZC,edge}}$ , similar as in the Laponite® system.

Formation of arrested states was characterized by the time  $t_c$  at which  $G' = G''$  at a fixed frequency. For a given clay mineral content strong attractive gels (high salt concentration) form much faster than weak gels (low salt concentration), and particularly the repulsive glass state (no added salt). Gels assumed to have preferred EF layer contacts at  $\text{pH} < \text{pH}_{\text{PZC,edge}}$  are stronger and are created much faster than gels with same layer content supposed to have prevailing FF contacts at  $\text{pH} > \text{pH}_{\text{PZC,edge}}$ . For Laponite® dispersions aging is much more pronounced for

## Conclusion

---

repulsive glasses than for attractive gels. For all strong gels of Laponite® dispersions  $G'$  increases only weakly for times  $t \gg t_c$  according to a power law  $G' \sim t^\alpha$  with  $\alpha = 0.11 \pm 0.03$ . For the repulsive glasses with 2 wt% Laponite®  $\alpha \approx 0.74 \pm 0.03$  is found and the exponent for the weak gels ( $\alpha \approx 0.36 \pm 0.01$ ) is in between.

Based on the rheological data of aged samples, state diagrams for the natural and synthetic clay minerals at their inherent pH have been established revealing that the clay mineral content required to form arrested states increases with increasing clay mineral layer diameter and higher salt concentrations are required to form attractive gel states of natural clay mineral dispersions due to their higher layer charge compared to Laponite®. Like in Laponite® system, gel formation takes place much faster than the transition from the sol to the repulsive glass state and attractive gels at  $\text{pH} < \text{pH}_{\text{PZC, edge}}$  form distinctly faster than at  $\text{pH} > \text{pH}_{\text{PZC, edge}}$  for natural clay mineral dispersions.

Aging has been studied at inherent pH of the respective natural clay mineral dispersions for a period of 8 weeks and turned out to be less pronounced for SHCa-0.2Na with  $\text{pH}_{\text{inh}} = 8.8 < \text{pH}_{\text{PZC, edge}} = 11$  compared to the arrested BV-M0.2Na dispersions with  $\text{pH}_{\text{inh}} = 9.7 > \text{pH}_{\text{PZC, edge}} = 6.5$ . In both cases aging is weaker in the glass state than for the investigated gels and was hardly detectable for the SHCa-0.2Na samples. These findings are in contrast to the strong aging observed for Laponite® in its repulsive glass state at  $\text{pH}_{\text{inh}} = 10 < \text{pH}_{\text{PZC, edge}} = 11$ . This might be related to the larger layer size distribution of natural clay minerals than Laponite®.

As typical for all kinds of materials in arrested states, the glass or gel-like clay mineral dispersions exhibit a constant value of  $G' \gg G''$  in the frequency range up to  $\omega = 100$  rad/s and the absolute modulus values increase with increasing clay mineral and ion concentration. At high frequencies a power law dependence  $G'' \sim \omega^\beta$  with  $\beta = 0.75 \pm 0.03$  for Laponite® dispersions,  $\beta = 0.72 \pm 0.03$  and  $\beta = 0.74 \pm 0.01$  for SHCa-0.2Na and BV-M0.2Na systems, respectively, was observed and the absolute values vary only weakly with clay mineral and salt concentration as well as pH. Consequently, the characteristic crossover

frequency  $\omega_c$  ( $G' = G''$ ) varies in a certain range depending on sample composition. However, the range of  $\omega_c$  values found for these natural clay mineral and Laponite® is distinctly different. For natural clay mineral dispersions this characteristic crossover occurs at lower frequencies than for Laponite® dispersions, i.e.  $\omega_c$  decreases with increasing layer size.

MPT data reveal a structural refinement on the sub-micrometer length-scale going on during aging, i.e. when the bulk modulus weakly increases and the characteristic crossover time  $t_c$  indicating structure formation increases with decreasing size of the tracers probing their viscoelastic environment. No such refinement is found in glass systems for Laponite® dispersions. This refinement is existent for weak or strong gels with EF or FF structure and most pronounced for weak gels at  $\text{pH}_{\text{inh}}$ . A pronounced structural heterogeneity occurs during formation of attractive gels as well as repulsive glasses, i.e. around  $t \approx t_c$ , this transient heterogeneity is most pronounced for the Laponite® gels with the EF structure formed at pH 8.5. At times  $t \gg t_c$  all arrested states appear homogenous on the length scale of 0.2  $\mu\text{m}$  for Laponite® system.

The kinetics of arrested state formation of natural clay mineral dispersions as obtained from bulk rheometry and MPT microrheology were compared. Crossover times  $t_c$  ( $G' = G''$ ) obtained with both methods agree very well for the BV-M0.2Na dispersions forming a glass or a strong gel (with FF contacts prevailing). Similar behavior was observed for Laponite® dispersions in the glass state. However, for the SHCa-0.2Na dispersion forming a weak gel primarily based on EF contacts gelation is delayed on the microscopic scale and  $t_c$  is shifted by about two orders of magnitude compared to bulk measurements, i.e. a structural refinement takes place long after the gel has formed on the macroscale. Qualitatively, this is in line with previous findings for Laponite® gels (but with FF contacts prevailing) and the fractal network model proposed by Pignon et al. (1997).

### 5.2 Outlook

The broad range of rheological comparison between natural and synthetic clay minerals corresponding their different octahedral structure, lateral layer size and layer charge represented in this study can shed new insight and perspective for optimizing of clay mineral dispersions in various fields of application and different processing techniques as well as for understanding the complex structure of plate-like charged particle systems.

Synthetic trioctahedral smectite Laponite® has been used as model system for most of natural clay minerals. Special attention should be paid to not use wrong model system for molecular simulation. For example, Laponite® should not be used as model system for Na-exchanged montmorillonite system, because most of their physicochemical properties, e.g. structural chemistry, layer charge distribution, lateral dimension and  $\text{pH}_{\text{PZC,edge}}$ , are different. At their corresponding  $\text{pH}_{\text{inh}}$  and at high electrolyte concentration the gel state of BV-M0.2Na dispersions have FF layer structure but Laponite® dispersions in gel state have EF layer structure, which has more heterogeneous microstructure than FF layer association. The  $\text{pH}_{\text{inh}}$  of BV-M0.2Na dispersions is higher than its  $\text{pH}_{\text{PZC,edge}}$  but Laponite® dispersions have lower  $\text{pH}_{\text{inh}}$  than its  $\text{pH}_{\text{PZC,edge}}$ .

As seen in this study, pH and electrolyte concentration have the significant effect on the rheological behavior of smectite dispersions. It could be very useful for geological application to be able to present a ternary phase diagram of clay mineral dispersions as a function of pH, solids and electrolyte concentrations considering the sample aging. For such a ternary phase diagram, the samples must be prepared in a certain steps of each control parameters. In this study, the samples were prepared only at three different pH; at their inherent pH, lower and higher pH than their  $\text{pH}_{\text{PZC,edge}}$ .

For most of clay mineral applications, it is very important to understand the complex flow behavior of dispersions, e.g. viscoelastic response at high frequency, structure deformation under strain, and structure rebuilding at rest, which are clarified in this study. But, in most processing operations the deformations can be large and rapid and it causes a nonlinear material property

that controls the system response. The nonlinear viscoelastic behavior of complex clay mineral dispersions could be investigated and quantified using Large Amplitude Oscillatory Shear (LAOS) (Yang et al. 2012).

For a further characterization of microstructural inhomogeneity of clay mineral dispersions in repulsive glass and attractive gel states, active microrheology could be applied (Rich et al. 2011a). In the passive measurements the dynamics of the embedded probes due to thermal motion is measured to obtain the viscoelastic response of the material, while in the active measurements, the response of probe particles to a known force, e.g. imposed by external magnetic or electric fields, is detected. By using active microrheology like magnetic tweezer, after local destroying in the clay mineral dispersions their complex microstructure might be understand more thoroughly.

Microstructural inhomogeneity is strongly influenced by layer interactions. Visualization of the layer contacts in aqueous medium is another important research area for clay mineral dispersions (Zbik et al. 2014). The pH dependent clay layer contacts could be monitored using cryogenic transmission electron microscope (Cryo-TEM).

## 6 List of Figures

- Figure 1. Building blocks of layer silicate minerals a) tetrahedral sheet b) trioctahedral sheet c) dioctahedral sheet d) an oblique view of a sheet sandwich (=layer), formed by two tetrahedral sheets bonded to an octahedral sheet e) a schematic representation of the layer in d) (web course materials [www.open.edu](http://www.open.edu), modified). .. 2
- Figure 2. Representation of the layer structure of the three-layer clay minerals (2: 1 layer silicates). The blue tetrahedrons represent the position of the  $[\text{SiO}_4]$ -tetrahedral sheet, the yellow octahedrons represent the  $[\text{Me}(\text{O},\text{OH})_6]$ -octahedral sheet. Depending on the clay mineral, the octahedral coordinated metal ions (yellow spheres) can be replaced by metal ions of different valence. Between the layers are counter-ions  $\text{Me}^{v+}$  (gray spheres) bound (ChemTube3D, University of Liverpool, [www.chemtube3d.com](http://www.chemtube3d.com), modified). ..... 3
- Figure 3. Swelling and complete delamination of clay mineral layers in aqueous dispersion. During dispersion, water or weak electrolyte solution is used to expand the distance between the individual plates. The  $\text{Na}^+$  ions are hydrated through water storage in the interlayers..... 4
- Figure 4. Development of surface charge heterogeneity on montmorillonite particles dispersed in aqueous solutions due to permanent negative charges on faces and surface pH-dependent charges on edges (Tombácz & Szekeres 2004, modified).... 6
- Figure 5. The diffuse electrical double layer showing the decay of potential away from the surface in fresh and saline water (Schramm 2006). ..... 9
- Figure 6. Two plate-like clay mineral layers approached to a separation distance,  $H$  with overlapping their diffuse double layers (Schramm 2006)..... 10
- Figure 7. Potential energy of interaction between two parallel colloidal plate-shaped particles as a function of separation distance (Luckham & Rossi 1999; Schramm 2006, modified). ..... 12
- Figure 8. Effect of electrolyte concentration and pH on surface charge and range of electrical double layer in clay mineral dispersions. Negative charges are marked in blue, positive charges in red. The different path ways of changing surface charge and electrostatic interaction are marked by arrows. The illustrations for arrested states of clay mineral dispersion in square frames were taken from Tanaka et al. (2004). ..... 14
- Figure 9. Illustration of change of kaolinite layer orientations subject to layer charges which are changing with adding NaOH or HCl into the medium (Lagaly 1989, modified)..... 16
- Figure 10. Photograph of samples in the concentration range  $0.1 \leq c_s \leq 1.2$  wt% of Laponite® at very long waiting time (about 30000 h). The sample with 1 wt% Laponite® aqueous dispersion shows evidence of a phase separation, while the

1.2 wt% gel sample remains homogeneous at all times (Ruzicka et al. 2010, modified)..... 18

Figure 11. Proposed non-equilibrium phase/state diagram for aqueous Laponite® dispersions. Various nonergodic states are possible at long aging time, depending on the ion concentration and the Laponite® concentration here given in weight % (Ruzicka & Zaccarelli 2011, modified). ..... 20

Figure 12. CEC values as a function of pH a) for natural and synthetic hectorite, SHCa-0.2Na and Laponite®, respectively. Data are submitted in Delavernhe et al. (2017, accepted) b) for Na-saturated montmorillonite BV-M0.2Na. Data are taken from Delavernhe et al. (2015)..... 28

Figure 13. Soluble structural cations of a) Laponite® and b) SHCa-0.2Na after 72 h equilibrium in dispersion (24 h without Cu-trien + 48 h after addition of Cu-trien solution). Dashed lines determined from the XRF analysis. Data are submitted in Delavernhe et al. (2017, accepted)..... 30

Figure 14. a) Types of time-independent flow behavior (Chhabra & Richardson 2008) b) Breakdown and re-formation of structure in a thixotropic dispersion (Chhabra & Richardson 2008)..... 34

Figure 15. Oscillatory shear strain ( - - ) out of phase with stress ( - ) by a phase angle  $\delta$ . ..... 36

Figure 16. a) Schematic diagram of a cone-plate geometry of a rotational rheometer with a diameter  $R$  and a cone angle  $\theta$ , b) Searle system of a rotational rheometer with rotating inner cylinder radius  $R_1$  and outer cylinder radius  $R_2$ ..... 37

Figure 17. a) Piezoelectric axial vibrator (PAV) used in this study b) longitudinal cut of the PAV c) transversal cut of PAV (Crassous et al. 2005) ..... 40

Figure 18. a) Structure formation for two arrested states of Laponite® dispersions at  $pH_{inh}=10$ . Filled up-triangle =  $G'$ , empty down-triangle =  $G''$ . b) Solids content and NaCl concentration effect on the crossover time  $t_c$  (where  $G' = G''$ ) of Laponite® dispersions..... 44

Figure 19. Effect of pH on kinetics of structure formation for a) 2 wt% Laponite® dispersion without NaCl and b) 1 wt% Laponite® dispersion at  $10^{-2}$  M NaCl concentration. Filled up-triangle =  $G'$ , empty down-triangle =  $G''$ . Blue, black and red symbols represent  $pH=8.5, 10$  and  $12$ , respectively. .... 46

Figure 20. Amplitude sweep experiments at different aging times for 2 wt% Laponite® dispersions with  $10^{-4}$  M added NaCl a) at  $pH=10$ , b) at  $pH=8.5$  and c) at  $pH=12$ . Filled up-triangle =  $G'$ , open down-triangle =  $G''$ . ..... 48

Figure 21. Normalized plateau moduli as a function of aging time for Laponite® dispersions at various solids content and NaCl concentrations at inherent pH of 10,

## List of Figures

---

- at set pH 12 and 8.5. Black, blue and red lines represent strong gel, weak gel and repulsive glass samples..... 49
- Figure 22. Linear viscoelastic a) storage modulus and b) loss modulus for 2 wt% Laponite® dispersions with and without NaCl at three pH. The broad frequency range was covered with the help of small amplitude oscillatory shear flow (square), squeeze flow (triangle) and DWS experiments (square). All experiments were performed on 8 weeks old samples..... 50
- Figure 23. a) Mean value of MSD of 0.21  $\mu\text{m}$  tracer particles embedded in a 3 wt% Laponite® dispersion with  $10^{-4}$  M NaCl at  $\text{pH}_{\text{inh}}=10$  at different waiting times. b) Frequency dependence of the storage and loss moduli of 3 wt% Laponite® dispersion with  $10^{-4}$  M NaCl on corresponding length scale (0.21  $\mu\text{m}$ ) at different waiting times. .... 52
- Figure 24. a) Glass structure; viscoelastic moduli as a function of time for 3 wt% Laponite® in deionized water at  $\text{pH}_{\text{inh}}=10$ . b) Gel structure; viscoelastic moduli as a function of time for 3 wt% Laponite® in  $10^{-4}$  M NaCl at  $\text{pH}=10$ . c) Gel structure with prevailing EF or FF; viscoelastic moduli as a function of time for 2 wt% Laponite® in  $10^{-4}$  M NaCl aqueous solution at  $\text{pH}=8.5$  (EF) and 12 (FF).  $G'$ (up-triangle) and  $G''$ (down-triangle)..... 53
- Figure 25. a) Heterogeneity ratio (HR) during sol-glass phase transition of Laponite® dispersions at  $\text{pH}=10$  measured by MPT method and using 0.21 and 0.52  $\mu\text{m}$  tracer particles b) HR during sol-gel phase transition of Laponite® dispersions at  $\text{pH}=10$  measured by MPT method and using 0.21  $\mu\text{m}$  tracer particle c) HR during phase transition of 2 wt% Laponite® in  $10^{-4}$  M NaCl aqueous solution at  $\text{pH}=8.5$  and 12 measured by MPT method and using 0.19  $\mu\text{m}$  tracer particle. The minimum HR for each tracer particle type was determined in homogeneous polymer hydrogel (Pluronic® F127) and plotted as horizontal dashed line. The phase transition point  $t_c$ , where  $G'$  and  $G''$  are equal, was marked at  $t/t_c = 1$  as vertical dotted line. .... 56
- Figure 26. Ensemble of individual MSD for simultaneously tracked tracer particles ( $d = 0.21 \mu\text{m}$ ) in a 3 wt% Laponite® dispersion with  $10^{-4}$  M NaCl at different times normalized by crossover time; a broad distributions of MSDs for the heterogeneous structure b) at  $t/t_c \approx 1$  and narrow distributions of MSDs for homogeneous structures a) at  $t/t_c \ll 1$  and c) at  $t/t_c \gg 1$  are clearly visible. .... 57
- Figure 27. Structure formation for two arrested states of a) Laponite® (the same of Figure 18a) b) SHCa-0.2Na and c) BV-M0.2Na dispersions at  $\text{pH}_{\text{inh}}=10, 8.8$  and 9.7, respectively. Filled up-triangle =  $G'$ , empty down-triangle =  $G''$ ..... 60
- Figure 28. Effect of pH on kinetics of structure formation for a) 5 wt% SHCa-0.2Na dispersion with  $10^{-3}$  M added NaCl and b) 5 wt% BV-M0.2Na dispersion with  $10^{-1}$  M NaCl concentration. Filled up-triangle =  $G'$ , empty down-triangle =  $G''$ . Black color represents samples at their inherent pH, red and blue colors represent higher and lower set pH than corresponding  $\text{pH}_{\text{PZC,edge}}$ , respectively. .... 62

- Figure 29. Normalized plateau moduli as a function of aging time for a) SHCa-0.2Na and b) BV-M0.2Na dispersions at various solids content and NaCl concentrations at their inherent pH of 8.8 and 9.7, respectively. Black and red colors represent the gel and glass arrested states of corresponding clay mineral dispersion, respectively. .... 63
- Figure 30. Estimated state diagrams a) for Laponite® dispersion from Tanaka et al. (2004) with blue symbols correspond the measured samples b) for SHCa-0.2Na dispersion with red symbols correspond the measured samples and c) for BV-M0.2Na dispersion with green symbols correspond the measured samples. All samples were analyzed using rotational and oscillatory shear rheometry during 8 weeks aging time. .... 65
- Figure 31. Linear viscoelastic storage modulus and loss modulus a) for SHCa-0.2Na and b) for BV-M0.2Na dispersions at their  $pH_{inh}$ . The broad frequency range was covered with the help of small amplitude oscillatory shear flow, squeeze flow and DWS experiments. All experiments were performed on 8 weeks old samples. .... 67
- Figure 32. The ratio of linear viscoelastic storage modulus ( $G'$ ) and loss modulus ( $G''$ ) of 2 wt% Laponite® (black line), 5 wt% SHCa-0.2Na (blue line) and 6 wt% BV-M0.2Na (red line) dispersions with  $10^{-2}$  added NaCl at their corresponding inherent pH over broad frequency range. All experiments were performed on 8 weeks old samples. 68
- Figure 33. a) Weak gel structure with prevailing EF; viscoelastic moduli as a function of time for 5 wt% SHCa-0.2Na in  $10^{-3}$  M NaCl at pH=8.8. b) Gel structure with prevailing FF; viscoelastic moduli as a function of time for 5 wt% BV-M0.2Na in  $10^{-1}$  M NaCl at pH=9.7. c) Glass structure; viscoelastic moduli as a function of time for 7 wt% BV-M0.2Na in  $10^{-2}$  M NaCl aqueous solution at pH=9.7.  $G'$ (up-triangle) and  $G''$ (down-triangle). .... 69

## 7 List of Tables

- Table 1. Physicochemical properties of synthetic and natural smectites..... 31
- Table 2. Clay mineral and NaCl concentrations in samples used in this study..... 32

# 8 References

- Abend, S. & Lagaly, G., 2000. Sol-gel transitions of sodium montmorillonite dispersions. *Applied Clay Science*, 16, pp.201–227.
- Alemdar, A. et al., 2005. Effects of polyethyleneimine adsorption on rheology of bentonite suspensions. *Colloids and Surfaces A: Physicochemical and Engineering Aspects*, 252, pp.2895–98.
- Ali, S. & Bandyopadhyay, R., 2016. Aggregation and stability of anisotropic charged clay colloids in aqueous medium in the presence of salt. *Faraday Discussions*, 186, pp.455–471.
- Arroyo, F. et al., 2000. Rheological and Electrokinetic Properties of Sodium Montmorillonite Suspensions. II.Low-Frequency Dielectric Dispersion. *Journal of Colloid and Interface Science*, 229, pp.118–122.
- Au, P.I. et al., 2015. Behaviour of laponite gels: Rheology, ageing, pH effect and phase state in the presence of dispersant. *Chemical Engineering Research and Design*, 101, pp.65–73.
- Avery, R.G. & Ramsay, J.D.F., 1986. Colloidal properties of synthetic hectorite clay dispersions. II. Light and small angle neutron scattering. *Journal of Colloid and Interface Science*, 109(2), pp.448–454.
- Awasthi, V. & Joshi, Y.M., 2009. Effect of temperature on aging and time-temperature superposition in nonergodic Laponite suspensions. *Soft Matter*, 5, pp.4991–4996.
- Baik, M.H., Cho, W.J. & Hahn, P.S., 2007. Erosion of bentonite particles at the interface of a compacted bentonite and a fractured granite. *Engineering Geology*, 91, pp.229–239.
- Barnes, A., 1997. Thixotropy. *Journal of Non-Newtonian Fluid Mechanics*, 70, pp.1–33.
- Benna, M. et al., 1999. Effect of pH on Rheological Properties of Purified Sodium Bentonite Suspensions. *Journal of Colloid and Interface Science*, 218, pp.442–455.
- Bonn, D. et al., 1998. Aging of a colloidal “Wigner” glass. *Europhysics Letters*, 45(1), pp.52–57.
- Bonn, D. et al., 2002. Laponite: aging and shear rejuvenation of a colloidal glass. *Physical Review Letters*, 89(1), p.15701.

- Bonn, D. et al., 1999. Laponite: What Is the Difference between a Gel and a Glass? *Langmuir*, 15, pp.7534–7536.
- Bosbach, D. et al., 2000. The dissolution of hectorite: In-situ, real-time observations using atomic force microscopy. *American Mineralogist*, 85(9), pp.1209–1216.
- Brandenburg, U. & Lagaly, G., 1988. Rheological properties of sodium montmorillonite dispersions. *Applied Clay Science*, 3, pp.263–279.
- Brigatti, M.F., Galan, E. & Theng, B.K.G., 2006. Chapter 2 - Structures and Mineralogy of Clay Minerals. *Developments in Clay Science*, 1, pp.19–86.
- Caruso, R.A., Susha, A. & Caruso, F., 2001. Multilayered titania, silica, and Laponite nanoparticle coatings on polystyrene colloidal templates and resulting inorganic hollow spheres. *Chemistry of Materials*, 13(2), pp.400–409.
- Chhabra, R.P. & Richardson, J.F., 2008. *Non-newtonian flow and applied rheology* 2. Edition., Oxford: Butterworth-Heinemann.
- Claire Greaves, R., Bond, S.P. & McWhinnie, W.R., 1995. Conductivity studies on modified laponites. *Polyhedron*, 14(23–24), pp.3635–3639.
- Crassous, J.J. et al., 2005. Characterization of the viscoelastic behavior of complex fluids using the piezoelastic axial vibrator. *Journal of Rheology*, 49(4), p.851.
- Crocker, J.C. & Grier, D.G., 1996. Methods of Digital Video Microscopy for Colloidal Studies. *Journal of Colloid and Interface Science*, 179, pp.298–310.
- Dawson, J.I. & Oreffo, R.O.C., 2013. Clay: New opportunities for tissue regeneration and biomaterial design. *Advanced Materials*, 25(30), pp.4069–4086.
- De Oliveira, T. & Guegan, R., 2016. Coupled Organoclay/Micelle Action for the Adsorption of Diclofenac. *Environmental Science and Technology*, 50(18), pp.10209–10215.
- Delavernhe, L. et al., 2015. Influence of mineralogical and morphological properties on the cation exchange behavior of dioctahedral smectites. *Colloids and Surfaces A: Physicochemical and Engineering Aspects*, 481, pp.591–599.
- Delavernhe, L., Pilavtepe, M. & Emmerich, K., 2017. Cation exchange capacity of natural and synthetic hectorite. *Applied Clay Science (accepted)*.

## References

---

- Delhomme, M. et al., 2010. Acid-base properties of 2:1 clays. I. modeling the role of electrostatics. *Langmuir*, 26(12), pp.9240–9249.
- Dijkstra, M., Hansen, J.P. & Madden, P.A., 1995. Gelation of a clay colloid suspension. *Physical Review Letters*, 75(11), pp.2236–2239.
- Durán, J. et al., 2000. Rheological and Electrokinetic Properties of Sodium Montmorillonite Suspensions. I. Rheological Properties and Interparticle Energy of Interaction. *Journal of Colloid and Interface Science*, 229, pp.107–117.
- Emmerich, K. et al., 2009. Clay profiling: The classification of montmorillonites. *Clays and Clay Minerals*, 57(1), pp.104–114.
- Eriksson, R. & Schatz, T., 2015. Rheological properties of clay material at the solid/solution interface formed under quasi-free swelling conditions. *Applied Clay Science*, 108, pp.12–18.
- Fossum, J.O., 1999. Physical phenomena in clays. *Physica A: Statistical Mechanics and its Applications*, 270(1), pp.270–277.
- Galamboš, M. et al., 2012. Comparative study of cesium adsorption on dioctahedral and trioctahedral smectites. *Journal of Radioanalytical and Nuclear Chemistry*, 293(3), pp.829–837.
- Ghezzehei, T. a. & Or, D., 2001. Rheological Properties of Wet Soils and Clays under Steady and Oscillatory Stresses. *Soil Science Society of America Journal*, 65, p.624.
- Giannakopoulos, E. et al., 2006. Adsorption and radical stabilization of humic-acid analogues and Pb 2+ on restricted phyllosilicate clay. *Langmuir*, 22(16), pp.6863–6873.
- Grangeon, S. et al., 2015. The influence of natural trace element distribution on the mobility of radionuclides. The example of nickel in a clay-rock. *Applied Geochemistry*, 52, pp.155–173.
- Houghton, H.A., Hasnain, I.A. & Donald, A.M., 2008. Particle tracking to reveal gelation of hectorite dispersions. *European Physical Journal E*, 25(2), pp.119–127.
- Ianni, F. et al., 2007. Aging after shear rejuvenation in a soft glassy colloidal suspension: Evidence for two different regimes. *Physical Review E*, 75(1), p.11408.
- Jabbari-Farouji, S. et al., 2012. Dynamical heterogeneity in aging colloidal

- glasses of Laponite. *Soft Matter*, 8, pp.5507–5512.
- Jabbari-Farouji, S., Atakhorrami, M., et al., 2008a. High-bandwidth viscoelastic properties of aging colloidal glasses and gels. *Physical Review E*, 78(6), p.61402.
- Jabbari-Farouji, S., Tanaka, H., et al., 2008b. Multiple nonergodic disordered states in Laponite suspensions: A phase diagram. *Physical Review E - Statistical, Nonlinear, and Soft Matter Physics*, 78(6), p.61405.
- Jabbari-Farouji, S., Wegdam, G.H. & Bonn, D., 2007. Gels and glasses in a single system: Evidence for an intricate free-energy landscape of glassy materials. *Physical Review Letters*, 99(6), p.65701.
- Janek, M. & Lagaly, G., 2001. Proton saturation and rheological properties of smectite dispersions. *Applied Clay Science*, 19, pp.121–130.
- Jasmund, K. & Lagaly, G., 1993. *Tonminerale und Tone*, Darmstadt: Steinkopff Verlag Darmstadt.
- Jönsson, B., Labbez, C. & Cabane, B., 2008. Interaction of nanometric clay platelets. *Langmuir*, 24(20), pp.11406–11413.
- Kaufhold, S. & Dohrmann, R., 2013. The variable charge of dioctahedral smectites. *Journal of Colloid and Interface Science*, 390(1), pp.225–233.
- Khandal, R.K. & Tadros, T.F., 1988. Application of viscoelastic measurements to the investigation of the swelling of sodium montmorillonite suspensions. *Journal of Colloid And Interface Science*, 125(1), pp.122–128.
- Kleshchanok, D. et al., 2012. Effects of added silica nanoparticles on hectorite gels. *Journal of Physical Chemistry B*, 116, pp.9532–9539.
- Knaebel, A. et al., 2000. Aging behavior of Laponite clay particle suspensions. *Europhysics Letter*, 52, pp.73–79.
- Kowalczyk, A., Oelschlaeger, C. & Willenbacher, N., 2015. Tracking errors in 2D multiple particle tracking microrheology. *Measurement Science and Technology*, 26(1), p.15302.
- Kroon, M., Vos, W.L. & Wegdam, G.H., 1998. Structure and formation of a gel of colloidal disks. *Physical Review E*, 57(2), pp.1962–1970.
- Labanda, J. & Llorens, J., 2008. Effect of aging time on the rheology of Laponite dispersions. *Colloids and Surfaces A: Physicochemical and Engineering Aspects*, 329, pp.1–6.

## References

---

- Lagaly, G., 1989. Principles of flow of kaolin and bentonite dispersions. *Applied Clay Science*, 4, pp.105–123.
- Lagaly, G. & Ziesmer, S., 2003. Colloid chemistry of clay minerals: The coagulation of montmorillonite dispersions. *Advances in Colloid and Interface Science*, 100–102, pp.105–128.
- Laribi, S. et al., 2005. Comparative yield stress determination for pure and interstratified smectite clays. *Rheologica Acta*, 44, pp.262–269.
- Larson, R., 1999. *The structure and rheology of complex fluids*, New York: Oxford University Press Inc.
- Lee, S.M. & Tiwari, D., 2012. Organo and inorgano-organo-modified clays in the remediation of aqueous solutions: An overview. *Applied Clay Science*, 59–60, pp.84–102.
- Levitz, P. et al., 2000. Liquid-solid transition of Laponite suspensions at very low ionic strength: Long-range electrostatic stabilisation of anisotropic colloids. *Europhysics Letters*, 49(5), pp.672–677.
- Lifshitz, I.M. & Slyozov, V.V., 1961. The kinetics of precipitation from supersaturated solid solutions. *Journal of Physics and Chemistry of Solids*, 19(1), pp.35–50.
- Loiseau, A. & Tassin, J., 2006. Model Nanocomposites Based on Laponite and Poly (ethylene oxide): Preparation and Rheology Model Nanocomposites Based on Laponite and Poly ( ethylene oxide ): Preparation and Rheology. *Macromolecules*, (39), pp.9185–9191.
- Loring, J.S. et al., 2012. In situ molecular spectroscopic evidence for CO<sub>2</sub> intercalation into montmorillonite in supercritical carbon dioxide. *Langmuir*, 28, pp.7125–8.
- Luckham, P.F. & Rossi, S., 1999. The colloidal and rheological properties of bentonite suspensions. *Advances in Colloid and Interface Science*, 82, pp.43–92.
- Madejová, J. et al., 1998. Comparative FT-IR study of structural modifications during acid treatment of dioctahedral smectites and hectorite. *Spectrochimica Acta Part A: Molecular and Biomolecular Spectroscopy*, 54(10), pp.1397–1406.
- Mason, T.G. & Weitz, D.A., 1995. Optical measurements of frequency-dependent linear viscoelastic moduli of complex fluids. *Physical Review Letters*, 74(7), pp.1250–1253.

- Meier, L.P. & Kahr, G., 1999. Determination of the cation exchange capacity (CEC) of clay minerals using the complexes of copper(II) ion with triethylenetetramine and tetraethylenepentamine. *Clays and Clay Minerals*, 47(3), pp.386–388.
- Meunier, A., 2005. *Clays*, Springer Science & Business Media.
- Michot, L.J. et al., 2006. Liquid-crystalline aqueous clay suspensions. *Proceedings of the National Academy of Sciences*, 103(44), pp.16101–16104.
- Michot, L.J. et al., 2004. Phase diagrams of wyoming Na-montmorillonite clay. Influence of particle anisotropy. *Langmuir*, 20(25), pp.10829–10837.
- Missana, T. & Adell, A., 2000. On the Applicability of DLVO Theory to the Prediction of Clay Colloids Stability. *Journal of Colloid and Interface Science*, 230, pp.150–156.
- Mohanty, R.P. & Joshi, Y.M., 2016. Chemical stability phase diagram of aqueous Laponite dispersions. *Applied Clay Science*, 119, pp.243–248.
- Mongondry, P., Tassin, J.F. & Nicolai, T., 2005. Revised state diagram of Laponite dispersions. *Journal of Colloid and Interface Science*, 283(2), pp.397–405.
- Mori, Y., Togashi, K. & Nakamura, K., 2001. Colloidal properties of synthetic hectorite clay dispersion measured by dynamic light scattering and small angle X-ray scattering. *Advanced Powder Technology*, 12(1), pp.45–59.
- Morrison, F. a, 2001. *Understanding Rheology*. Oxford University Press, pp.387–394.
- Mourad, M.C.D. et al., 2009. Sol - Gel Transitions and Liquid Crystal Phase Transitions in Concentrated Aqueous Suspensions of Colloidal Gibbsite Platelets. *Journal of Physical Chemistry B*, 113, pp.11604–11613.
- Mourad, M.C.D. et al., 2008. Structure of the repulsive gel/glass in suspensions of charged colloidal platelets. *Journal of Physics: Condensed Matter*, 20(49), p.494201.
- Mourchid, A. et al., 1998. On Viscoelastic, Birefringent, and Swelling Properties of Laponite Clay Suspensions: Revisited Phase Diagram. *Langmuir*, 14(17), pp.4718–4723.
- Mourchid, A. et al., 1995a. Phase Diagram of Colloidal Dispersions of Anisotropic

## References

---

- Charged Particles: Equilibrium Properties, Structure, and Rheology of Laponite Suspensions. *Langmuir*, 11(6), pp.1942–1950.
- Mourchid, A., Delville, A. & Levitz, P., 1995b. Sol-gel transition of colloidal suspensions of anisotropic particles of laponite. *Faraday Discussions*, 101, pp.275–285.
- Nicolai, T. & Cocard, S., 2000. Light scattering study of the dispersion of laponite. *Langmuir*, 16(21), pp.8189–8193.
- Nicolai, T. & Cocard, S., 2001. Structure of gels and aggregates of disk-like colloids. *European Physical Journal E*, 5, pp.221–227.
- Norrish, K., 1954. The swelling of montmorillonite. *Discussions of the Faraday Society*, 18, pp.120–134.
- Odriozola, G., Romero-Bastida, M. & Guevara-Rodríguez, F.D.J., 2004. Brownian dynamics simulations of Laponite colloid suspensions. *Physical Review E*, 70, pp.1–15.
- Oelschlaeger, C. et al., 2009. Linear-to-Branched Micelles Transition: A Rheometry and Diffusing Wave Spectroscopy (DWS) Study. *Langmuir*, 25, pp.716–723.
- Okamoto, M. et al., 2001. A House of Cards Structure in Polypropylene/Clay Nanocomposites under Elongational Flow. *Nano Letters*, 1(6), pp.295–298.
- Oppong, F.K., Coussot, P. & De Bruyn, J.R., 2008. Gelation on the microscopic scale. *Physical Review E*, 78(2), pp.1–10.
- Paineau, E., Bihannic, I., et al., 2011a. Aqueous suspensions of natural swelling clay minerals. 1. structure and electrostatic interactions. *Langmuir*, 27(9), pp.5562–5573.
- Paineau, E., Michot, L.J., et al., 2011b. Aqueous suspensions of natural swelling clay minerals. 2. Rheological characterization. *Langmuir*, 27(12), pp.7806–7819.
- Pálková, H. et al., 2010. Laponite-derived porous clay heterostructures: I. Synthesis and physicochemical characterization. *Microporous and Mesoporous Materials*, 127(3), pp.228–236.
- Penner, D. & Lagaly, G., 2001. Influence of anions on the rheological properties of clay mineral dispersions. *Applied Clay Science*, 19, pp.131–142.
- Petit, L. et al., 2009. Size dependence of tracer diffusion in a laponite colloidal

- gel. *Langmuir*, 25(20), pp.12048–12055.
- Pignon, F. et al., 1997. Yield stress thixotropic clay suspension: Investigation of structure by light, neutron, and x-ray scattering. *Physical Review E*, 56(3), pp.3281–3289.
- Pilavtepe, M. et al., 2017. Macro- and microscale structure formation and aging in different arrested states of Laponite dispersions. *Journal of Rheology* (submitted).
- Ramos-Tejada, M.M., de Vicente, J., et al., 2011a. Effect of humic acid adsorption on the rheological properties of sodium montmorillonite suspensions. *Journal of Rheology*, 45(5), p.1159.
- Ramos-Tejada, M.M., Arroyo, F.J., et al., 2011b. Scaling Behavior of the Rheological Properties of Montmorillonite Suspensions: Correlation between Interparticle Interaction and Degree of Flocculation. *Journal of Colloid and Interface Science*, 235(2), pp.251–259.
- Rand, B. et al., 1980. Investigation into the existence of edge-face coagulated structures in Na-montmorillonite suspensions. *Journal of the Chemical Society, Faraday Transactions 1*, 76, pp.225–235.
- Reiche, T., Noseck, U. & Schäfer, T., 2016. Migration of Contaminants in Fractured-Porous Media in the Presence of Colloids: Effects of Kinetic Interactions. *Transport in Porous Media*, 111(1), pp.143–170.
- Rich, J.P., Lammerding, J., et al., 2011a. Nonlinear microrheology of an aging, yield stress fluid using magnetic tweezers. *Soft Matter*, 7(21), p.9933.
- Rich, J.P., McKinley, G.H. & Doyle, P.S., 2011b. Size dependence of microprobe dynamics during gelation of a discotic colloidal clay. *Journal of Rheology*, 55(2), p.273.
- Rives, V., del Arco, M. & Martín, C., 2014. Intercalation of drugs in layered double hydroxides and their controlled release: A review. *Applied Clay Science*, 88–89, pp.239–269.
- Rozalén, M., Brady, P. V. & Huertas, F.J., 2009. Surface chemistry of K-montmorillonite: Ionic strength, temperature dependence and dissolution kinetics. *Journal of Colloid and Interface Science*, 333(2), pp.474–484.
- Ruzicka, B. et al., 2008. Arrested state of clay-water suspensions: Gel or glass? *Physical Review E*, 77(2), p.20402.
- Ruzicka, B. et al., 2010. Observation of empty liquids and equilibrium gels in a

## References

---

- colloidal clay. *Nature Materials*, 10(1), pp.56–60.
- Ruzicka, B. & Zaccarelli, E., 2011. A fresh look at the Laponite phase diagram. *Soft Matter*, 7, pp.1268–1286.
- Ruzicka, B., Zulian, L. & Ruocco, G., 2006. More on the phase diagram of laponite. *Langmuir*, 22(3), pp.1106–1111.
- Ruzicka, B., Zulian, L. & Ruocco, G., 2004. Routes to gelation in a clay suspension. *Physical Review Letters*, 93(25), p.258301.
- Savin, T. & Doyle, P.S., 2005. Static and dynamic errors in particle tracking microrheology. *Biophysical Journal*, 88(1), pp.623–638.
- Savin, T. & Doyle, P.S., 2007. Statistical and sampling issues when using multiple particle tracking. *Physical Review E*, 76(2), p.21501.
- Schnetzer, F. et al., 2016. Unraveling the Coupled Processes of (De)hydration and Structural Changes in Na<sup>+</sup>-Saturated Montmorillonite. *Journal of Physical Chemistry C*, 120(28), pp.15282–15287.
- Schramm, L.L., 2006. *Emulsions, Foams, and Suspensions: Fundamentals and Applications*, Weinheim: Wiley VCH Verlag GmbH & Co. KGaA.
- Secor, R.B. & Radke, C.J., 1985. Spillover of the diffuse double layer on montmorillonite particles. *Journal of Colloid and Interface Science*, 103(1), pp.237–244.
- Shahin, A. & Joshi, Y.M., 2010. Irreversible aging dynamics and generic phase behavior of aqueous suspensions of laponite. *Langmuir*, 26(6), pp.4219–4225.
- Shalkevich, A. et al., 2007. Cluster, glass, and gel formation and viscoelastic phase separation in aqueous clay suspensions. *Langmuir*, 23(7), pp.3570–3580.
- Shaw, D.J., 1992. *Colloid & Surface Chemistry*, Oxford: Butterworth-Heinemann.
- Sohm, R. & Tadros, T.F., 1989. Viscoelastic properties of sodium montmorillonite (Gelwhite H) suspensions. *Journal of Colloid and Interface Science*, 132(1), pp.62–71.
- Sposito, G., 1992. Characterization of particle surface charge. *Environmental Particles*, 1, pp.291–314.
- Sposito, G., 2008. *The Chemistry of Soils* 2. Edition., New York: Oxford

- University Press.
- Sposito, G., 1981. The operational definition of the zero point of charge in soils. *Soil Science Society of America Journal*, 45, pp.292–297.
- Sridharan, A. & Satyamurty, P. V., 1996. Potential-distance relationships of clay-water systems considering the stern theory. *Clays and Clay Minerals*, 44(4), pp.479–484.
- Strachan, D.R., Kalur, G.C. & Raghavan, S.R., 2006. Size-dependent diffusion in an aging colloidal glass. *Physical Review E*, 73(4), p.41509.
- Struik, L.C.E., 1978. *Physical aging in amorphous polymers and other materials*, New York: Elsevier Scientific Pub. Co.
- Tanaka, H., Meunier, J. & Bonn, D., 2004. Nonergodic states of charged colloidal suspensions: Repulsive and attractive glasses and gels. *Physical Review E*, 69, p.31404.
- Tawari, S.L., Koch, D.L. & Cohen, C., 2001. Electrical Double-Layer Effects on the Brownian Diffusivity and Aggregation Rate of Laponite Clay Particles. *Journal of Colloid and Interface Science*, 240, pp.54–66.
- Tombácz, E. et al., 1990. The pH-dependent colloidal stability of aqueous montmorillonite suspensions. *Colloids and Surfaces*, 49, pp.71–80.
- Tombácz, E. & Szekeres, M., 2004. Colloidal behavior of aqueous montmorillonite suspensions: The specific role of pH in the presence of indifferent electrolytes. *Applied Clay Science*, 27, pp.75–94.
- Tournassat, C., Greneche, J.M., et al., 2004a. The titration of clay minerals: I. Discontinuous backtitration technique combined with CEC measurements. *Journal of Colloid and Interface Science*, 273(1), pp.224–233.
- Tournassat, C., Ferrage, E., et al., 2004b. The titration of clay minerals: II. Structure-based model and implications for clay reactivity. *Journal of Colloid and Interface Science*, 273(1), pp.234–246.
- Tripathy, S., Bag, R. & Thomas, H.R., 2014. Effect of Stern-layer on the compressibility behaviour of bentonites. *Acta Geotechnica*, 9, pp.1097–1109.
- Trizac, E. et al., 2002. Effective interactions and phase behavior for a model clay suspension in an electrolyte. *Journal of Physics: Condensed Matter*, 14, pp.9339–9352.
- Vali, H. & Bachmann, L., 1988. Ultrastructure and flow behavior of colloidal

## References

---

- smectite dispersions. *Journal of Colloid and Interface Science*, 126(1), pp.278–291.
- Van Olphen, H., 1977. *An introduction to clay colloid chemistry, for clay technologists, geologists, and soil scientists*. 2nd editio., New York: John Wiley & Sons, New York.
- Willenbacher, N. et al., 2007. Broad bandwidth optical and mechanical rheometry of wormlike icelle solutions. *Physical Review Letters*, 99(6), p.68302.
- Willenbacher, N., 1996. Unusual thixotropic properties of aqueous dispersions of Laponite RD. *Journal of Colloid and Interface Science*, 182(2), pp.501–510.
- Willenbacher, N. & Georgieva, K., 2013. Rheology of Disperse Systems. In *Product Design and Engineering*. Weinheim: Wiley VCH Verlag GmbH & Co. KGaA, pp. 7–49.
- Winter, H.H. & Chambon, F., 1986. Analysis of Linear Viscoelasticity of a Crosslinking Polymer at the Gel Point. *Journal of Rheology*, 30(2), p.367.
- Wolters, F. et al., 2009. A comprehensive characterization of dioctahedral smectites. *Clays and Clay Minerals*, 57(1), pp.115–133.
- Yang, Y.-R. et al., 2012. Large amplitude oscillatory shear rheology of Laponite gels. *Gaodeng Xuexiao Huaxue Xuebao/Chemical Journal of Chinese Universities*, 33(4), pp.818–822.
- Yariv, S. & Cross, H., 1979. *Geochemistry of Colloid Systems: For Earth Scientists*. Springer-Verlag, 457, pp.220–222.
- Yildiz, N., Sarikaya, Y. & Calimli, A., 1999. The effect of the electrolyte concentration and pH on the rheological properties of the original and the. *Applied Clay Science*, 14, pp.319–327.
- Zbik, M.S. et al., 2014. The formation of a structural framework in gelled Wyoming bentonite: Direct observation in aqueous solutions. *Journal of Colloid and Interface Science*, 435, pp.119–127.
- Web course materials [www.open.edu](http://www.open.edu), An introduction to minerals and rocks under the microscope.
- University of Liverpool, ChemTube3D, <http://www.chemtube3d.com/solidstate/SS-Hectorite.html>